

# A Three-Dimensional Printing Machine to Facilitate Observation of Printing Phenomena

by

Akobuije Chijioke

B.S.E., Mechanical Engineering and Materials Science

Duke University, 1996

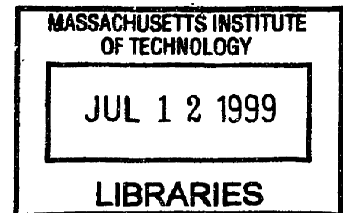
Submitted to the Department of Mechanical Engineering  
in Partial Fulfillment of the Requirements for the Degree of  
Master of Science in Mechanical Engineering

at the

Massachusetts Institute of Technology


June 1998

©1998 Massachusetts Institute of Technology  
All rights reserved




**ARCHIVES**

Signature of Author . . . . .

  
Department of Mechanical Engineering  
May 8, 1998

Certified by . . . . .

  
Emanuel M. Sachs  
Professor of Mechanical Engineering  
Laboratory for Manufacturing and Productivity  
Thesis Supervisor

Accepted by . . . . .

  
Ain A. Sonin  
Chairman, Department Committee on Graduate Students

# **A Three-Dimensional Printing Machine to Facilitate Observation of Printing Phenomena**

by

Akobuije Chijioke

Submitted to the Department of Mechanical Engineering on May 8,  
1998 in partial fulfillment of the requirements for the Degree of  
Master of Science in Mechanical Engineering

## **ABSTRACT**

The understanding of binder-powder interaction during the Three Dimensional Printing process is critical to improving the characteristics of parts produced by this process. The ability to observe the binder-powder interaction taking place could aid its investigation greatly. In the case of Three Dimensional Printing of fine ceramics, in which powderbeds are deposited as a liquid slurry before printing with a binder is done, the deposition of the powderbed itself is a part of the process the investigation of which could benefit from convenient automated image acquisition.

Such observation requires flexible imaging capabilities of a nature that cannot easily be realized by using attachments to existing Three Dimensional Printing machines. This motivated the design and construction of a specialized imaging-oriented Three Dimensional Printing machine, the droplet impact observation station, which this thesis documents. The requirements of the machine are presented, the realized design and operation of the machined described, the results of initial tests of operation presented and areas for further work and improvement outlined.

The droplet impact observation station constructed moves a carriage back and forth over a travel of up to 46.5 inches, at speeds of up to 2 m/s with a total velocity ripple of approximately 0.007 m/s. In the station's primary mode of operation, the moving carriage transports a powderbed, while the printhead remains stationary. Tests in which strobe-illuminated images of crosshairs mounted on the moving carriage were obtained have demonstrated the ability to time a strobe flash to within +/- 1-2 microns. Strobe-illuminated images of continuous-jetted droplets produced by the observation station have been obtained.

Thesis Supervisor: Emanuel M. Sachs

Title: Professor of Mechanical Engineering

## **Acknowledgements**

The development of the droplet impact observation station has been anything but a solo project. Ely, Dave and I have worked on the project as a team, and these two senior partners have provided guidance for which I am grateful. Several others have also contributed to the project.

Ely gave me this wonderful opportunity and has taught me several important lessons over the past two years, while putting up with my shortcomings. I hope that in return I have been able to give something of value to the larger project.

Dave has steered me away from trouble many times and lifted me out of it when despite his efforts I have managed to wade in. He is a debugging genius among many other things. Furthermore, several of the best parts of the station are basically entirely Dave's work: the strobe delay scheme, the rod-end cable connection, the velocity profiling routine and the crosshair image analysis routine all come to mind.

Jim Serdy has been a great help with jetting, and has many a time provided me with necessary components, tools and instruction on their use. Jim is also an inspiring example of dedication and professionalism.

I have been very fortunate to have the opportunity to learn some machining from the likes of Fred Cote, Gerry Wentworth and Victor Lerman.

Diana Buttz, Vedran Knezevic, Ben Polito and Akan Oton have all made significant contributions to this project, for which I thank them.

Adam, Akan, Vedran, Drew, Costas, Pat, Bjorn - it's been a pleasure to work, learn and play with you all. All the best in your future endeavours.

# TABLE OF CONTENTS

ABSTRACT	2
ACKNOWLEDGEMENTS	3
TABLE OF CONTENTS	4
LIST OF FIGURES	9
LIST OF TABLES	12
1.0 INTRODUCTION	13
1.1 Three Dimensional Printing	13
1.2 Previous Work on Observing Droplet Impacts	15
1.3 Organization of this Thesis	21
2.0 REQUIRED CAPABILITIES AND OVERALL DESIGN	22
2.1 Desired Images	22
2.1.1 Strobe-Illuminated Single Image	23
2.1.2 Imaging a Series of Impacts Per Pass with Controlled Phase Advance between Images	24
2.1.3 Imaging at Long Times after Printing	25
2.1.4 Motion of Camera, Jet and Powderbed	26
2.1.5 Adaptability to New Tasks	28
2.2 Controlled Motion	28
2.2.1 Axis Labels	29
2.2.2 Acceleration and Length of Travel	29
2.2.3 Velocity Fluctuation and Transverse Position Error	32
2.3 Printing	31
2.3.1 Continuous-Jet Printing	32



2.3.2 Drop-On-Demand Printing	34
2.3.3 Slurry Printing	35
2.3.4 Geometry of Printed Features	35
2.3.5 Accommodation of Printing Requirements	36
2.4 Conclusion	36
3.0 LINEAR BEARINGS	40
3.1 Bearing Type	40
3.2 Air Bearing Selection	41
3.2.1 Dover Box Slide	41
3.2.2 New Way Box Slide	42
3.2.3 Space Electronics Cylindrical Sleeves	42
3.2.4 New Way Porous Graphite Bearings	45
3.3 Conclusion	45
4.0 MOVING CARRIAGE	46
4.1 Powderbed	46
4.2 Encoder Readhead	46
4.3 Bearing Couplings	48
4.3.1 Deflections to be accommodated	48
4.3.2 Maximum bearing loads	51
4.3.3 Flexible coupling design	56
4.3.4 Potted coupling	63
4.3.5 Assembly procedure	65
4.3.6 Electrical monitoring of bearing contact	66
4.4 Cable Connection	67
4.5 Umbilical	67
4.6 Center of Gravity Tuning	69
4.7 Conclusion	72

<b>5.0 DRIVE SYSTEM</b>	<b>73</b>
5.1 Cable	73
5.2 Drive Pulley Assembly	77
5.3 Idler Pulley Assembly	79
5.4 Motor	79
5.5 Conclusion	84
<b>6.0 OVERALL LAYOUT AND STRUCTURE</b>	<b>86</b>
6.1 Camera and Printhead Mounting	86
6.2 Encoder Plate	88
6.3 Frame	88
<b>7.0 ELECTRONIC SYSTEM OVERVIEW</b>	<b>90</b>
7.1 Tasks Performed by the System	90
7.2 Parts of the System	90
7.3 Flow of Information	93
7.4 Signal Timing	96
7.5 Synchronous Operation	96
7.5.1 Synchronous Operation and Encoder Resolution	98
7.5.2 Synchronous Operation and Droplet Breakoff Timing	102
7.6 Computer	102
7.7 Software	102
<b>8.0 MOTION CONTROL</b>	<b>104</b>
8.1 Encoder	104
8.1.1 Signals	104
8.1.2 Scale and Limit Switch Mounting	106
8.1.3 Readhead Mounting	107
8.2 Motion Controller	108
8.3 Amplifier	108

<b>9.0 PRINTING AND IMAGING</b>	<b>110</b>
9.1 Encoder	110
9.1.1 Quadrature Decoder Chip	110
9.2 Drop Excitation	113
9.2.1 Flip-Flop Gate	114
9.3 Drop Charging	115
9.4 Strobe Triggering	115
9.4.1 Strobe Delay Circuit	115
9.5 Frame Grabber Triggering	117
9.6 Camera	118
9.7 Frame Grabber	118
<b>10.0 TESTS OF OPERATION</b>	<b>120</b>
10.1 Gains Testing	120
10.2 Velocity Ripple	122
10.3 Test of Encoder Counting: Repositioning Test	123
10.4 Strobng Moving Crosshairs: Repeatability of Strobe Flash Timing	127
10.5 Strobng Moving Crosshairs: Test of Strobe Delay	129
10.6 Synchronous Generation of Droplets	129
10.7 Strobng Drops	131
<b>11.0 FURTHER WORK AND IMPROVEMENTS</b>	<b>132</b>
11.1 Strobng Drops with Phase Delay	132
11.2 Printing Lines	132
11.3 Adding charging, deflection and catching	132
11.4 High-Speed Frame Grabbing	133
11.5 Electronics Mounting	133
11.6 Steel Band	133

11.7 Pulley and Idler Fits	134
11.8 Strobe Delay Circuit	134
<b>REFERENCES</b>	<b>136</b>
<b>APPENDIX A: Machine Drawings</b>	<b>137</b>
<b>APPENDIX B: Mass Moment of Inertia Calculations</b>	<b>168</b>
<b>APPENDIX C: VI Documentation</b>	<b>172</b>

# LIST OF FIGURES

## Chapter 1. Introduction

1.1 Steps in the Three Dimensional Printing Process	13
1.2 Droplet impact on loose powderbed	16
1.3 Droplet impact on pre-treated powderbed	16
1.4 Schematic diagram of Fan's impact observation station	17
1.5 Mechanical assembly used by Fan	18
1.6 Overall sketch of droplet impact observation station	20

## Chapter 2. Required Capabilities and Overall Design

2.1 Visualization of a series of images with droplet phase advance between images	24
2.2 Axis labels	29
2.3 Experimental assembly for testing powderbed tolerance of acceleration	30
2.4 Continuous-jet printing	33

## Chapter 3. Linear Bearings

3.1 Sketch of Dover Air Bearing Slide	41
3.2 Continuously-supported round shafts require a gap in the bearing	43
3.3 Space Electronics cylindrical sleeve air bearing with gap	43
3.4 New Way porous graphite air bearing	44

## Chapter 4. Moving Carriage

4.1 Carriage Layout	47
4.2 Bearing Motions	49
4.3 Maximum bearing torques and forces to be measured	51
4.4 Experimental arrangement for measuring force $F$ at bearing contact	52
4.5 Experimental arrangement for measuring torque $T_1$	53

4.6 Experimental arrangement for measuring torque T2	54
4.7 Flexible coupling stiffness and dimension labels	56
4.8 Potted coupling	63
4.9 Potted coupling accommodates some errors that otherwise cause f-rotation of Bearings	64
4.10 Bearing block height variation and necessary shimming	65
4.11 Drive cable connection	67
4.12 Hanging umbilical	68
4.13 Rolling Umbilical	68
4.14 Loads and displacements related to center-of-gravity discussion	69
4.15 Arrangement for measuring center-of-gravity position	71
<b>Chapter 5. Drive System</b>	
5.1 Drive pulley assembly	76
5.2 Idler pulley assembly	78
<b>Chapter 6. Overall Layout and Structure</b>	
6.1 Camera mounting assembly	87
6.2 Photograph of machine on frame	88
<b>Chapter 7. Electronic System Overview</b>	
7.1 Overall electronic system	91
7.2 Flow of information. Broad view	93
7.3 Flow of information. Detailed view	94
7.4 Signal timing diagram	97
<b>Chapter 8. Motion Control</b>	
8.1 Parts of electronic system concerned with motion control	105
8.2 Readhead mounting scheme	107

## **Chapter 9. Printing and Imaging**

9.1 Parts of the electronic system related to printing and imaging	111
9.2 Quadrature decoding circuit	112
9.3 Output Pulse Width ( $T_{ow}$ ) versus $R_1$ ( $R_{bias}$ )	112
9.4 Flip-flop gate circuit	114
9.5 Strobe delay circuit	116

## **Chapter 10. Tests of Operation**

10.1 Grabbed image of droplet breakoff, illuminated by single strobe flash	131
--	-----

## **Chapter 11. Further Work and Improvements**

11.1 Alternate Strobe Delay Scheme	135
------------------------------------	-----

## **LIST OF TABLES**

### **Chapter 2. Required Capabilities and Overall Design**

2.1 Possible combinations of motion of printhead, powderbed and camera	27
2.2 Summary of functional requirements and design decisions	38

### **Chapter 4. Moving Carriage**

4.1 Motion requirements of bearing 3 relative to bearings 1 and 2	51
4.2 Design goals for flexible coupling stiffnesses	57
4.3 Material properties of Ultem 1000	58
4.4 Stiffness formulae	59
4.5 Constraints used in Solver optimization	60
4.6 Solver results	61

### **Chapter 5.**

5.1 Manufacturer's specifications for motor used	80
--	----

### **Chapter 7**

7.1 Frequencies in Hz available at given speeds	100
7.2 Speeds in m/s available at given frequencies	101

### **Chapter 10.**

10.1 Result of gains testing	121
10.2 Measured velocity ripple	122
10.3 Repositioning test #1 data	123
10.4 Repositioning test #2 data	125
10.5 Repeatability of image analysis	126
10.6 Strobing crosshairs moving at 0.02 m/s	127
10.7 Strobing crosshairs moving at 0.5 m/s	128
10.8 Strobing crosshairs moving at 2.0 m.s	128
10.9 Testing of strobe delay	129



## 1.0 INTRODUCTION

### 1.1 THREE DIMENSIONAL PRINTING

Three Dimensional Printing is a prototyping and manufacturing technique in which a liquid binder is used to selectively join powder particles to form a rigid part. The placement of liquid binder is controlled by information extracted from a Computer-Aided Design (CAD) file. The printed part is either used in its as-printed state, or processed further such as by sintering and subsequent infiltration with a molten metal.

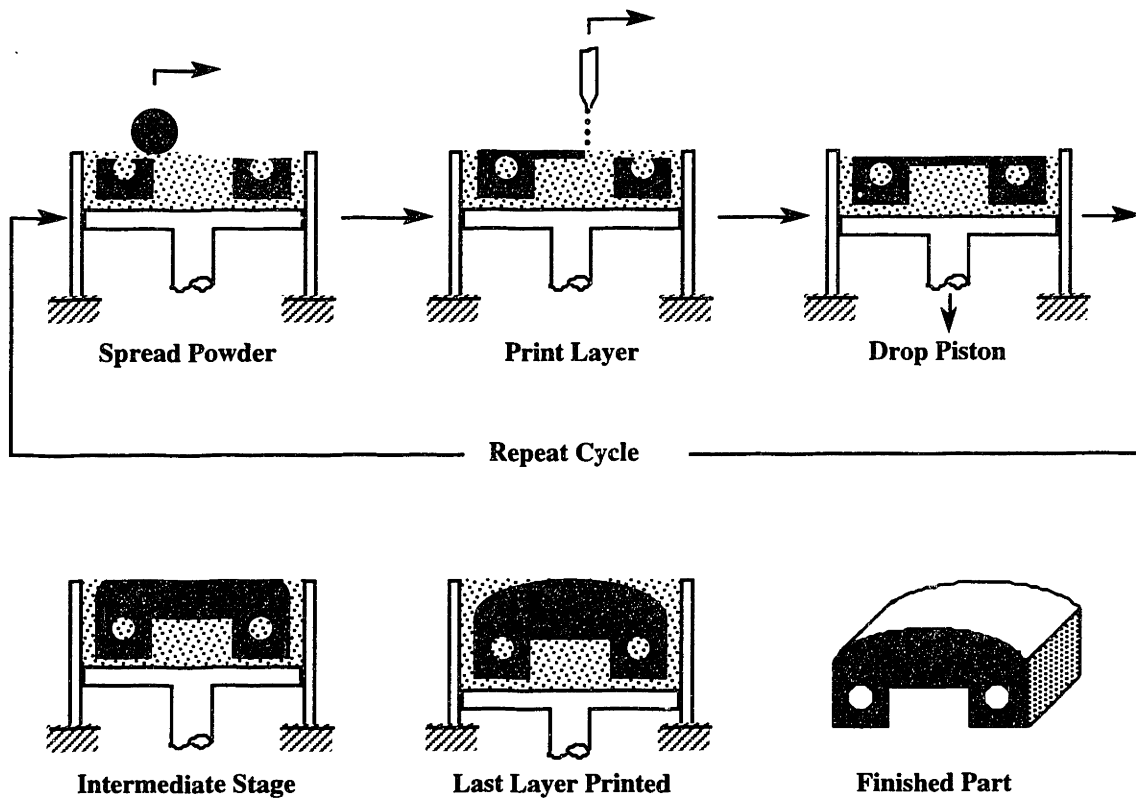


**Figure 1.1.** Steps in the Three Dimensional Printing process.

Figure 1.1 illustrates the Three Dimensional Printing process. First, a layer of powder is spread. Then a printhead is rastered over a powderbed, depositing binder in

areas to be joined. After printing for the layer has been completed, the powderbed is lowered, a new layer of powder spread, and the binder for the next layer printed. In this way a part is built up. When the part is completed it is removed from the powderbed and may be sintered and infiltrated with a molten metal (Sachs et. al.).

In doing Three Dimensional Printing with fine ceramics, it is generally the case that each layer of the powderbed is not spread as a dry powder, but is deposited as a slurry.

Three Dimensional Printing is a technology that reduces the time that it takes to bring some new products to market, in several possible ways. One way in which it reduces time-to-market is by allowing rapid prototyping of part designs. Another is by allowing the rapid production of tooling for injection molding, a manufacturing step that routinely takes months with current industry standard practice. Investment casting is another manufacturing process greatly accelerated by the use of Three Dimensional Printing, as the production of casting shells directly from CAD models via Three Dimensional Printing eliminates several steps from the traditional lost-wax technique.

Three Dimensional Printing also allows the production of some parts that are difficult or impossible to produce by other available manufacturing techniques. Examples are parts with complex internal geometries, and parts with local compositional variation.

The standard measures of the performance of Three Dimensional Printing as a manufacturing and prototyping technology are dimensional control, surface finish, and part strength and hardness. The understanding of binder-powder interaction during the printing process is critical to improving these characteristics. The ability to conveniently acquire images of this interaction taking place could aid its investigation greatly. In the

case of Three Dimensional Printing with fine ceramics, the deposition of the powderbed itself is a part of the process the investigation of which could benefit from automated image acquisition.

Such observation requires high-speed imaging of a nature that cannot easily be accomplished using attachments to existent Three Dimensional Printing machines. This motivated the design and construction of a specialized imaging-oriented Three Dimensional Printing machine, which this thesis documents.

## **1.2 PREVIOUS WORK ON OBSERVING DROPLET IMPACTS**

The first pictures of droplet impacts in the 3DP™ process were taken by Steve Michaels and are shown in Figures 1.2 and 1.3. Michaels used a single strobe flash to illuminate an open-shutter 35-millimeter camera image. Michaels' pictures showed the damage to loose powderbeds that could be caused by droplet impact, and that such damage could be prevented by pre-treating the powderbed.

Tailin Fan did a detailed study of single droplet impacts on loose alumina powderbeds (Fan). The arrangement used by Fan is shown in Figures 1.4 and 1.5, and consisted of the following:

- A printhead to generate droplets, mounted on a micro-positioning stage;
- A catcher to catch unprinted droplets;
- Droplet charging and deflection electrodes, each pair of electrodes separately mounted on a micro-positioning stages (The entire assembly of printhead, catcher, electrodes and their respective positioning stages was mounted on a z-axis positioning stage);

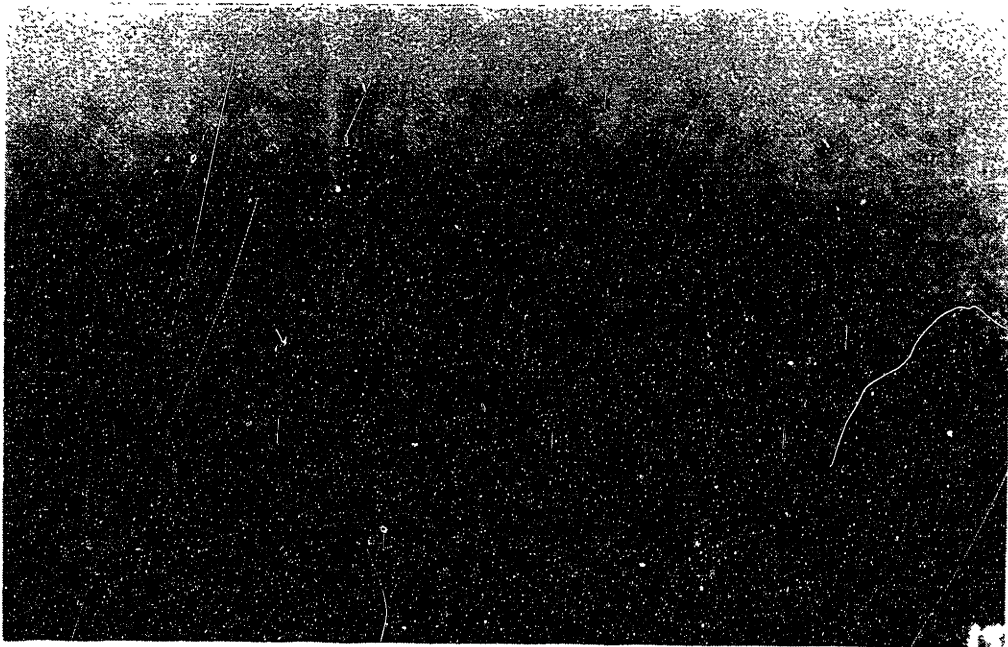


**Figure 1.2.** Droplet impact on loose powderbed (Courtesy of S. Michaels).

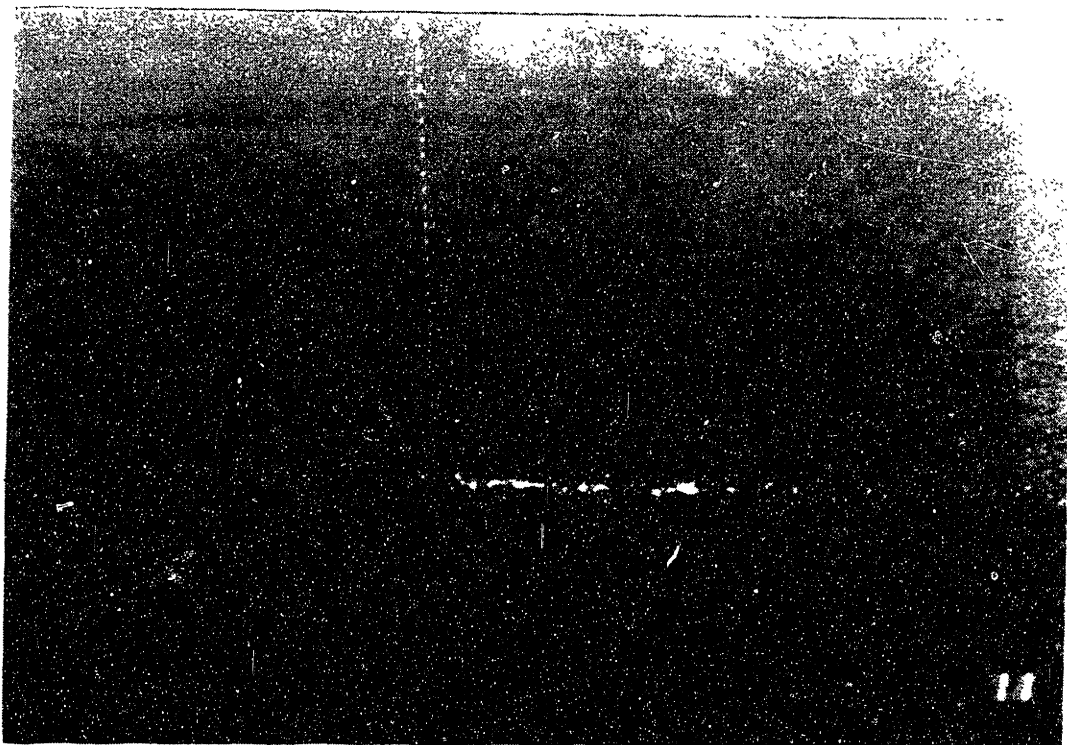


**Figure 1.3.** Droplet impact on pre-treated powderbed (Courtesy of S. Michaels).

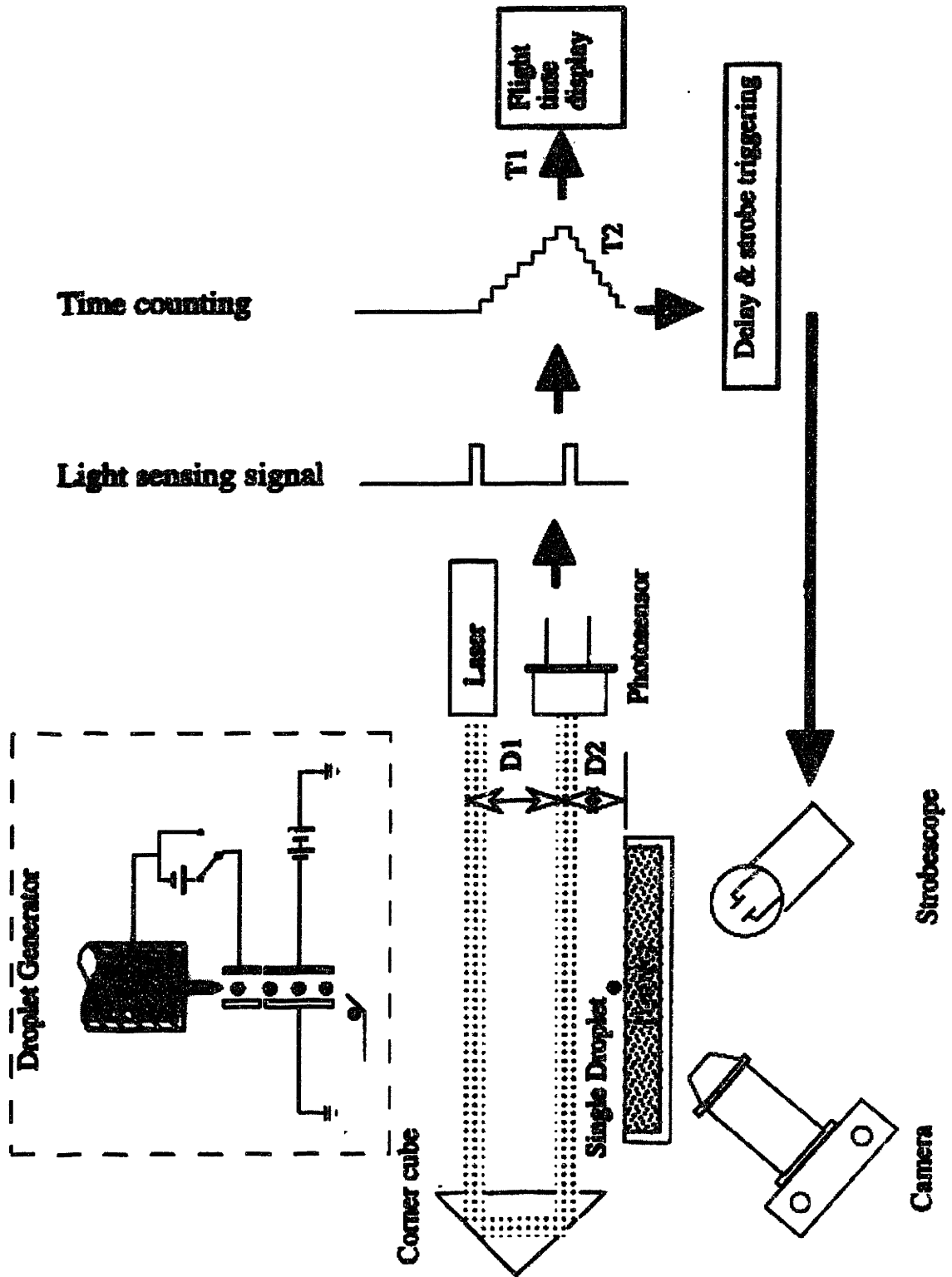


Figure 1.4. Schematic diagram of Fan's observation station (Courtesy of Tailin Fan).

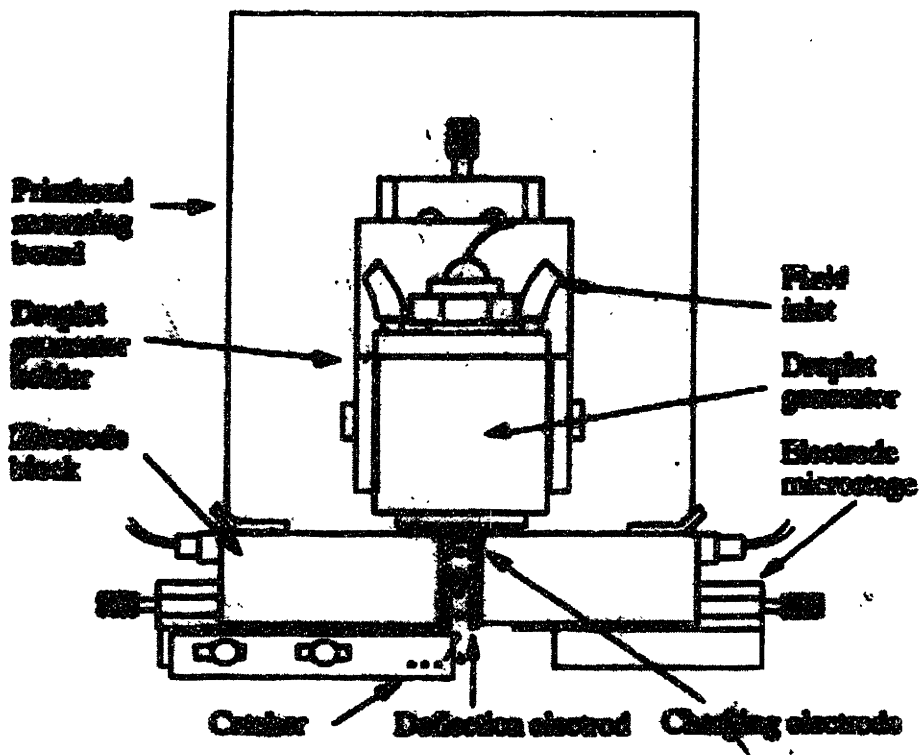


Figure 1.5. Mechanical assembly used by Fan (courtesy of T. Fan).

- Control circuitry that enabled a drop to fall to the powderbed when the user wished to take a picture;
- A powderbed mounted on a micro-positioning stage;
- A laser speed-trap to measure the speed of a droplet in flight;
- A strobe light;
- A strobe triggering circuit, to time the strobe flash to occur after the desired period after droplet impact;
- A first-surface mirror set at a 45-degree angle to the powderbed to enable the top of the powderbed to be photographed within the space constraints;
- A 35-mm camera with an auto extension tube and a 20-mm micro-lens, achieving a 9X total magnification.

Like Michaels, Fan used the 35-mm camera with an open shutter in a dark room, using a strobe flash to illuminate the subject. Fan's observations showed the simultaneous evolution of binder-particle aggregate formation and powderbed cratering.

Tara Arthur used video observation to study the infiltration time of Hewlett Packard drop-on-demand ink droplets into fine ceramic powderbeds. She observed that it takes about 30-60 milliseconds for a droplet to infiltrate a powderbed, the time being dependent on the surface finish of the powderbed, and that splashing might be taking place as one droplet impacts into other droplets that were previously deposited but are still on the surface (Arthur).

In order to extend these observations to observations of single droplet impacts on moving powderbeds, impacts on powderbeds in which a pattern is being printed, and

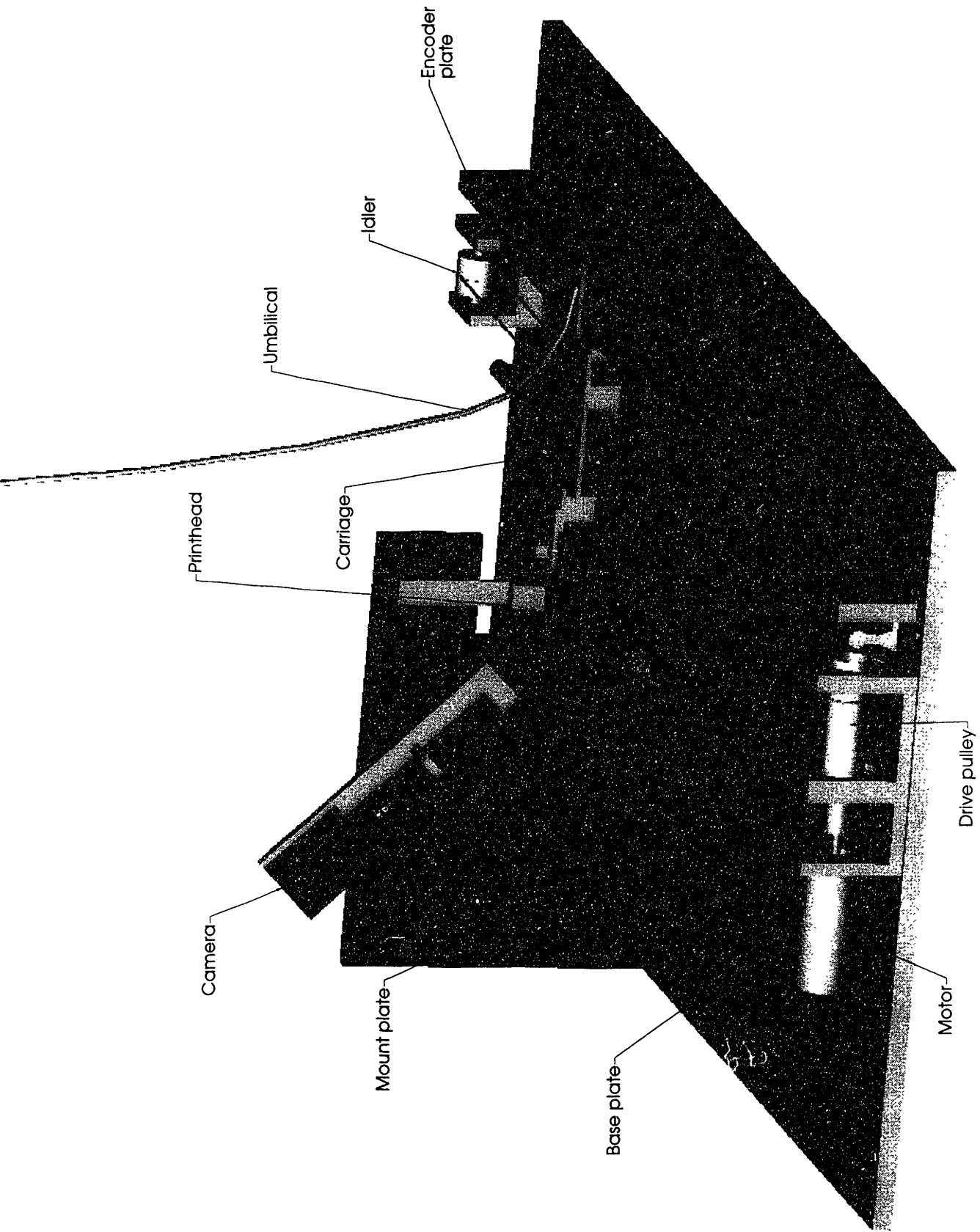


Figure 1.6. Overall sketch of droplet impact observation station.



impacts over the wide range of printing conditions that occur in the several variations of the 3DP™ process, it was deemed worthwhile to design and construct an observation-oriented Three Dimensional Printing machine.

### **1.3 ORGANIZATION OF THIS THESIS**

This thesis is divided into four sections. The first two chapters constitute the first section. The present chapter presents the motivation for this work, and chapter two presents the functional requirements for the droplet impact observation station and the means by which these were addressed. The second section discusses the mechanical design of the station, an overall picture of which is shown as Figure 1.6: chapter three deals with the linear bearing system, chapter four with the moving carriage, chapter five with the drive system, and chapter six with the overall structure and the location of the various parts. The third section discusses the electronic design of the station: chapter seven discusses the overall electronic scheme, chapter eight discusses motion control, and chapter nine discusses the generation of signals to control printing and imaging. The final section consists of two chapters: chapter ten presents the results of tests of various aspects of the operation of the station and chapter eleven discusses possible improvements to the station. Appendices contain machine drawings, calculations of mass moments of inertia of moving parts and documentation of the software created for the machine.

## **2.0 REQUIRED CAPABILITIES AND OVERALL DESIGN**

### **2.1 DESIRED IMAGES**

In an ideal design process, the functional requirements are clearly stated before the design is begun and are not altered after the design is complete and construction has begun. In the present case, however, the principal functional requirements, namely the imaging capabilities of the machine, were not clearly known at the outset. Indeed, it was recognized that studies performed with the aid of the machine would likely indicate what image-taking capabilities were important. The only requirement in the area of imaging that could be specified with certainty was that the machine should be a flexible platform, easily adaptable to as many different imaging schemes as possible, and to as many different subjects as possible. The viewing angle should in general be variable from a top view to a horizontal profile view.

Nevertheless, certain perceived imaging requirements were identified at the start of the design process. But even these approximate targets underwent drastic revision as design and concurrent construction moved forward, and the limitations of available pieces of equipment became apparent. In its present form, the observation station performs such imaging as is possible with equipment currently possessed, and has been built to perform certain other imaging functions with the modular addition of pieces of equipment that fit into the overall framework of the machine. Subsections 2.1.1 and 2.1.3 describe imaging tasks that the machine is currently capable of performing. Subsection 2.1.2 describes a task that has been kept in mind during design and construction, but which requires equipment not currently possessed in order to be effected.

### **2.1.1. Strobe-Illuminated Single Image**

A fundamental requirement of the observation station is the ability to take a stop-action picture of a droplet impact on a moving powderbed, at a specific phase in the droplet cycle. For typical continuous-jet frequencies used in the 3DP™ process, a droplet cycle has a period of about 20 microseconds. A stop-action picture should therefore have an exposure duration of no more than 2 microseconds, one tenth of the droplet cycle duration. Precisely locating the image within the droplet cycle requires the synchronization of imaging and droplet generation, and requires adjustability of the image timing with a resolution of 2 microseconds or better. At the minimum, a single image should be acquired per pass.

The identified means of achieving this is to use a strobe light to illuminate an image acquired by a video camera run under computer control. A strobe lamp on hand with a flash duration of approximately 1.2 microseconds and a variation in the strobe flash timing relative to a trigger signal of less than 2 microseconds, electronically triggered at a predetermined delay of several microseconds after drop excitation, provides the desired precisely timed stop-action imaging. Further details of this electronic scheme will be given in chapters seven and nine. The use of a video camera under computer control allows the machine to be used under normal lighting, and provides for the convenient storage and retrieval of images. The camera possessed can also be used for other imaging schemes (e.g. see 2.1.3).

### 2.1.2 Imaging a Series of Impacts per Pass with Controlled Phase Advance between Images

An improvement over the ability to acquire a single image per pass at a predetermined position within an impact cycle would be the ability to acquire a series of images per pass, not all of the same specific impact, but each occurring a bit later in droplet phase than the previous image. This is illustrated by Figure 2.1.

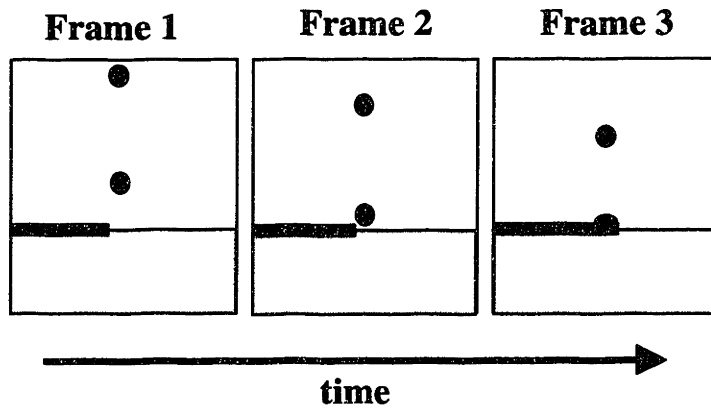


**Figure 2.1.** Visualization of a series of images with droplet phase advance between images.

Three consecutive images show a horizontal profile view of an imagined jet of liquid printing into an imagined powderbed. Each consecutive image is advanced in droplet phase with respect to the previous one. A typical camera field of view at the magnifications desired is at best only one or two millimeters wide, so the acquisition of more than one or two images in a single printing pass at typical continuous-jet printing speeds requires that the camera and liquid jet remain stationary relative to each other. To allow for possibly bulky or heavy cameras and light sources, it was decided to design the machine to have a moving powderbed, stationary printhead and stationary camera in its primary mode of operation.

This imaging task requires only a monochromatic camera and frame grabber, and a single strobe lamp. However at typical printing speeds, and with powderbeds of reasonable length\*, the ability to acquire more than a few images in a pass requires a camera and frame grabber that run at a higher speed than do the equipment currently possessed. For example, a series of ten images at a printing speed of 2 meters per second would require a camera and frame grabber operating at 80 frames per second. This is calculated as follows:

$$\begin{aligned}
 \text{Frame rate} &= \frac{\# \text{ of frames}}{\text{time powderbed is in field of view}} = \\
 \left( \frac{\# \text{ of frames}}{\left( \frac{\text{length of powderbed}}{\text{speed of powderbed}} \right)} \right) &= \left( \frac{10 \text{ frames}}{\left( \frac{0.254 \text{ m}}{2 \frac{\text{m}}{\text{s}}} \right)} \right) = 79 \frac{\text{frames}}{\text{s}} \quad (2.1)
 \end{aligned}$$

The same electronic scheme used for the single-image-per-pass application can be used for this multiple-image-per-pass application, once a functional high speed camera and frame grabber have been obtained.

### 2.1.3. Imaging at Long Times after Printing

At a speed of 2 meters per second and with a powderbed ten inches long, the powderbed would be in the camera field of view for about 130 milliseconds. It is quite possible that it will be desired to observe a powderbed for times on the order of seconds, minutes or even hours. It is also quite possible that it will be desired to combine such observation with observation of a short time impact event. To accommodate such applications, provision was made in the design and construction of the machine for

---

\* Less than or equal to ten inches, dictated by the necessity of getting the powderbed moving at a constant typical printing speed using an allowable acceleration, as explained in subsection 2.2.1.

mounting the powderbed on a stationary stand and mounting the printhead on the moving carriage, reversing their respective standard locations. The electronic equipment and arrangement used for single-image-per-pass strobe imaging is capable of performing this type of imaging.

#### **2.1.4 Motion of Camera, Jet and Powderbed**

As mentioned earlier in subsection 2.1.2, the desire to acquire several images of droplet impacts per pass requires that the camera and liquid jet remain stationary relative to each other. On the other hand, the long-time imaging application discussed in subsection 2.1.3 requires that the camera and powderbed remain stationary relative to each other. These are conflicting requirements, as the powderbed and liquid jet must move relative to each other for printing to occur. Accommodation of both applications thus requires that the machine have two separate modes of operation.

It is useful at this point to review all the possible combinations of motion that can occur between the camera, jet and powderbed. These are summarized in Table 2.1. The printhead must move relative to the powderbed, so cases 1, 4, 5 and 8 are disallowed. As far as imaging is concerned, cases 2 and 7 are identical, and cases 3 and 6 are identical. In cases 2 and 7, the camera is moving relative to the powderbed and fixed relative to the jet. The jet remains stationary in the picture. Each frame in a series is of a different bunch of powder and liquid, but the layout of the picture remains the same. The number of pictures that can be acquired in a pass is limited by the length of the powderbed, not by the width of the camera field of view. One of these two cases is necessary in order to perform the imaging described in section 2.1.2 - Imaging a series of impacts per

Case #	Powderbed	Liquid Jet	Camera	Allowed?
1	Stationary	Stationary	Stationary	No
2	Moving	Stationary	Stationary	Yes
3	Stationary	Moving	Stationary	Yes
4	Moving	Moving	Stationary	No
5	Stationary	Stationary	Moving	No
6	Moving	Stationary	Moving	Yes
7	Stationary	Moving	Moving	Yes
8	Moving	Moving	Moving	No

Table 2.1. Possible combinations of motion of printhead, powderbed and camera.

with controlled phase advance between images. It was judged that it would be easier to move a small bed of powder than a possibly bulky or heavy camera and strobe light along with a printhead, so case 2 was selected over case 7.

In cases 3 and 6, the camera is fixed relative to the powderbed and moving relative to the jet. The jet moves through the picture, while the camera remains focused on the same bunch of powder (and liquid, once that is printed). This is necessary in order to look at a single impact point for long times, as described in subsection 2.1.3. Case 3 would require mounting the powderbed on a support fixed to the base, and mounting the printhead on the moving carriage. Case 6 would involve mounting the camera and light source on the moving carriage along with the powderbed, while the printhead remained stationary as in case 2. Case 3 was judged to be the easier than case 6, and was therefore selected.

Two modes of operation were thus selected for the impact observation station. The first case has a moving powderbed a stationary jet, and a stationary camera. The second case has a moving jet, a stationary powderbed and a stationary camera.

### **2.1.5 Adaptability to New Tasks**

The most useful images that could be acquired will probably only be known after some imaging work has been done with the observation station. These may differ significantly from the imaging tasks outlined in 2.1.1 – 2.1.3, and therefore as much flexibility as possible is desired of the machine. Mechanically, the station is designed to have plenty of space to mount various cameras, lights and other optical apparatus, and has a grid of uncommitted mounting holes. It is difficult to predict what additional equipment and electronic circuitry may be required.

## **2.2 CONTROLLED MOTION**

A basic requirement of the droplet impact observation station is that it provide relative linear motion between the printhead and powderbed at speeds of up to 2 meters per second, which is toward the high end of current continuous-jet Three Dimensional Printing speeds, and at speeds as low as 1 millimeter per second, which is toward the low end of drop-on demand printing speeds. The distance over which this speed is maintained should be at least 2 inches, to allow lines of over 1 inch in length to be printed. The motion must be performed repeatedly, under automatic control.

Based on experience gathered from building other Three Dimensional Printing machines, the selected means of providing such motion is to use a direct current servo motor to move the carriage back and forth, with closed loop control provided via encoder



feedback to a computer-based motion control card. A round cable is used in a belt-drive configuration.

### 2.2.1 Axis Labels

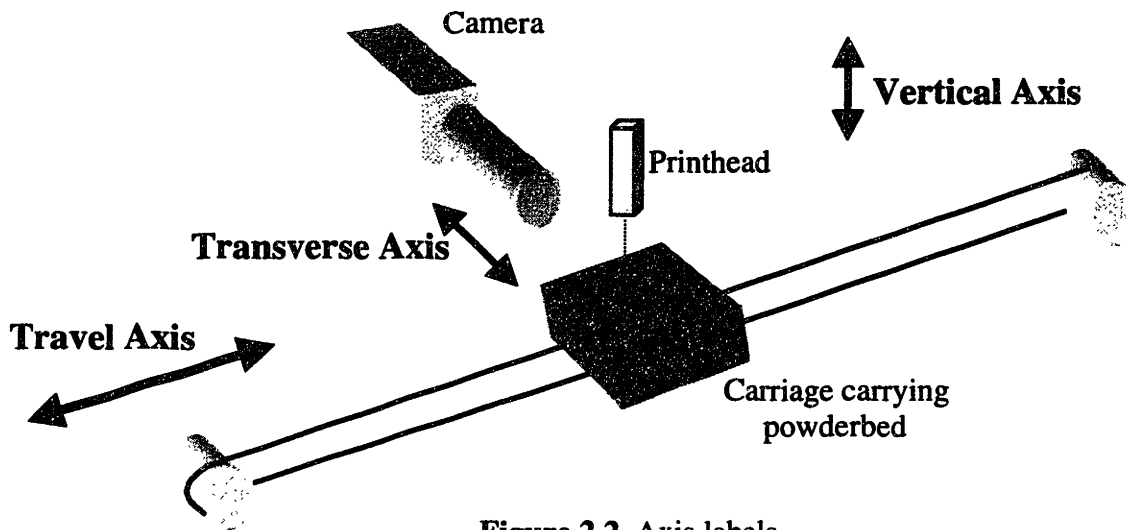


Figure 2.2. Axis labels.

The terms used for the three orthogonal axes of the observation station are illustrated in Figure 2.1. These terms will be used in the rest of this chapter and the remainder of this thesis.

### 2.2.2 Acceleration and Length of Travel

Since the powderbed was chosen to be the moving item, it is necessary to provide enough travel that the acceleration of the powder can be kept low enough that the powder remains undisturbed. An experiment was performed to measure how high an acceleration a powderbed could withstand. The arrangement is illustrated in Figure 2.1. A 2 inch x 1/2 inch x 1/2 inch box filled with -170/+325 mesh spherical stainless steel powder (particle diameter ranging from 45 to 90 microns) was supported on the moving carriage of

M.I.T.'s production Three Dimensional Printing machine, the Alpha Machine. This powder is typical of the metal powders used in Three Dimensional Printing. A video camera was rigidly mounted at one end of the travel of the carriage, and focused on the surface of the powderbed. The surface of the powderbed was displayed on a television monitor in real time. A tiny piece of plastic that could be clearly distinguished from the

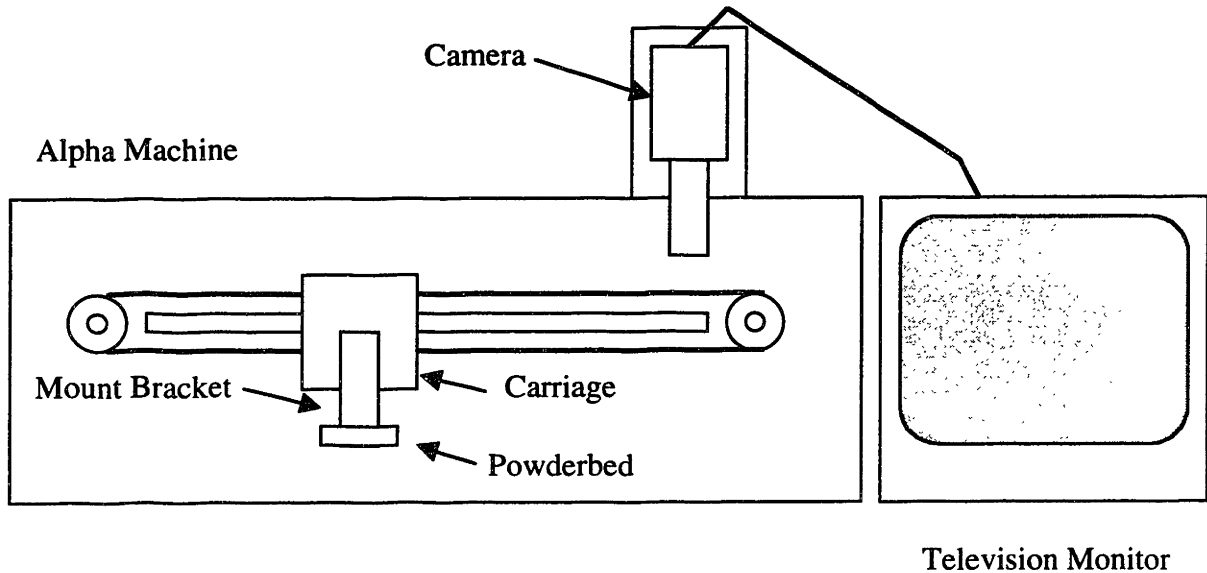


**Figure 2.3.** Experimental assembly for testing powderbed tolerance of acceleration.

powder particles was put in the powderbed. The location of this piece of plastic on the screen was marked and the position of the powderbed along the fast axis noted. The latter is reported to within 10 microns by the alpha machine. The resolution of the screen image was about 5 microns per pixel. The powderbed was then moved back and forth ten times over a 30-inch travel, with a set acceleration and deceleration. After the series of ten passes, the position of the piece of plastic on the screen relative to the position of the powderbed was noted. The acceleration and deceleration used were increased in steps, starting from  $3 \text{ m/s}^2$ , and the procedure repeated. It was found that at accelerations up to

5.2 m/s<sup>2</sup> the plastic marker did not move relative to the powderbed, while at 7.8 m/s<sup>2</sup> the powder was thrown from the powderbed during acceleration and deceleration.

Based on this result, it was decided to make 5 m/s<sup>2</sup> an upper design limit for the acceleration of the moving carriage of the droplet impact observation station. This resulted in the requirement that the length of travel be at least 85 centimeters, calculated as follows:

$$\begin{aligned}
 x &= x_{accel} + x_{const.spd.} + x_{decel} \\
 &= \left( \frac{v^2}{2a} \right) + 0.0508 \text{ m} + \left( \frac{v^2}{2a} \right) \\
 &= \left( \frac{\left( 2 \frac{m}{s} \right)^2}{2 \times 5 \frac{m}{s^2}} \right) + 0.0508 \text{ m} + \left( \frac{\left( 2 \frac{m}{s} \right)^2}{2 \times 5 \frac{m}{s^2}} \right) = 0.851 \text{ m}
 \end{aligned} \tag{2.2}$$

### 2.2.3 Velocity Fluctuation and Transverse Position Error

In addition to the requirements on speed and acceleration, velocity fluctuation and transverse position error should be kept below tolerable limits. Velocity fluctuation should be no greater than 0.01 meters per second. For a typical continuous-jet droplet time-of-flight of 3 milliseconds and a printhead speed of 2 meters per second, this level of velocity fluctuation results in a droplet placement error of 30 microns, calculated as follows:

$$\Delta x = \Delta v \times t = 0.01 \frac{m}{s} \times 0.003 \text{ s} = 30 \times 10^{-6} \text{ m} \tag{2.3}$$

Transverse position repeatability on consecutive passes should be ten microns or better, which is a requirement of the bearing system and the carriage.

## 2.3 PRINTING

The observation station must print, and must be adaptable to a variety of printing methods. The current printing varieties used in Three Dimensional Printing are continuous-jet printing, drop-on-demand printing, and jetting of liquid slurries.

### 2.3.1 Continuous-Jet Printing

In continuous-jet printing, illustrated in Figure 2.4, a jet of liquid is ejected from a nozzle. The jet quickly breaks up into a stream of droplets, and the frequency of this breakup can be controlled by exciting the liquid stream at the desired frequency, such as by using a piezoelectric element. A continuous-jet printhead is constructed such that droplet breakoff occurs between two electrodes, which cause the droplets to acquire electric charge as they break off. As the droplets fall, they pass between another pair of electrodes that deflect the droplets toward one or the other electrode, depending on the charge on the droplets. This deflection is used to either deflect the droplets into a catcher, which prevents them from hitting the powderbed, or to allow them to fall to the powderbed. In the latter case, the transverse position at which the droplet lands can be controlled by the charge voltage. This is referred to as *proportional deflection*.

In continuous-jet printing, the distance from the print nozzle exit to the powderbed is typically about one inch. Droplet frequencies range between 20 kHz and 150 kHz. Droplet diameters are typically in the range of 20 to 100 microns (about 90 microns with the printhead currently used on the Alpha 3DP™ machine), and print speeds are typically 1-2.5 meters per second. Droplet spacings vary from 20 to 60 microns.

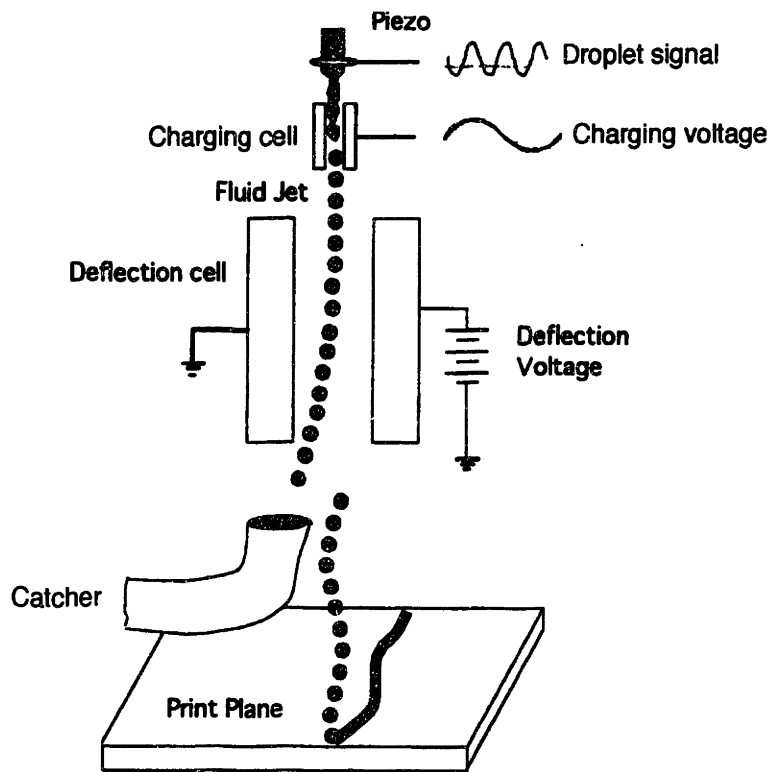


**Figure 2.4.** Continuous-jet printing. (Courtesy of Christopher Shutts).

Continuous-jet printing requires two separate electrical signals, one to excite droplet breakoff at the desired frequency and another to set the charging electrode voltage. The voltage between the deflection electrodes is held constant. It was decided to endow the droplet impact observation station with the capability to synchronize the charging signal with the droplet excitation signal. This is not a general practice in continuous-jet printing and the absence of such synchronization can lead to incorrectly charged droplets, which are then deflected incorrectly, and to charging voltages being “lost” in that they are not applied to any droplets.

Continuous-jet printheads require that the fluid to be printed be externally supplied. Also, the unprinted fluid, either caught by the catcher or allowed to fall when the powderbed is not beneath the printhead, must be taken care of.

A final consideration for accommodating continuous-jet printing is that provision must be made to mount the printhead.

### **2.3.2 Drop-On-Demand Printing**

In drop-on-demand printing an electrical pulse is used to excite the ejection of a single droplet from a printhead. A drop is only printed when needed, so unlike continuous-jet printing, there is no need to catch unprinted drops. The distance from printhead to powderbed in drop-on-demand printing is much smaller than in continuous-jet printing, typically a millimeter or less. These two factors – the lack of a need to catch droplets and the short distance from printhead to powderbed – result in charging and deflection not being implemented in drop-on-demand printing. Drop-on-demand droplet frequencies range from 10 Hz to several kHz. The distance from the printhead to the powderbed ranges from a few tenths of a millimeter to several millimeters. Droplets have a diameter in the same range as continuous-jet droplets.

Drop-on-demand printing requires only a single electrical signal, the droplet excitation pulse train. A means of mounting the printhead must be supplied. Drop-on-demand printheads typically incorporate their own liquid reservoir, so an external fluid supply system is not required.

### **2.3.3 Slurry Printing**

The ceramic powders used in the three dimensional printing of ceramic parts are often too fine to be spread as dry powder, the means by which coarser powders are deposited. One means of depositing such ceramic powder is to print it as a liquid slurry in a continuous jet. Such printing does not involve charging and deflection, and droplet breakoff does not occur. Printing is done at speeds ranging from a meter per second to over 2 meters per second.

Slurry printing does not require any electrical signals. It requires provision for mounting the printhead, and a fluid supply. It also requires a provision to catch the printed slurry when the powderbed is not underneath the printhead, since this stream runs continuously throughout the deposition of a layer.

### **2.3.4 Geometry of Printed Features**

To study powderbed interaction over the broad range of real printing conditions, it is necessary to observe droplets that are part of a line being printed, with and without lines printed next to the current line, and with and without layers printed underneath the current layer. Therefore it is necessary to accommodate the three-dimensional building of parts of several layers depth, of several lines width and of appreciable length. It was specified that the impact observation station be able to print lines 1 inch long, 1/2 inch wide and four layers deep.

In addition to the requirements on part size, the machine should accommodate the variety of patterns that are used and anticipated in Three Dimensional Printing. These include proportionally-deflected patterns and repeat-path printing with registration of

droplets between passes, such as when droplets are printed sixty microns apart in a first pass, and then in a second pass droplets are printed midway between the droplets that were printed in the first pass. Registration of droplets between passes in such repeat-path printing should be within ten microns. Droplet spacing in general should be variable from 10 microns to 500 microns.

### **2.3.5 Accommodation of Printing Requirements**

Mechanical accommodation of the different printheads and printing methods to be used with the observation station consists of providing:

- a generic mount to which various printheads can be attached;
- space and mounting holes for a fluid supply for cases in which one is needed;
- the capability to run a fluid umbilical line to a moving printhead;
- a catch tray directly beneath the printhead location and beneath the travel of the powderbed.

Electrically, drop excitation and charging voltage signals must be supplied, and these must be synchronized with each other and with strobing and picture-taking signals. This can be achieved using a commercially-available computer-plug-in multifunction signal generation card. The electronic scheme will be discussed in more detail in chapters seven through nine.

## **2.4 CONCLUSION**

In summary, the capabilities required of the droplet impact observation station can be broken into the three areas of imaging, motion and printing. In imaging, the biggest



requirement is flexibility, since the imaging to be done with the station is to a large extent unknown. The station is designed to perform strobe-illuminated single-image-per-pass imaging of droplet impacts, and to be extendable to other imaging tasks with the addition of some hardware. The imaging capabilities desired require synchronized and repeatable printing, strobing and frame-grabbing. The motion capability required is automatic controlled linear motion motion between the powderbed and the printhead at speeds of up to 2 meters per second. Since it is the powderbed that moves in the machine's primary mode of operation, the permissible acceleration is limited. Specifically, it was determined that an upper design limit on the acceleration is  $5 \text{ m/s}^2$ , resulting in a minimum travel distance of 85 centimeters. Velocity fluctuation should be no more than 0.01 m/s, and transverse error from pass to pass should be no more than 10 microns. In the area of printing, the machine must electrically and mechanically accommodate continuous-jet printing with charging and deflection, drop-on-demand printing and slurry printing. It must allow three-dimensional printing of parts up to 1-inch long, 1/2-inch wide and 4 layers deep, and must accommodate repeat path printing and proportional deflection. The desired capabilities and resulting requirements and design decisions are summarized in Table 2.2. Italicized features require equipment not currently possessed to be possible with the impact observation station.

Area	Desired Capability	Resulting requirements and decisions
Imaging	1. Flexibility	Space and support for mounting a camera over a 90-degree range of viewing angles; Space and holes for mounting new attachments; Flexible and powerful PC-based multifunction electronic signal card.
	2. Single image per pass imaging	CCD video camera with computer-based frame-grabber; Synchronization of printing and strobing signals via a multifunction signal card; Sub-2-microsecond strobe flash with less than 2 microseconds of jitter; Adjustable electronic strobe flash delay.
	3. <i>Multiple image per pass imaging</i>	High-speed video camera; High-speed frame grabber; Moving powderbed.
	4. Observing powderbeds for long times	Convertibility to operation with stationary powderbed and moving printhead.
Controlled Motion	Up to 2 meters per second Without disturbing the powderbed, with velocity fluctuations less than 0.01 m/s and transverse repeatability no worse than 10 microns.	D.C. servo-motor powered belt drive; Closed loop motion control via encoder feedback to a P.C.-based motion controller; Length of travel $\geq 85$ cm.

Printing	1. Continuous-jet printing, with proportional deflection	Space and support and holes for mounting printhead and fluid supply; Capability to run fluid supply to a moving printhead; P.C.-based multifunction signal card;
	2. Drop-on-demand printing	Same as 1.
	3. Slurry printing	Same as 1.
	4. 1 inch x 1/2 inch x 4 layer parts	Powderbed dimensions greater than this; Repeatability of printing signals from pass to pass to ensure registration of drops; Transverse motion; Capability to spread several layers;
	5. Repeat-path printing with variable drop spacing	Repeatability of printing signals from pass to pass; Flexible control of drop-generating signal;

**Table 2.2.** Summary of functional requirements and design decisions.

### **3.0 LINEAR BEARINGS**

In order to move the carriage back and forth along its trajectory some sort of linear bearing system is required. Such a system must provide linear motion at the speeds required, with a straightness over the middle four inches of travel of 10 microns, and a repeatability of transverse location of 10 microns over the same section of travel. The vertical repeatability over the middle section should also be within 10 microns, and the motion must be vibration-free. The bearing system must have a life of at least three years in an environment contaminated with abrasive powders.

#### **3.1 BEARING TYPE**

There were three practical alternative bearing types for the present application, namely rolling element bearings, sliding bushings and air bearings. Rolling element bearings are prone to vibration, and the rolling elements would be subject to rapid wear by the abrasive powders being observed with the machine. These considerations eliminated rolling element bearings as a viable option. Sliding bushings are less prone to vibration, and some are available which avoid the deleterious effects of abrasive particles via the capability to embed a significant amount of such particulate matter in the sliding surface. However, no such bushings were found which were rated to perform as needed at the speeds desired. This left air bearings as the only remaining choice. Air bearings are generally used in Three Dimensional Printing machines, so the performance of one variety of them is known and satisfactory. Their principal disadvantage is cost.

### 3.2 AIR BEARING SELECTION

Air bearings are generally constructed such that air is supplied to the moving bearings, which run along some sort of solid rail. This has the disadvantage of requiring an air supply umbilical connected to the moving carriage, which can affect the behavior of the carriage in ways that are not easy to analyze. Therefore a preliminary investigation was made of the possibility of constructing an air bearing system in-house, in which the air is supplied to the rail rather than to the moving bearing. When it became apparent that realizing a functional system of this sort would take more time than was available, if it was at all possible, the effort was abandoned in favor of selection of a commercially available system. Several alternatives were considered, and these are summarized in the following subsections.

#### 3.2.1 Dover Box Slide

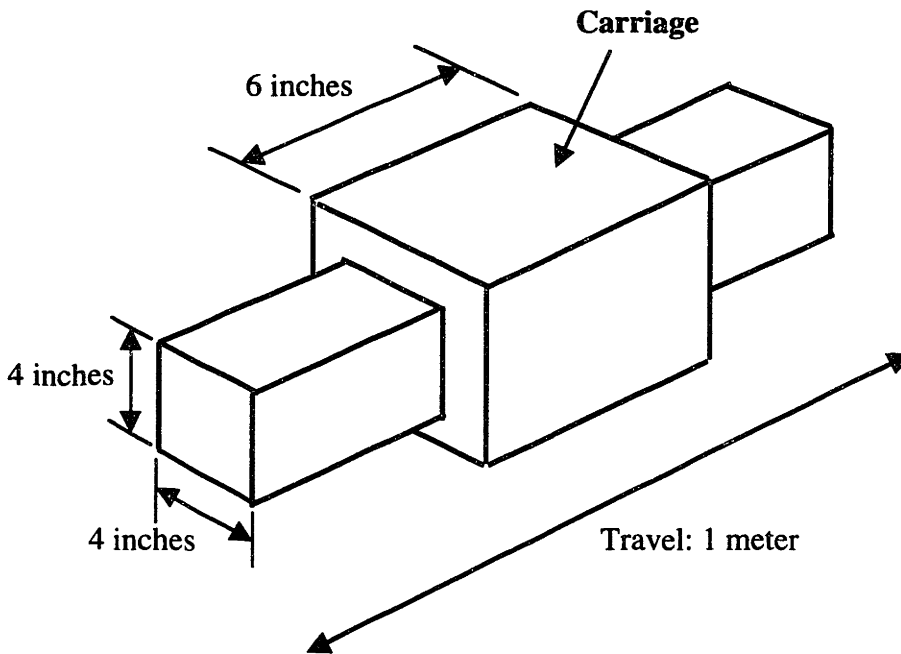


**Figure 3.1.** Sketch of Dover air bearing slide.

Dover Instrument Corporation has been the supplier of air bearing slides for three dimensional printing machines previously built at M.I.T. A quotation was obtained from Dover for a slide with one meter of travel that consisted of a six-inch-long sliding box that fit around a four-inch-square bar, sketched in Figure 3.1. The quoted price was \$9000.00.

### **3.2.2 New Way Box Slide**

A quotation for an air slide similar to that quoted by Dover was obtained from New Way Machine Components Incorporated. The dimensions of the sliding box considered were 5.25 inches (width) by 5.375 inches (height) by 4 inches (length). The dimensions of the hard-anodized aluminum rail were 50 inches (length) by 4 inches (height) by 4 inches (width). The quoted price was \$4000.00.

### **3.2.3. Space Electronics Cylindrical Sleeves**

An alternative to a box that fits around a square rail is a set of three cylindrical sleeves that run on two parallel rails (two on one rail and one on the other, providing a kinematic mount). Due to the length of travel required, the rails have to be continuously-supported to avoid excess vertical deflection, given the diameters of sleeves and rails that are commercially available. Continuously-supported rails require a gap in the air bearing sleeves to accommodate the rail support, as shown in Figure 3.2.

A quotation for a set of 4 cylindrical air bearings was obtained from Space Electronics Incorporated. A diagram such a bearing is presented as Figure 3.3. The quoted price was \$9,948 for a set of four sleeves. The shafts would have to be obtained

separately from a supplier such as Thomson Industries Incorporated, and would cost around \$400 for a pair.

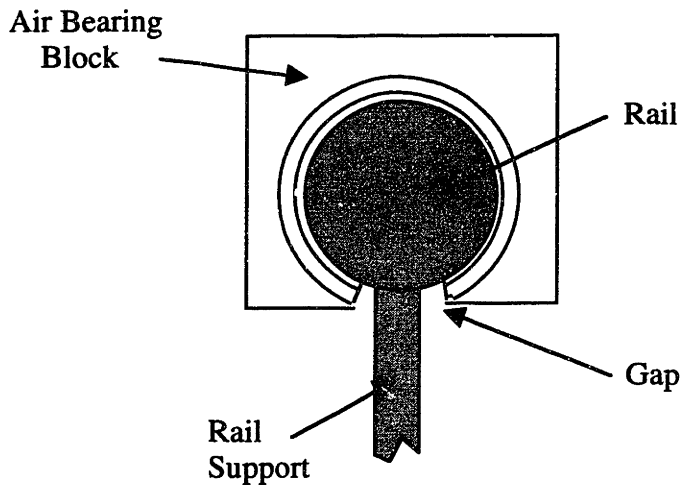


**Figure 3.2.** Continuously-supported round shafts require a gap in the bearing.

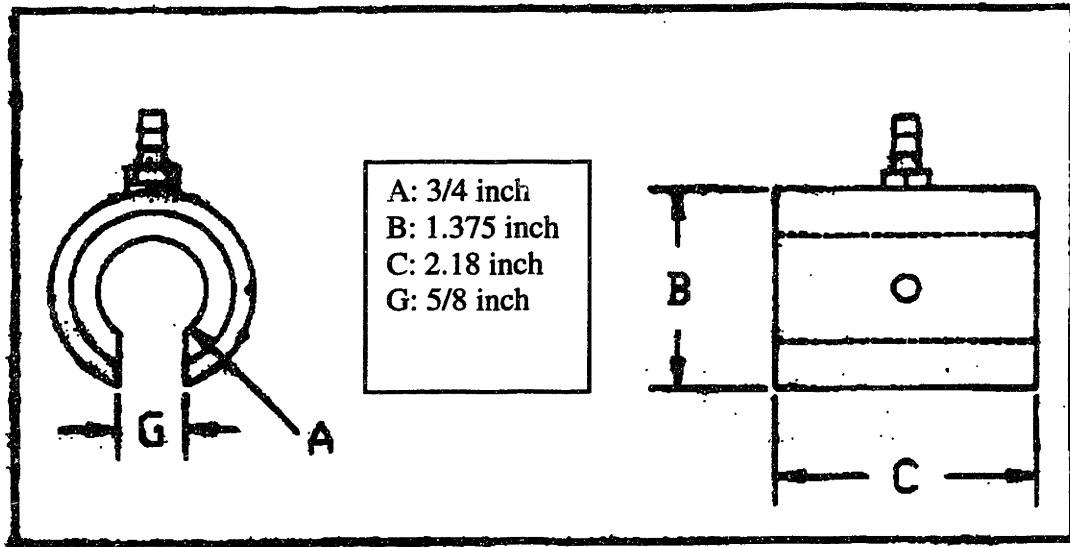


**Figure 3.3** Space Electronics cylindrical sleeve air bearing with gap.

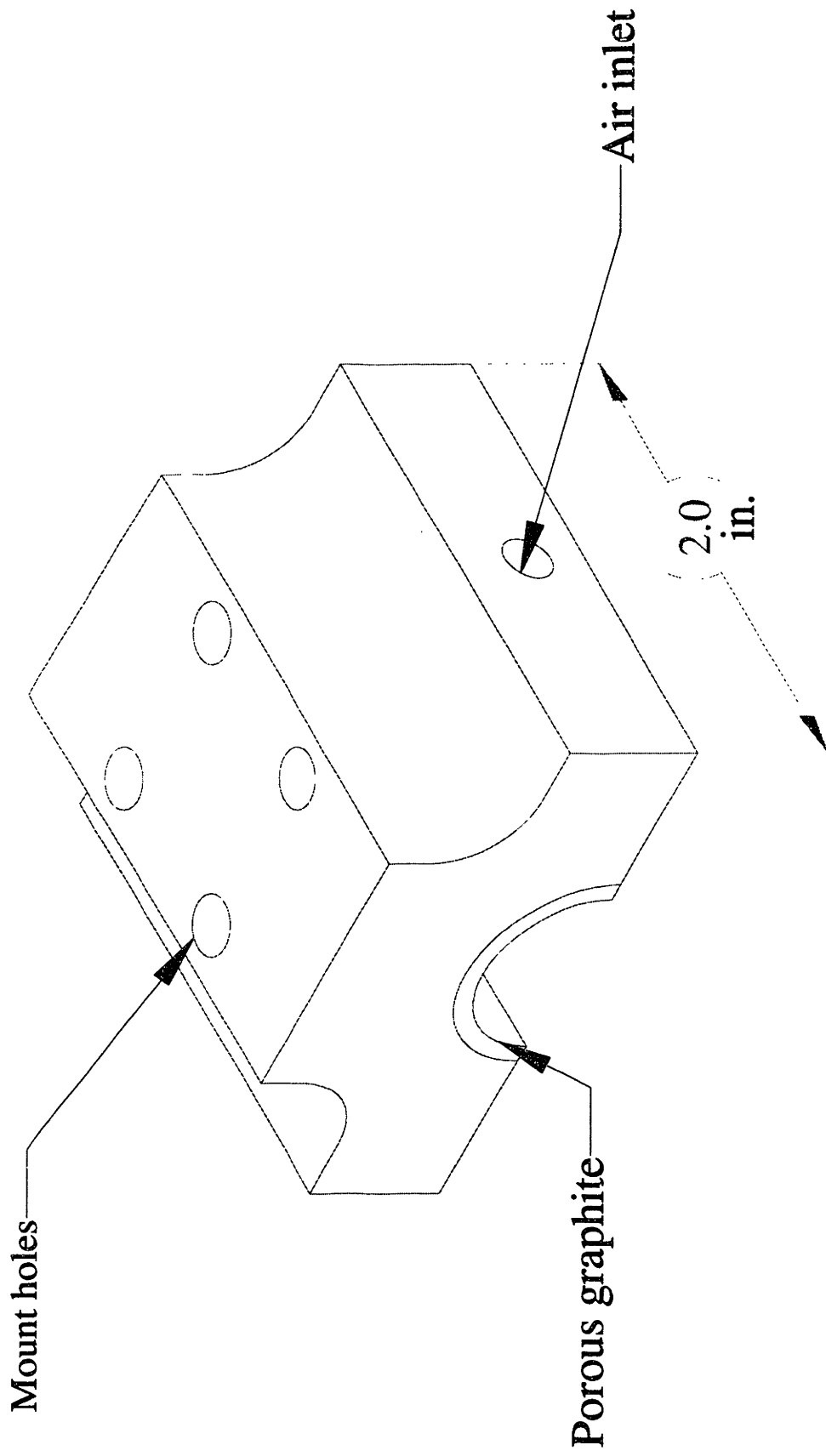


Figure 3.4. New Way porous graphite air bearing



### **3.2.4 New Way Half-Round Porous Graphite Bearings**

New Way Machine Components Incorporated also manufactures partial cylinder air bearings. These are half-cylinder bearings which have a porous graphite surface through which air is supplied to the air layer between the bearing and the rail. A picture of one is shown in Figure 3.4. The quoted price for the bearings was \$359 each. As with the Space Electronics bearings, the shafts would have to be obtained from a supplier such as Thomson Industries Incorporated. The quoted price for a pair of 55-inch stainless steel rails of the necessary tolerance was \$1,452.

### **3.3 CONCLUSION**

From among the options identified, a set of three New Way porous graphite bearings were selected, due to the cost advantage over the alternatives, the mass advantage over a box-slide and the desire to explore alternatives to the Dover air slide system generally used on 3DP™ machines. Experience with the bearings has since shown their performance to be inferior to that of a Dover box slide. The bearings are very sensitive to side loads, and it has proven difficult to operate the machine without rubbing any of the bearings against a rail.

## **4.0 MOVING CARRIAGE**

The function of the carriage is to transport the powderbed and the readhead for the linear encoder. There are several parts of the carriage: the air bearings on which it sits, couplings by which the rest of the carriage is mounted on the air bearings, a carriage plate that provides the primary structural connection, a micropositioning stage on which to mount a powderbed, a connection for a drive cable, and an electrical umbilical. The layout of the carriage is shown in Figure 4.1. Machine drawings for the machined parts of the carriage are included in Appendix A.

### **4.1. POWDERBED**

In order to allow for printing of several lines side by side, a means of moving the powderbed transverse to the direction of travel must be provided. Therefore the powderbed is mounted on a micropositioning stage as shown in Figure 4.1. The stage used provides a travel of 1/2 inch. The powderbed is mounted overhanging one of the rails. This simplifies arrangements for catching jetted liquid when the powderbed is not underneath the printhead.

### **4.2 ENCODER READHEAD**

The linear encoder is mounted along the carriage's path of travel, on the opposite side from where printing takes place. A readhead for the encoder must thus be mounted on this side of the carriage. The readhead is mounted via a two-piece bracket that allows adjustment of its orientation relative to the carriage and the encoder scale.

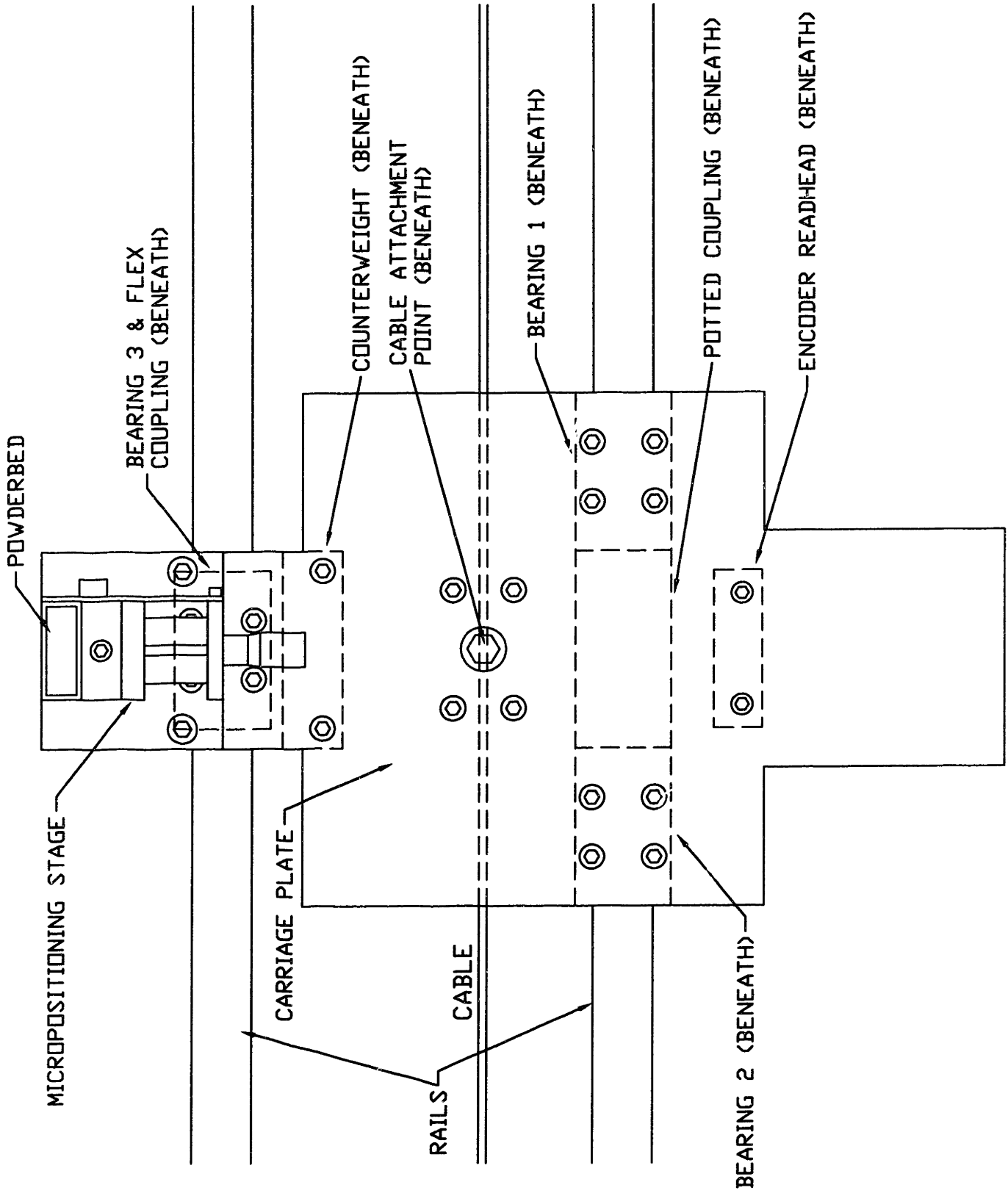


Figure 4.1. Carriage Layout.

### **4.3 BEARING COUPLINGS**

The air bearings must be coupled to the carriage in such a way as to prevent any of them from rubbing against a rail during carriage traverse, while at the same time maintaining the maximum possible stiffness of the couplings. Rubbing must be avoided because it may damage the bearings and may cause vibrations that disturb the powder or cause errors in drop placement. Stiffness is important in order to maximize the robustness of the carriage and because compliance in the couplings may itself lead to vibrations.

Because the manufacturing tolerance of the rails allows for variation in their straightness of a magnitude larger than can be accommodated by the 20-micron bearing air gap, it is necessary to allow some transverse relative motion between bearings riding on different rails. This was done by mounting the single bearing riding on the print-side rail via a flexible coupling. The pair of bearings riding on the encoder-side rail were potted in place using epoxy. The following subsections present the details of the coupling system design.

#### **4.3.1 Deflections to be Accommodated**

The bearing coupling system must accommodate certain motions of the bearings relative to one another. Figure 4.2 labels the linear motions and rotations of a bearing relative to the other bearings that can occur. Motion **a** is unnecessary and undesired, and should be limited as much as possible. Motion **b** is necessary for bearing 3 relative to bearings 1 and 2 in order to accommodate rail straightness error. The quoted rail straightness tolerance is 0.002 inches over the entire length of a rail. This implies a worst-case rail separation variation of 0.004 inches, which is the magnitude of deflection **b** of

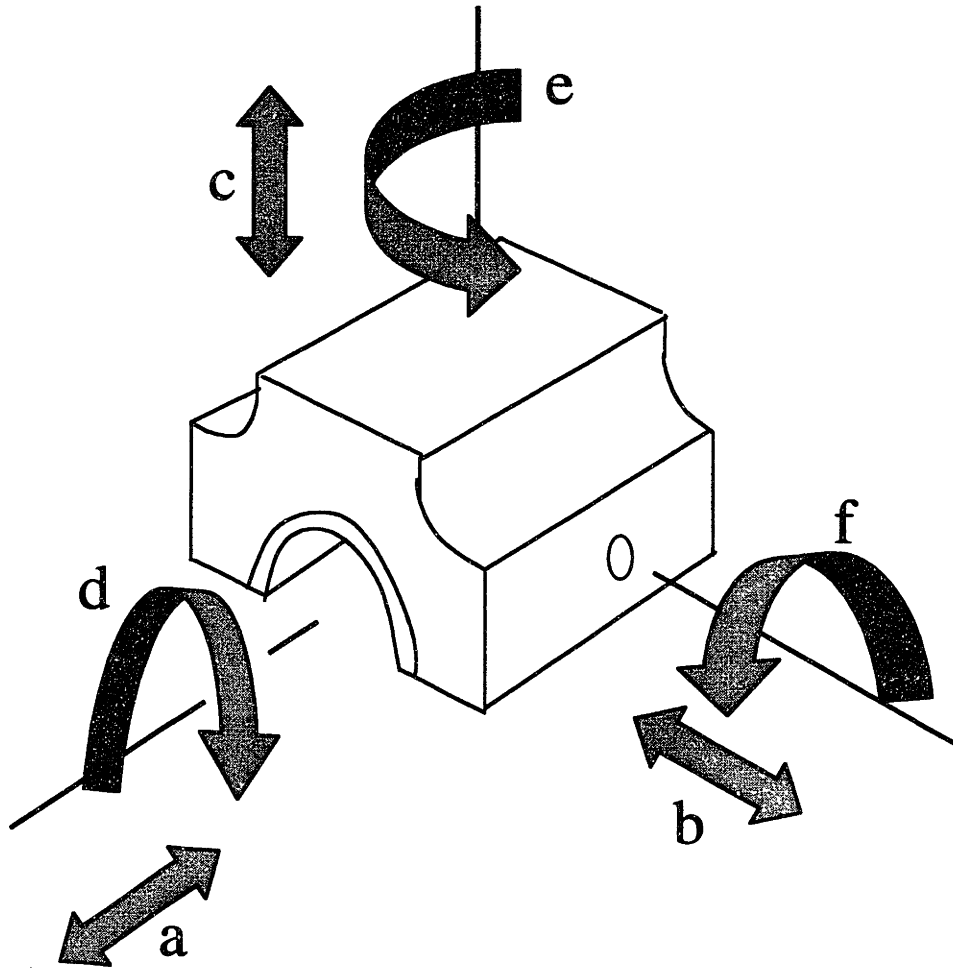


**Figure 4.2.** Bearing motions

bearing 3 relative to bearings 1 and 2 that should be accommodated. Motion **c** is not necessary and should be limited as much as possible. A certain degree of rotation **d** of bearing 3 relative to bearings 1 and 2 must be accommodated. This rotation accommodates parallelism mismatch between the carriage plate surface (over the region in which it is attached to the coupling) and the top surface of the air bearing block. Such mismatch has several sources: parallelism mismatch between the graphite bearing surface and the bearing block top surface, bearing block height differences and rail height

mismatch of less than 0.0005 inch<sup>\*</sup>, and flatness error of the carriage plate. It is difficult to firmly specify the amount of rotation **d** required. An approximate estimate of the maximum possible value is 0.004 radians, corresponding to 0.004 inch over the 1-inch width of the bearing block top surface, which is the dimension over which the flexible coupling is fixed flush to both the air bearing and the carriage plate. Rotation **e** is necessary for bearing 3 in order to accommodate rail straightness errors. The amount of rotation necessary in the worst case can be determined by adding the maximum angular deflection that can occur over the 6.5-inch carriage length on the encoder-side rail to the maximum angular deflection that could occur over the 2-inch bearing length on the printhead-side rail. In each case, the maximum rail straightness error is 0.001 inch, so the total rotational deflection is

$$\theta = \frac{0.001 \text{ inch}}{6.5 \text{ inches}} + \frac{0.001 \text{ inch}}{2.0 \text{ inches}} = 6.5 \times 10^{-4} \text{ rad} \quad (4.1)$$

Rotation **f** accommodates variations in rail height and plate flatness that occur over the 2-inch length of a bearing. In the case of the single bearing on the printhead-side rail, the effect of bearing block height variation beyond that which can be accommodated by shimming must also be included<sup>\*\*</sup>. A rough estimate of the amount of motion to be accommodated is 0.001 inch over the 2-inch length of a bearing block, or  $5 \times 10^{-4}$  radians. Table 4.1 summarizes the deflection requirements for the coupling system.

---

<sup>\*</sup> Larger magnitudes can be eliminated by shimming.

<sup>\*\*</sup> The pair of bearings on the encoder side rail are potted in place. The design of the potted coupling eliminates the effect of bearing block height variation. See subsection 4.3.4.

Motion	Requirement
a	As small as possible
b	0.004 inch
c	As small as possible
d	0.004 radians
e	$6.5 \times 10^{-4}$ radians
f	$5 \times 10^{-4}$ radians

**Table 4.1.** Motion requirements of bearing 3 relative to bearings 1 and 2.

#### 4.3.2 Maximum Bearing Loads

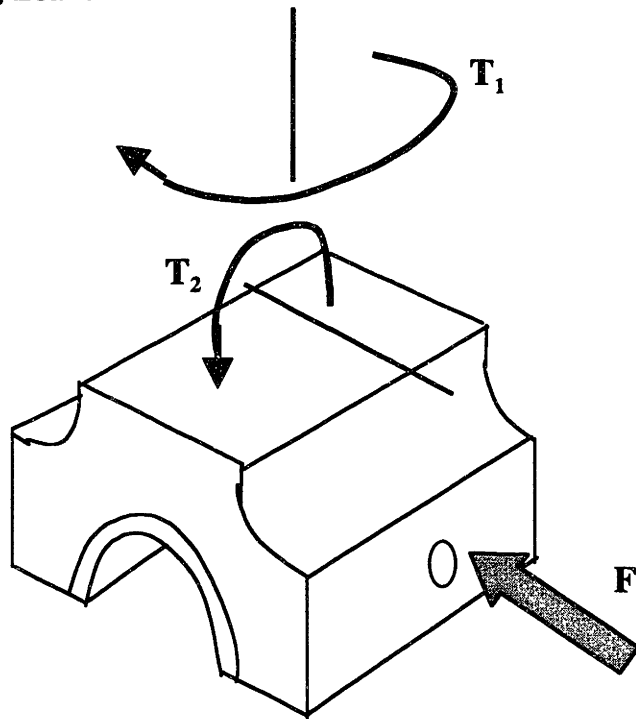


**Figure 4.3.** Maximum bearing torques and forces to be measured.

Together with measurements of the loads and torques that a bearing can be subjected to without grounding, the maximum deflections discussed in the previous section determine the required coupling stiffness. An experiment was performed to measure the magnitudes of the torques and force illustrated in Figure 4.3 that cause contact of the bearing surface with the rail. The experimental arrangement is illustrated in Figures 4.4, 4.5 and 4.6 and

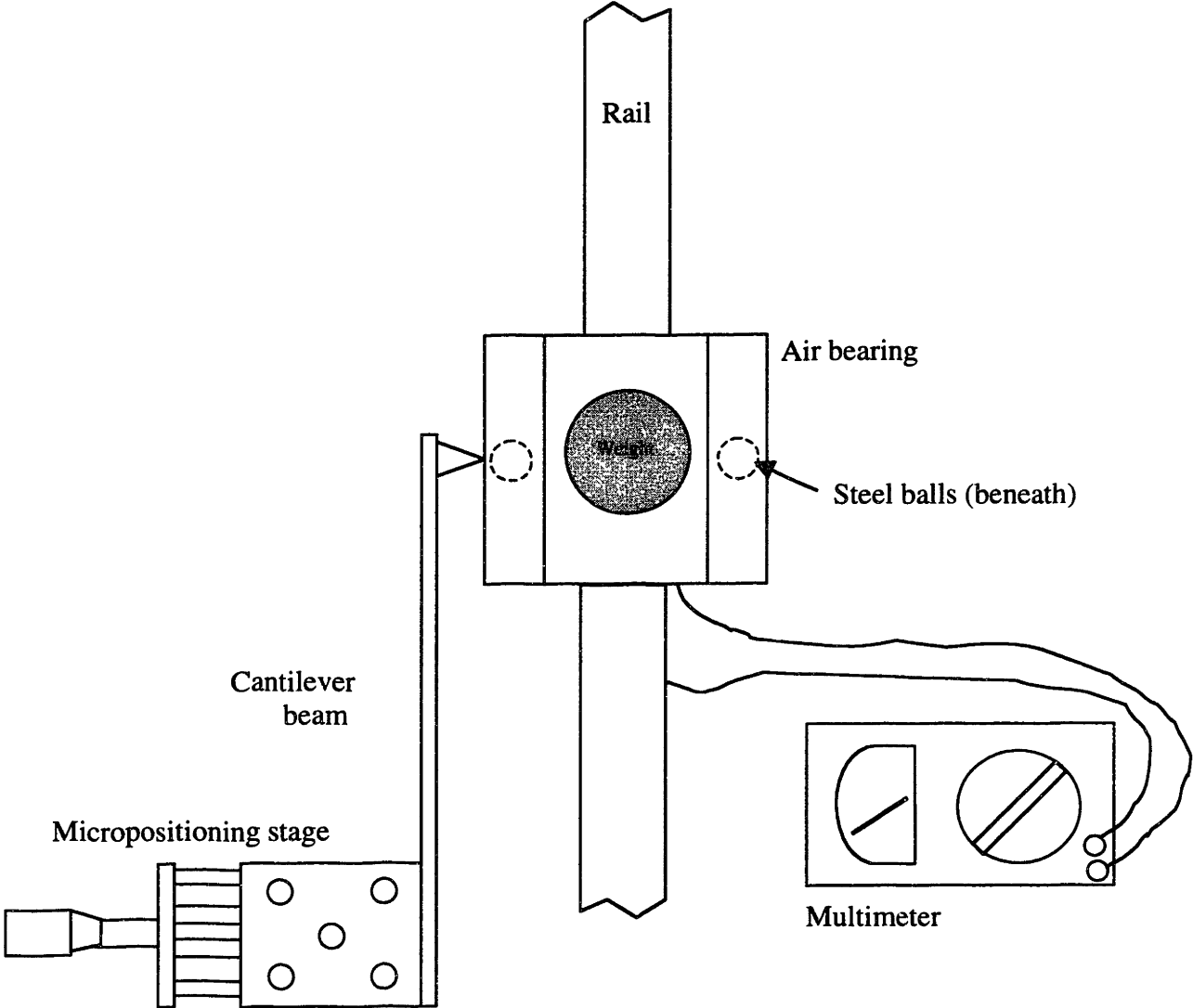


**Figure 4.4.** Experimental arrangement for measuring force  $F$  at bearing contact.



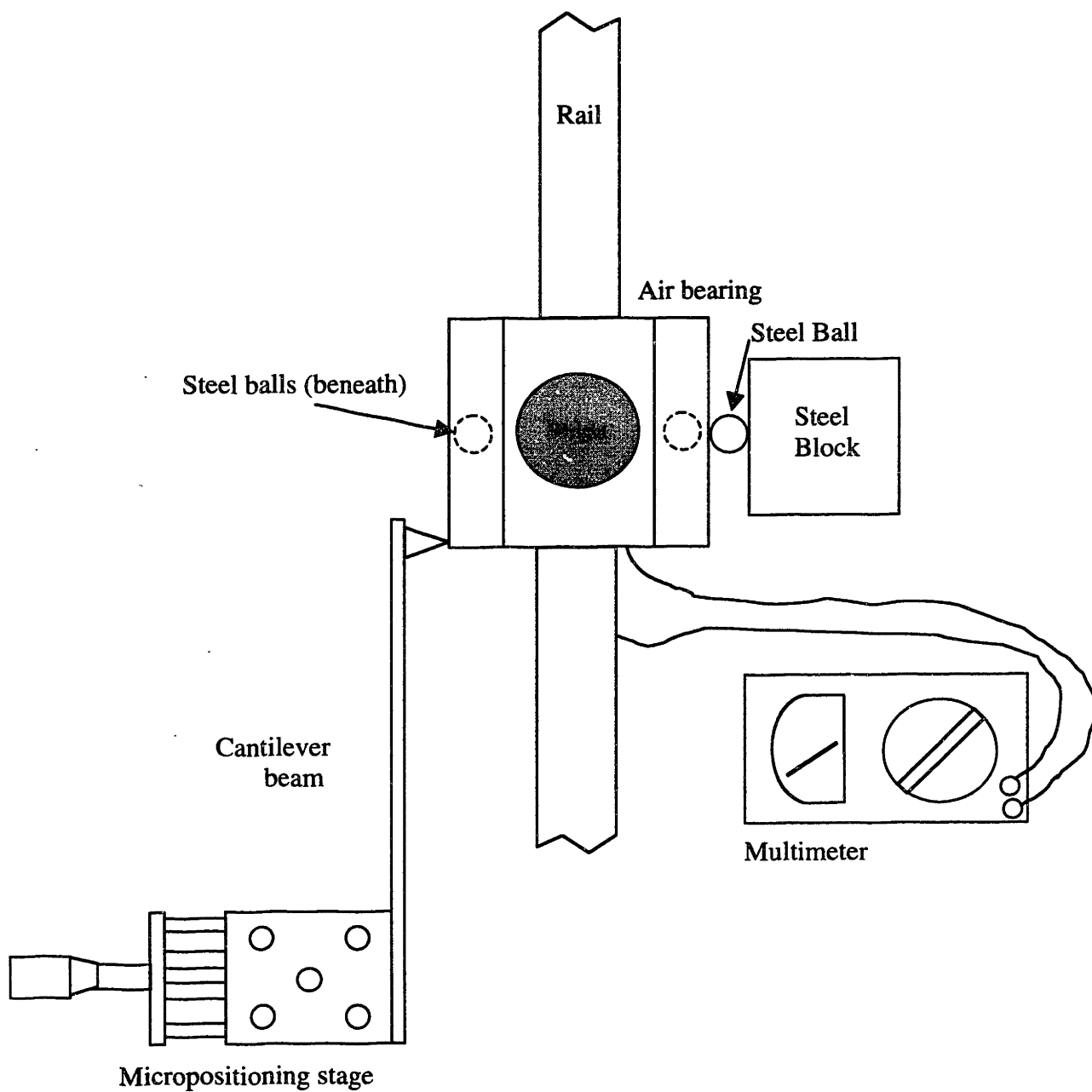


**Figure 4.5.** Experimental arrangement for measuring torque  $T_1$ .

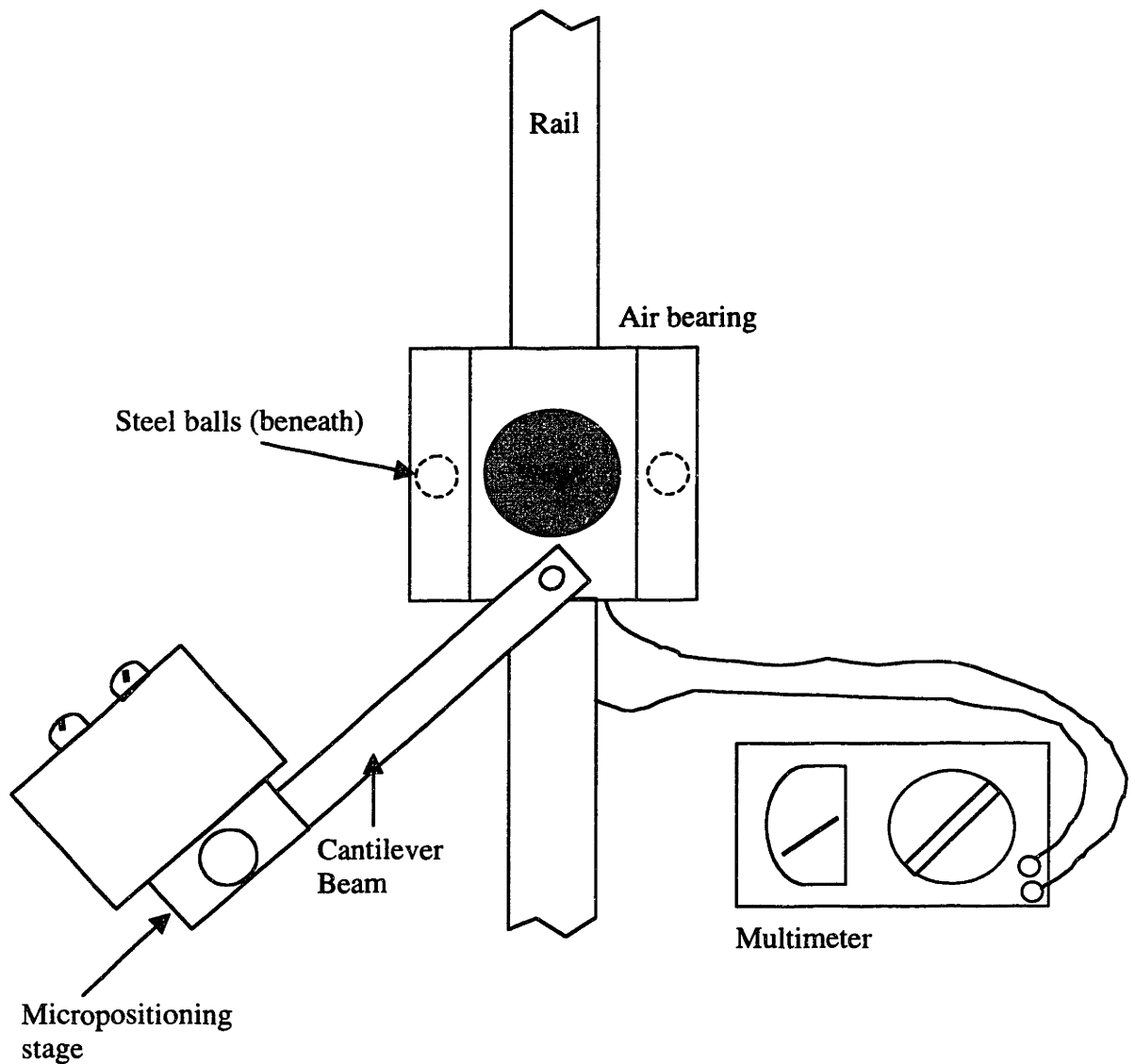


**Figure 4.6.** Experimental arrangement for measuring torque  $T_2$ .

described as follows.

Figure 4.4 shows the arrangement used to measure the side force  $F$  that can be borne by a bearing. A bearing was placed on a rail, and to prevent it from rolling off the rail, was supported on either side by a steel ball that made contact with the bearing at the bearing centerline. A mass of approximately 1.2-kilograms was placed on top of the

bearing, centered, to load the bearing. A cantilever beam attached to an anchored micro-positioning stage was used to apply a load to the center of one side of the bearing block. The deflection of the beam as determined by the micro-positioning stage was used to determine the load, the stiffness of the beam having been experimentally confirmed. The presence or absence of contact between the bearing surface and the rail was monitored by measuring the resistance between the graphite surface of the bearing and the stainless steel rail using a digital multimeter. Contact was observed at a load of approximately **0.12 lbs.**

Figure 4.5 shows the variation of the arrangement used to measure torque  $T_1$  that can be borne by a bearing. The two differences between this arrangement and the one used to measure side force are that:

- an additional steel ball backed by a steel block was placed against the center of one side of the bearing in order to prevent sideways linear deflection of the entire bearing;
- the cantilever beam load was applied not at the center of the bearing, but at one end of the bearing, an inch away from the center.

The torque at contact was measured to be **0.042lb-in.**

Figure 4.6 shows how torque  $T_2$  at contact was measured. In this case, the cantilever beam load was applied on the top of the bearing, at one end, an inch away from the center. The torque at contact was measured to be **0.80 lb-in.**

The contact torques and forces were measured at a supply air pressure of 80 psi.

### 4.3.3 Flexible Coupling Design

As mentioned earlier, the chosen means of coupling the bearings to the carriage was to pot the two encoder-side bearings in place and attach the printhead-side bearing using a flexible coupling. The loads and deflections determined as described in the previous two subsections determine the design stiffnesses of the flexible coupling. This coupling is designed as a small plate, approximated as a short cantilever beam. A picture of the coupling, with deflections and dimensions labeled, is shown in Figure 4.7.

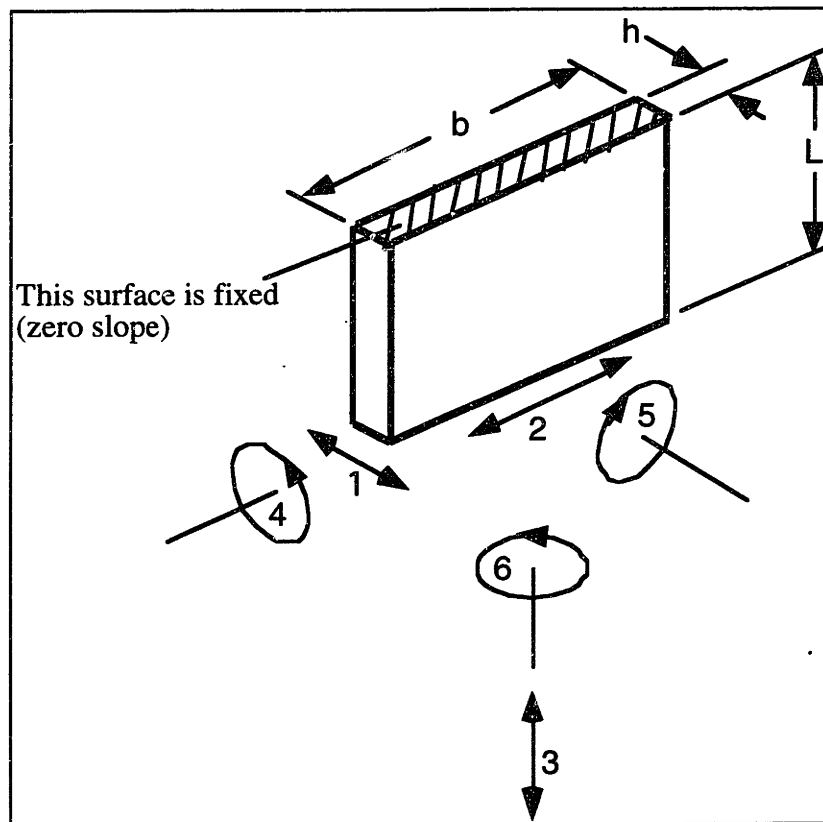


Figure 4.7. Flexible coupling stiffness and dimension labels .

The design stiffnesses are calculated from the loads and deflections discussed in subsections 4.3.1 and 4.3.2 and are summarized in Table 4.2.

Stiffness	Design Goal	Implication
S1	<30 lb/in	Minimize
S2	Large enough	Maximize
S3	Large enough	Maximize
S4	<18 lb-in/rad	Minimize
S5	1280 lb-in/rad < S5 < 1600 lb-in/rad*	Keep within range
S6	<65 lb-in/rad	Minimize

**Table 4.2.** Design goals for flexible coupling stiffnesses.

The material used for the coupling was Ultem 1000™, an engineering plastic the relevant properties of which are shown in Table 4.3.

---

\* The design parameters of a torque of 0.8 lb-in and a deflection of  $5 \times 10^{-4}$  radians result in a requirement that S5 be less than 1600 lb-in/rad. However, it is desired that S5 not be too low, so as to limit motion a of

Material Property	Value
Elastic Modulus (E)	480,000 psi
Shear Modulus (G)	<p>≈ 190,000 psi  calculated from the elastic modulus as follows, given that the material is isotropic:</p> $G = \frac{E}{2(1 + \nu)}$ <p>where <math>\nu</math> is Poisson's ratio and is generally between 0.25 and 0.4. A value of 0.25 is used, the worst-case value within this range.</p>
Yield Strength	22,000 psi

**Table 4.3.** Material properties of Ultem 1000.

The Microsoft® Excel™ spreadsheet software from Microsoft Corporation includes an optimization routine named *Solver*. Solver optimizes a user-defined objective function of values from a spreadsheet subject to user-defined constraints. Solver was used to optimize the dimensions of a model flexible coupling. The flexible coupling was modeled as a cantilever beam with the top end fixed and the bottom end free. Calculations of stiffnesses **S1** and **S2** were also done for the case where the bottom end is forced to maintain zero slope. The stiffnesses were calculated as summarized in Table 4.4.

---

the bearing. The value of 1280 lb/in was selected based on the experience with various couplings described in the final paragraph of this subsection.

Stiffness	Formula
$S1_{\text{free}}$	$\frac{3E}{L^3} \left( \frac{bh^3}{12} \right)$
$S1_{\text{zero slope}}$	$\frac{12E}{L^3} \left( \frac{bh^3}{12} \right)$
$S2_{\text{free}}$	$\frac{3E}{L^3} \left( \frac{hb^3}{12} \right)$
$S2_{\text{zero slope}}$	$\frac{12E}{L^3} \left( \frac{hb^3}{12} \right)$
$S3$	$\frac{E}{L}(bh)$
$S4$	$\frac{E}{L} \left( \frac{bh^3}{12} \right)$
$S5$	$\frac{E}{L} \left( \frac{hb^3}{12} \right)$
$S6$	$\frac{G}{L}K$ , where $K = \frac{bh^3}{16} \left[ \frac{16}{3} - 3.36 \frac{h}{b} \left( 1 - \frac{h^4}{12b^4} \right) \right]$ (Roark, 348)

**Table 4.4.** Stiffness formulae

The approach taken for the optimization was to minimize the stiffnesses **S1**, **S4** and **S6** subject to the constraints on **h**, **L** and **S5** listed in Table 4.4.

Constraint	Reason
<b>L</b> = 0.600 in.	Appropriate value given space available, and desire to have thick coupling webs.
<b>h</b> 0.050 in	To make the coupling machinable without great difficulty
1600 lb/in <b>S5</b> 1280 lb/in	The design parameters of a torque of 0.8 lb-in and a deflection of $5 \times 10^{-4}$ radians result in a requirement that <b>S5</b> be less than 1600 lb-in/rad. However, it is desired that <b>S5</b> not be too low, so as to limit motion <b>a</b> of the bearing. The value of 1280 lb/in was selected based on the experience with various couplings described in the final paragraph of this subsection.

**Table 4.5.** Constraints used in Solver optimization.

To simultaneously minimize the values of each of the three stiffnesses, the following objective function was minimized subject to the above-noted constraints:

$$\text{Objective Function} = S1^2 + S4^2 + S6^2 \quad (4.2)$$

Table 4.6 presents the results of the Solver solution and re-lists the design goals of Table 4.2 for comparison.



Parameter	Value	Units	Design Goal
b	0.727	inches	
h	0.050	inches	
L	0.600	inches	
S1 <sub>free</sub>	50.5	lbs/inch	<30
S1 <sub>zero slope</sub>	202	lbs/inch	
S2 <sub>free</sub>	10700	lbs/inch	Large enough
S2 <sub>zero slope</sub>	42800	lbs/inch	
S3	29100	lbs/inch	Large enough
S4	6.06	lb-in/rad	<18
S5	1280	lb-in/rad	1280<S5<1600
S6	9.06	lb-in/rad	<65
Buckling Load	24.9	lbs	

**Table 4.6.** Solver™ results.

The parameters **b**, **h**, and **L** are the values of the dimensions returned by the Solver optimization. **L** was specified as a constraint, while the values of **b** and **h** are the ones that minimize the objective function subject to the constraints used. It is noted that the value returned for **h** is the minimum allowed by the constraint, and that if this constraint were relaxed a lower value would result. **S1-S6** are the stiffnesses previously presented in Figure 4.7, Table 4.2 and Table 4.5. The goal was to find a set of stiffnesses that met the

requirements listed in the last column of Table 4.6. It is seen that the design goals for stiffnesses **S4**, **S5** and **S6** are met by the model, while the stiffness returned for **S1** is 1.7 times as large as the design maximum. The Euler buckling load of the recommended dimensions was also checked, and found to be 25 lbs, indicating sufficient resistance to buckling, even though the coupling is not strictly a slender beam. It is recognized that the model used is somewhat rough, as the length of the coupling  $L$  is of the same order of magnitude as the width. A more accurate model would make corrections for this (e.g. see Roark). The purpose of the model was not to provide strictly accurate results, but to provide a starting point for the coupling design, to be modified if necessary after trial operation of the machine with the coupling.

The implementation of a flexible coupling on the single bearing side and a potted coupling on the other was preceded by several other coupling system design attempts. Rigid bolting of the two encoder-side bearings combined with a single print-side flexible coupling failed. It was found that rigid bolting of the encoder-side bearings forced them to lie non-parallel to one another (and therefore to the rail surface), and caused the carriage to bind on the rails. A system combining flexible couplings on both sides, allowing rotation of the encoder-side bearings was found to allow too much flexibility. Finally, the approach of potting the encoder side bearings in place while attaching the printside bearing via a flexible coupling was pursued. In the course of this testing of various systems, several different flexible coupling dimensions were experimented with. Combining this experience with the Solver optimization of the beam model of the coupling, the following coupling dimensions were chosen:

$$\begin{aligned}
 b &= 0.700 \text{ inch} \\
 h &= 0.050 \text{ inch} \\
 L &= 0.600 \text{ inch}
 \end{aligned}
 \tag{4.3}$$

These are the dimensions of the flexible coupling currently in use.

#### 4.3.4 Potted Couplings

The two encoder-side bearings were potted in place using Devcon 2-Ton™ epoxy. This was done with the carriage fully assembled and riding on the rails, and with the air running as the epoxy cured. The design of the potted coupling is shown in Figure 4.8.

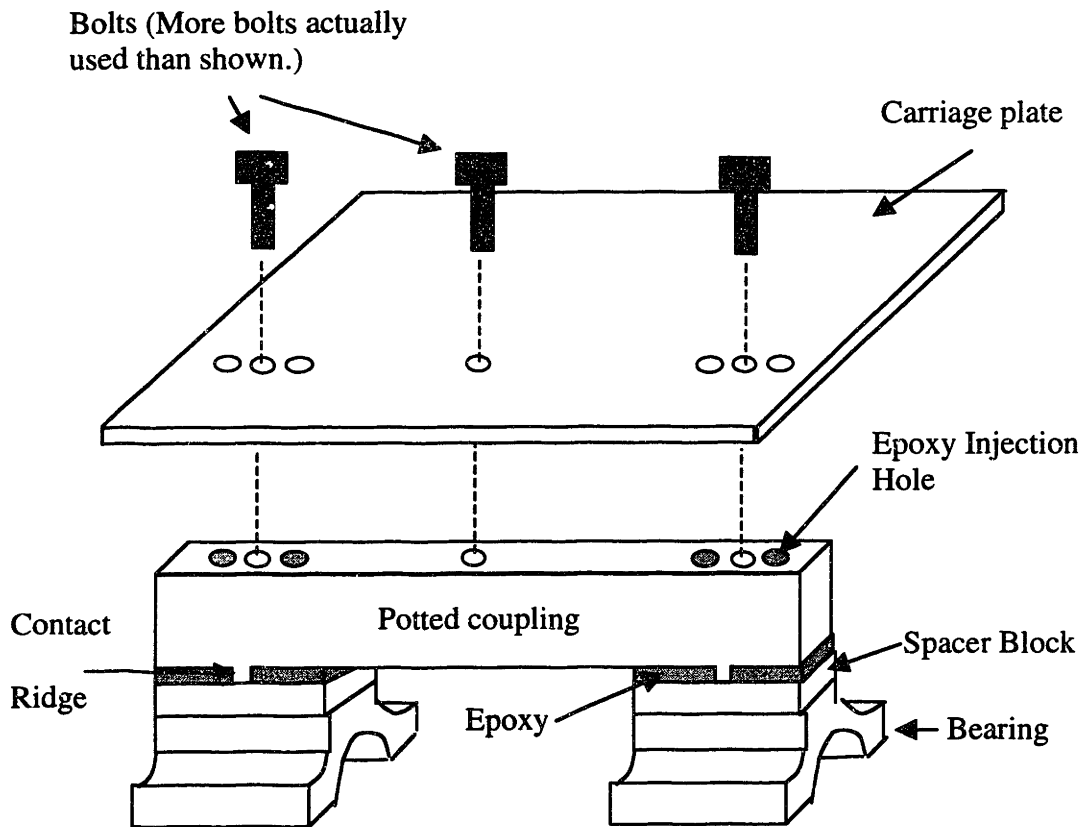


**Figure 4.8.** Potted Coupling

The rigid potting does not accommodate rotation  $f$  of these bearings relative to one another and to bearing 3, rotation which may be necessary. However, the design of the couplings causes much less of this rotation to be required by these bearings than by the printhead-side bearing. By contacting each bearing only at its centerline, the design of the potted coupling allows each bearing to orient itself properly in the  $f$  direction before potting. This eliminates one source of error that requires  $f$  direction rotation, namely parallelism error between the surface of the bearing blocks and the graphite bearing surfaces. The encoder-side bearings are also shielded from the effect of bearing block height variation (beyond that which is eliminated by shimming). The  $f$ -rotation required by such variation is transferred to the printhead-side bearing. Figure 4.9 illustrates the way in which the potted coupling reduces the need for  $f$ -rotation of the encoder-side bearings.

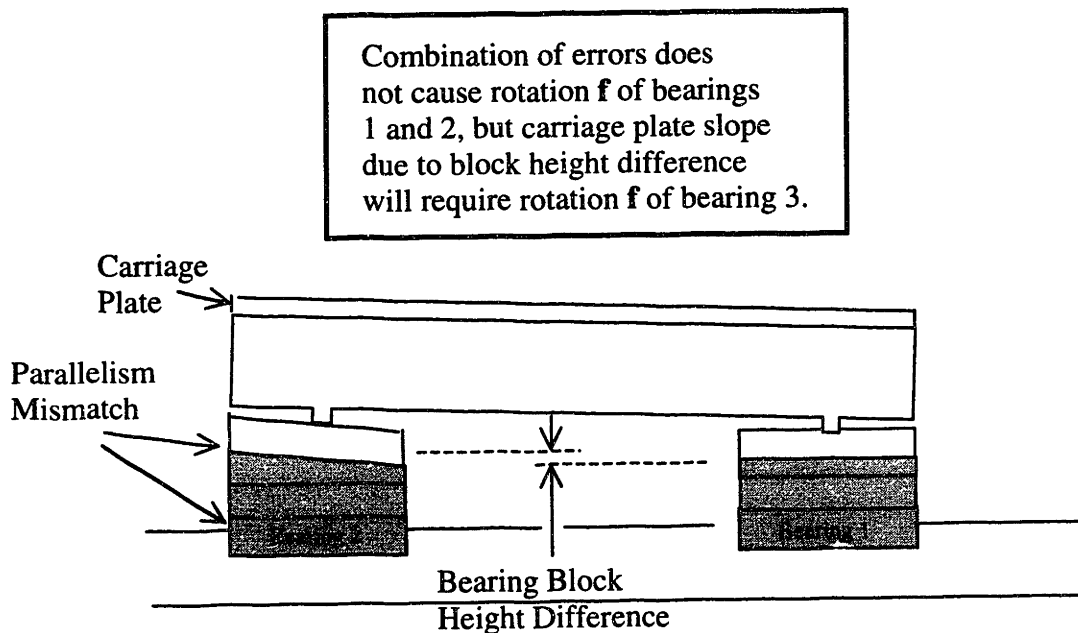


**Figure 4.9.** Potted coupling accommodates some errors that otherwise cause  $f$ -rotation of bearings.

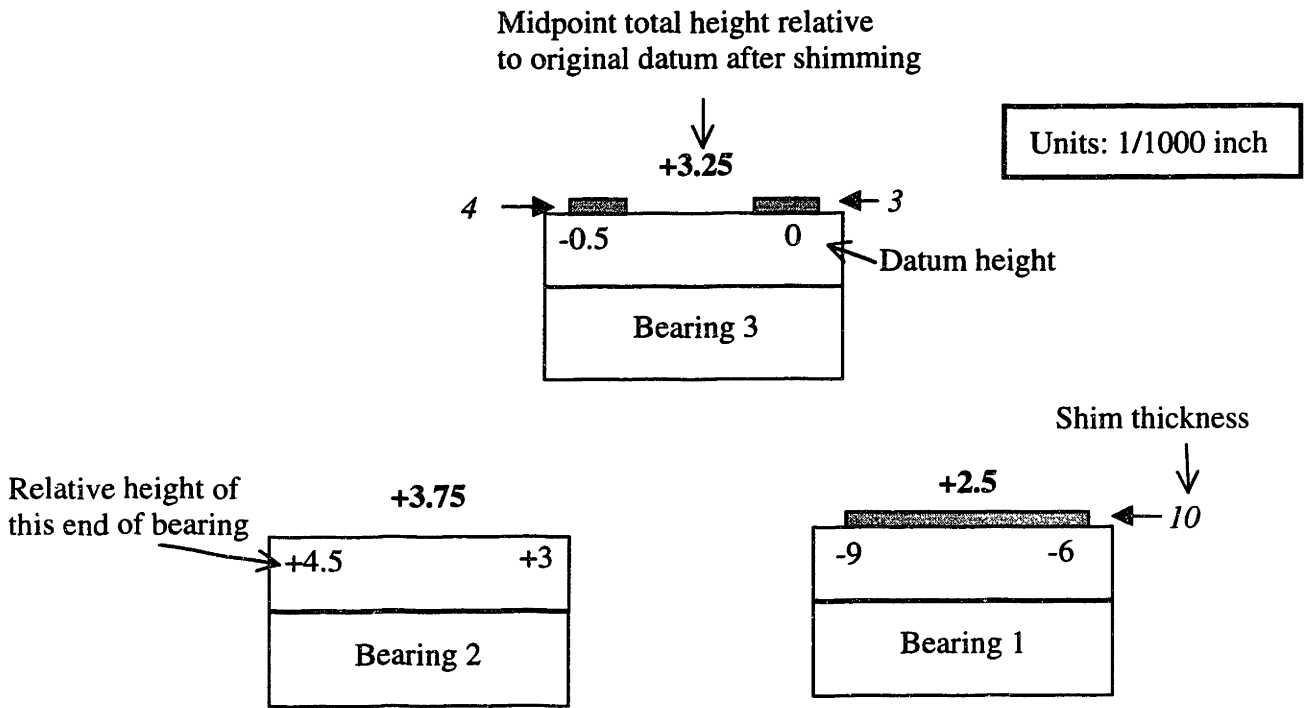


**Figure 4.10** Bearing block height variation and necessary shimming.

#### 4.3.5 Assembly Procedure

As the bearing block top surfaces were not all at the same height above the rail and were not perfectly parallel to the rails, the first step in the assembly of coupling system was putting appropriate shims on the bearing blocks. Figure 4.10 illustrates the bearing block height variations and the shims used. It is noted that there is an overall slope of the carriage plate, which could have been avoided by more careful shimming. Spacers of equal thickness were then bolted to the encoder-side bearings. These spacers are present to allow the air bearings to be separated from the potted coupling, should this

become necessary and the epoxy prove difficult to remove. In such an instance, one would cut through the spacers and the bolts embedded in them in order to free the bearings. Air was supplied to the bearings at a pressure of 80psi throughout the remainder of the assembly. The flexible coupling was next bolted to the printhead side bearing. The potted coupling was then bolted to the carriage plate, and the carriage plate assembly set onto the three bearings. The printhead-side bearing and its accompanying flexible coupling were properly located with respect to the carriage with the bolts to be used to attach them to the carriage, but these bolts were not tightened. A 1.2-kilogram weight was placed on the carriage, and the assembly was then run back and forth along rails, using electrical contact to make sure that none of the bearings was making contact with a rail. Epoxy was then injected into the gap between the potted coupling and the spacers on top of the encoder-side bearings. The epoxy was allowed to cure overnight with air running to the bearings.

#### **4.3.6 Electrical Monitoring of Bearing Contact**

As mentioned in connection with the measurement of bearing contact torques and forces, because the bearing sleeves are graphite, electrical contact can be used to determine whether the bearings are grounding. This is taken advantage of in the droplet observation station by using a set of light emitting diodes (L.E.D.s) to indicate any contact that occurs during operation of the carriage. A separate L.E.D. is connected between each bearing and a 5-volt supply, with a series resistor for each L.E.D. The rails are earthed, so that whenever a bearing makes contact with its rail, the L.E.D. for that bearing turns on.

#### 4.4 CABLE CONNECTION

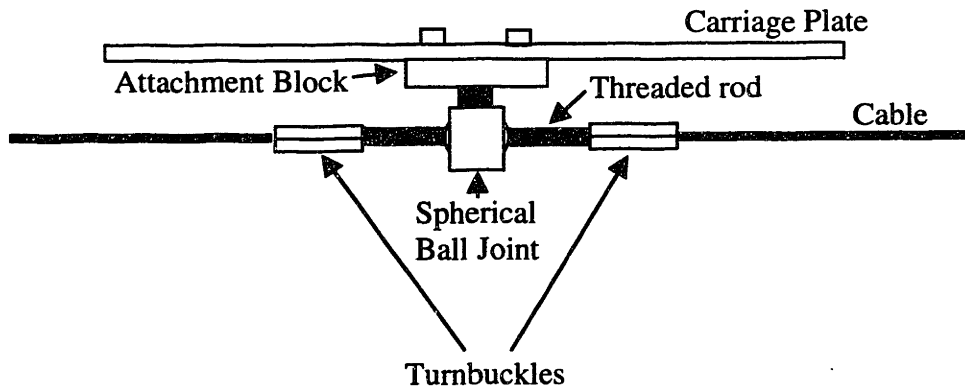


**Figure 4.11.** Drive cable connection.

The connection of the drive cable to the carriage is critical, as it is important that the cable does not exert any side load or torque on the carriage. Such loading is avoided by connecting the cable to the carriage via a spherical ball joint as illustrated in Figure 4.11. The two ends of the cable are attached to the threaded rod that passes through the center of the spherical ball joint via turnbuckles, providing a means of tensioning the cable. A spherical ball joint with a plastic lining is used in order to eliminate backlash.

#### 4.5 UMBILICAL

The air supply for the bearings, the electrical signals for the encoder readhead and the 5-volt supply for the bearing contact indicator L.E.D.s must all be connected to the moving carriage. This is done as illustrated in Figure 4.12. The required wire and tubing is hung from a central point 3 feet above the carriage, and swings back and forth as the carriage travels.

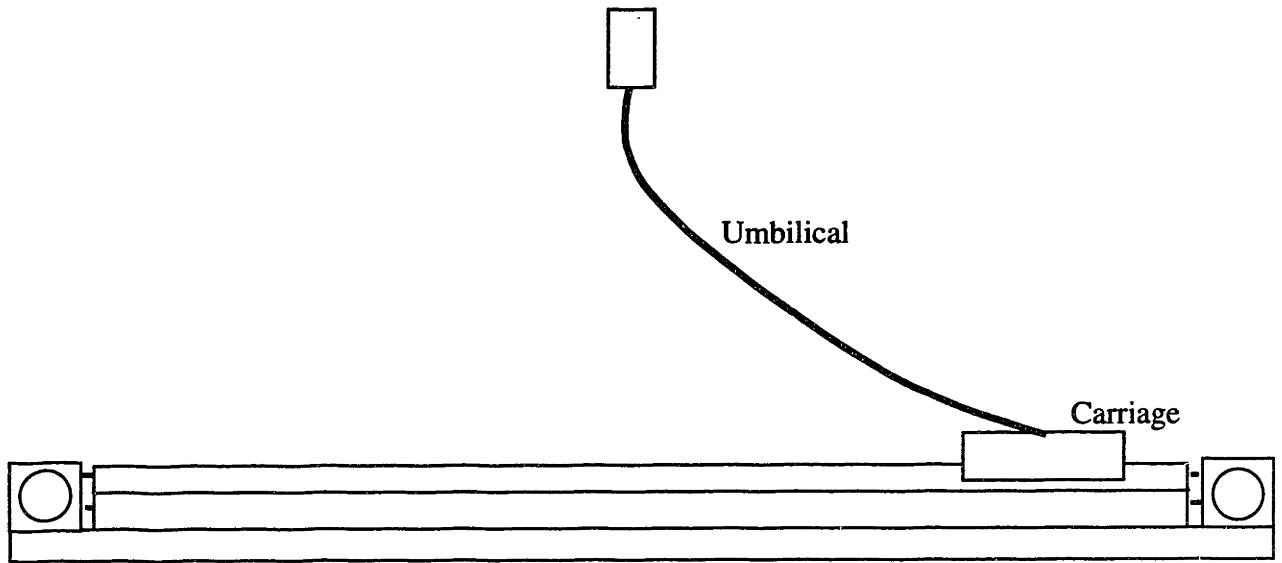


**Figure 4.12.** Hanging umbilical.

An alternate umbilical arrangement is to have a rolling umbilical as shown in Figure 4.13. A flat strip of tubing and electrical cable lies on the table and is folded

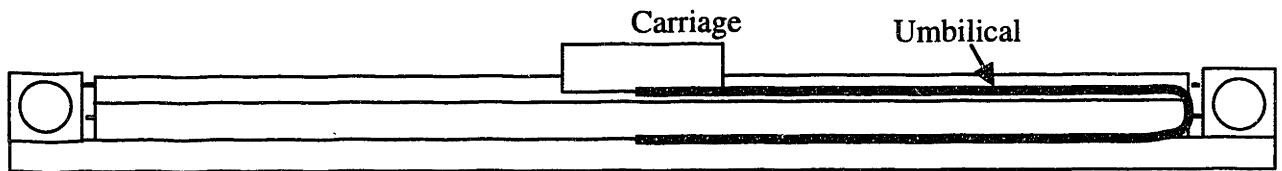


**Figure 4.13.** Rolling Umbilical.



through 180 degrees to where it is connected to the carriage. As the carriage moves back and forth, the cable rolls and unrolls without sliding. To make provision for an umbilical of this sort, the carriage plate was machined with a section protruding beyond the encoder location to provide an attachment area for a rolling umbilical.

#### 4.6 CENTER OF GRAVITY TUNING

If the carriage is not driven through its center of gravity, loads are imparted on the bearings that tend to push the bearings against the rails. As noted earlier, the bearings are especially sensitive to side loads, so the location of the center of gravity in the transverse direction is especially important. To illustrate, suppose that it is desired to limit the side load caused by center of gravity misalignment to one quarter of the grounding side load of 0.12 lbs. Figure 4.14 illustrates the loads and displacements under discussion.

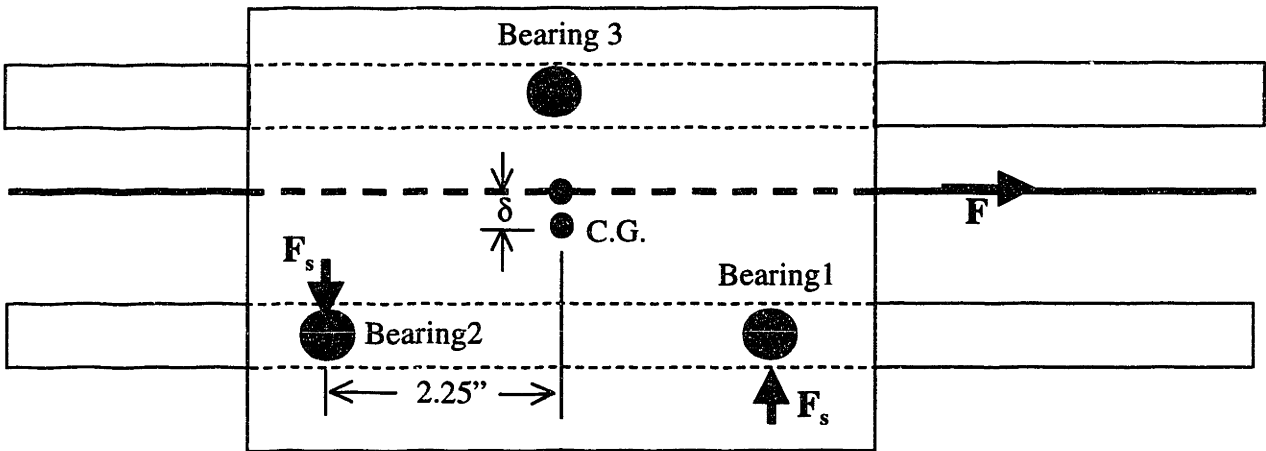


**Figure 4.14.** Loads and displacements related to center-of-gravity discussion.

The force on the carriage causing acceleration is calculated as

$$F = ma = 1.8kg \times 5 \frac{m}{s^2} = 9N = 2.02lb \quad (4.4)$$

In order to limit the side load  $F_s$  imparted on the bearings to 0.03 lb, the transverse displacement  $\delta$  from the center of gravity to the point through which the carriage is driven must be no more than

$$\delta = \frac{2 \times 2.25in \times 0.030lb}{2.02lb} = 0.067 in \quad (4.5)$$

Attention was paid during the design of the machine's overall layout to the need to drive the carriage through its center of gravity. But as construction moved forward and modifications were made to the carriage (e.g. a different encoder readhead than that originally contemplated, the bearing coupling system discussed in section 4.3), the center of gravity inevitably moved. It thus became necessary to use a set of counterweights to move the center of gravity back as close as possible to the drive point. The location of these weights is shown in Figure 4.1. The amount of weight to attach was determined by hanging the carriage from a cable attached directly above the drive point and adding and subtracting weight until the top edge of the carriage was parallel to leveled surface. This is illustrated in Figure 4.15. Space constraints made movement of the vertical location of the center of gravity more difficult. The drive point is currently approximately 0.2 inch above the center of gravity.

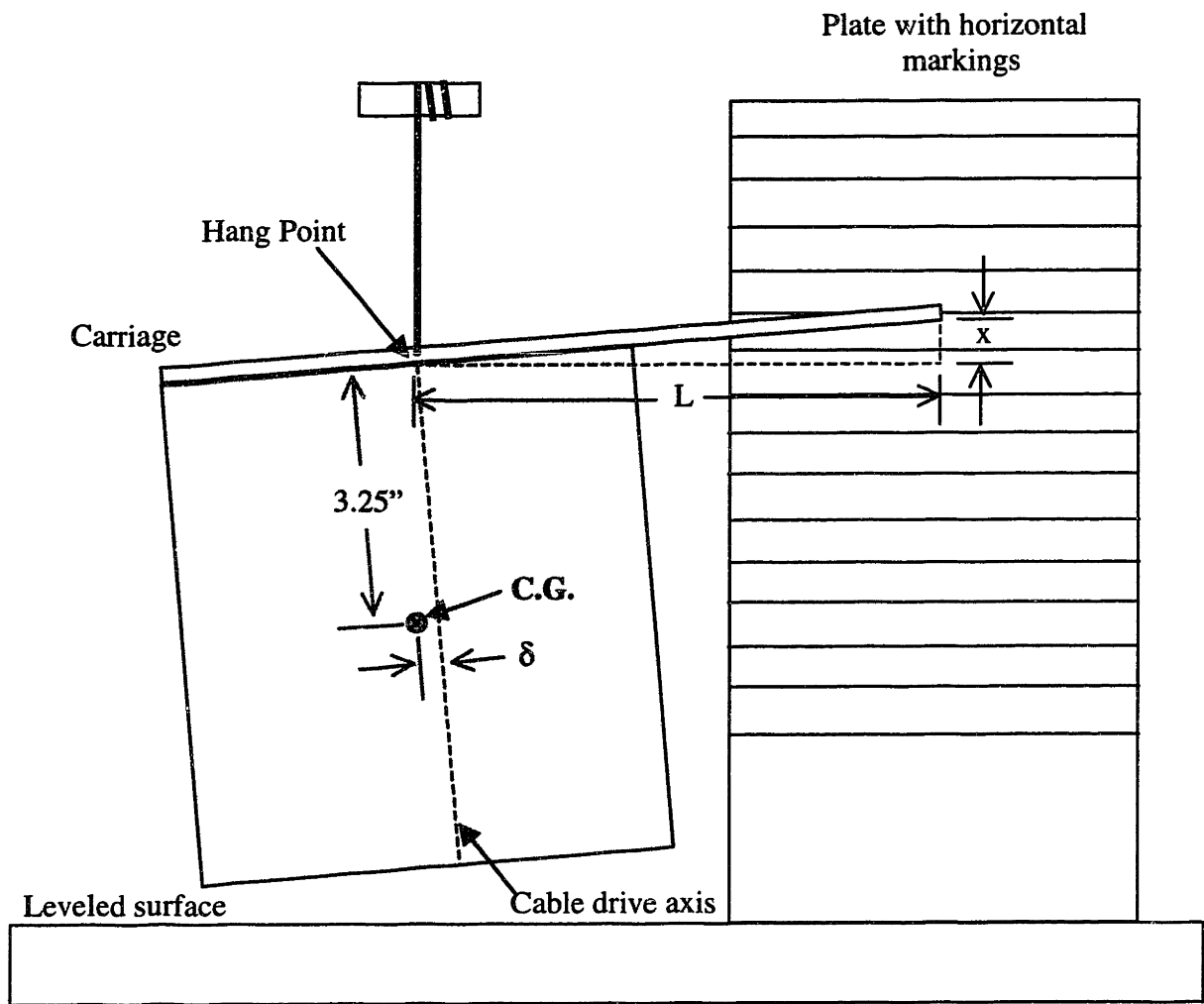


**Figure 4.15.** Arrangement for measuring center-of gravity position.

As illustrated in the diagram:

$$\delta = 3.25in \times \frac{x}{L} \quad (4.6)$$

If additional mass is added to the carriage and not centered over the drive point and current center of gravity, the center of gravity will shift. The center of gravity will have to be moved back to the drive point by addition or subtraction of weight from the carriage at the appropriate distance from the center of gravity. The transverse distance between the drive point and the location of the balancing weights currently used is 2.15 inches. If for example a 250 gram payload is added to the carriage at a transverse distance of 0.5 inches from the center of gravity in the direction away from the location of the current balancing weights, some additional weight will have to be added. If this additional weight is placed at the same transverse location as the current balancing weight, the mass that must be added is:

$$M_{balance} = \frac{(0.5 \text{ in} \times 250 \text{ g})}{2.15 \text{ in}} \quad (4.7)$$

#### 4.7. CONCLUSION

The moving carriage has proven to be the most critical part of the machine. A large effort has made in order to get it to function properly. Its present operation is adequate, but it is still probably the weakest link in the system.

## **5.0 DRIVE SYSTEM**

A belt drive system using a round nylon-sheathed steel cable running over stainless steel pulleys is used. The drive system consists of the cable, the drive pulley assembly, the idler pulley assembly and the motor. The design or selection of each of these items will be briefly discussed in the following sections. Machine drawings for all machined parts are included in Appendix A.

### **5.1. CABLE**

The selection of an appropriate cable is primarily a tradeoff between bending flexibility and axial stiffness. Sava Industries Incorporated manufactures a variety of highly flexible round stainless steel cable from which the cable used was selected.

The first cable tried was a 7 x 49 ply nylon-coated cable with a core diameter of 0.054 inches (total diameter of 0.063 inches). With a pulley diameter of 1.6 inches, the pulley-to-cable diameter ratio was 30, resulting in a strength efficiency of 93% of the nominal value of 250lbs, according to the Sava design guide. This is more than adequate for the present application. The 7 x 49 construction is the most flexible offered by Sava. The quoted axial stiffness of the cable is 1470 lb/in for a ten inch length. Tests of the motion of the carriage with this cable in place showed oscillations in the travel axis direction. These oscillations were measured by an accelerometer attached to the carriage. The frequency of oscillation observed with the carriage running under power was about 90Hz +/- 20Hz, though it varied a bit from the beginning of a pass through the middle to the end. With the carriage at the midpoint of its traverse and power disconnected from the motor, the carriage was tapped and the resulting vibration observed using the

accelerometer. The frequency was found to match that observed during a powered traverse. The natural frequency of a two-body model of the system can be calculated for comparison, as:

$$f = \frac{1}{2\pi} \sqrt{\frac{k}{\mu}} \quad (5.1)$$

where  $\mu$  is the reduced mass of the two-body system. The mass of the moving carriage is 1.8kg. For the drive pulley assembly, an equivalent mass is calculated based on the rotational inertia. This rotational inertia is calculated in Appendix B as 0.000308 kg·m<sup>2</sup>. The radius at which the cable goes over the pulley is 0.0212 m, so the equivalent mass is:

$$m_{eq} = \frac{I}{r^2} = \frac{0.000308 \text{ kg} \cdot \text{m}^2}{(0.0212 \text{ m})^2} = 0.69 \text{ kg} \quad (5.2)$$

The reduced mass of the system  $\mu$  is thus

$$\mu = \frac{m_1 m_2}{m_1 + m_2} = \frac{1.8 \text{ kg} \times 0.69 \text{ kg}}{1.8 \text{ kg} + 0.69 \text{ kg}} = 0.50 \text{ kg} \quad (5.3)$$

As length of cable between the two masses varies from 5 inches to 50 inches (about the range of lengths that occur over a pass), its nominal stiffness varies from 2940 lb/in (515,000 N/m) to 294 lb/in (51,500 N/m). This gives a natural frequency ranging from

$$f = \frac{1}{2\pi} \left( \sqrt{\frac{51500 \frac{N}{m}}{0.50kg}} \right) = 51Hz \quad (5.4)$$

to

$$f = \frac{1}{2\pi} \left( \sqrt{\frac{515000 \frac{N}{m}}{0.50kg}} \right) = 162Hz \quad (5.5)$$

The observed frequency of vibrations does indeed fall within this range.

The drive cable was replaced with a stiffer version, the replacement being a 7 x 19 ply nylon-coated cable with a core diameter of 0.063 inches (total diameter of 0.093 inches). The pulley to cable diameter ratio with a pulley of 1.6 inches is 25, resulting in a strength efficiency of 92% of the specified value of 480lbs, again more than adequate. The quoted axial stiffness of this cable is 2820 lb/in for a 10 inch length. The performance of the drive system with this cable has been satisfactory thus far. At the motion control system gains currently used (derivative gain KD = 50, proportional gain KP = 1, integral gain KI = 0) and with a servo loop time of 500 microseconds (the minimum possible), no vibrations have been observed. The servo loop time can be adjusted in 125 microsecond increments. Increasing it beyond 625 microseconds causes vibrations to occur. KI as small as 0.1 causes oscillation, though this is oscillation at a lower frequency than that observed to be caused by increasing TM. Changing KP and KD does not cause vibrations until the motor itself starts to vibrate. Tuning of the motion control system gains is discussed further in chapter 10.

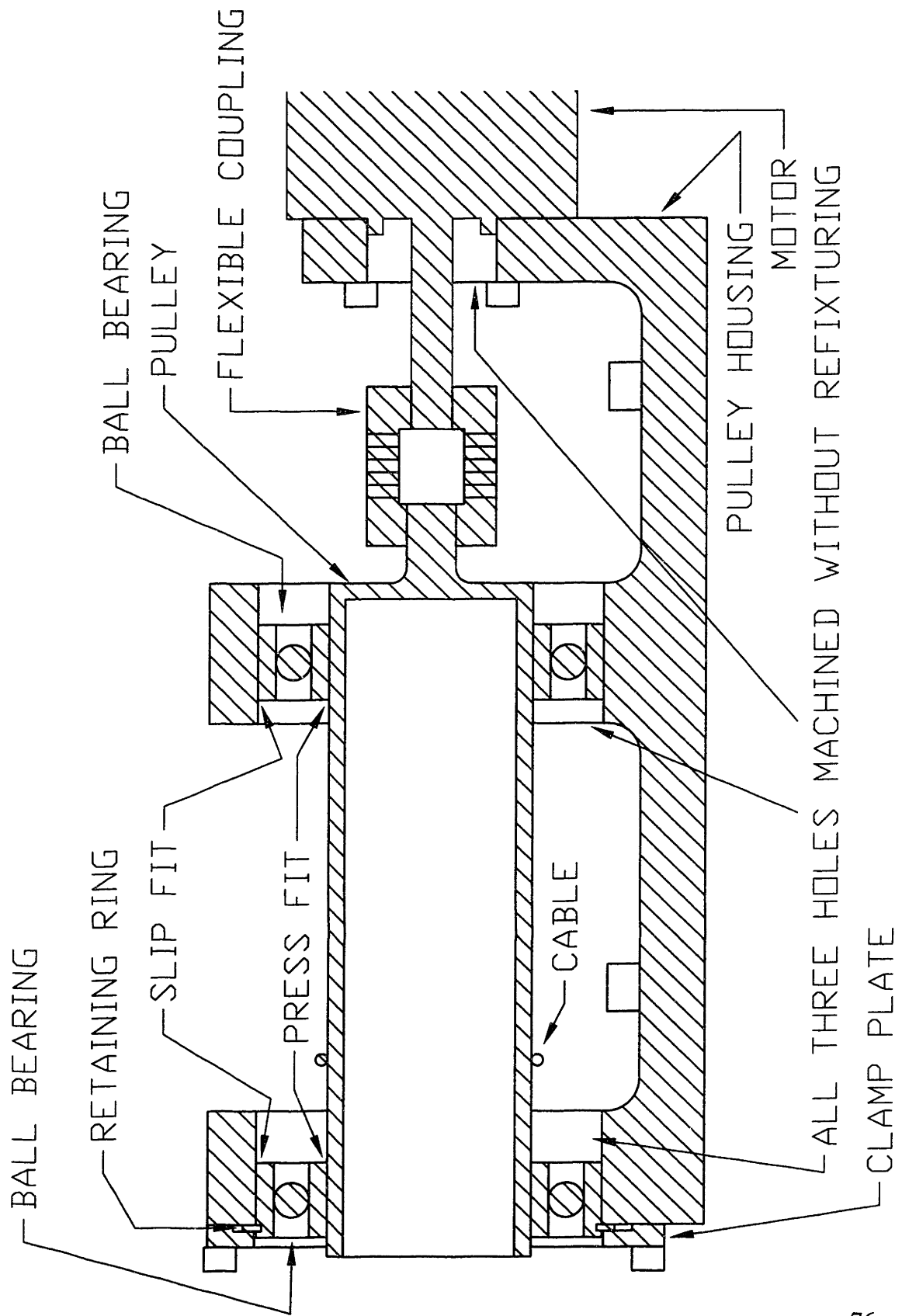


Figure 5.1. Drive Pulley Assembly



As mentioned in section 4.4, tensioning of the cable is achieved via turnbuckles on each end of the cable that screw onto a piece of threaded rod.

## **5.2 DRIVE PULLEY ASSEMBLY**

Figure 5.1 shows a cross-section of the drive pulley assembly. The pulley is supported by two ball bearings that sit in a pulley housing. The entire housing is machined out of a single block, and supports both the pulley and the motor. The holes in the housing are all machined without refixturing the workpiece so as to minimize concentricity errors. The motor shaft and pulley are connected via a flexible coupling, so as to accommodate some misalignment of the two.

The two ball bearings are pressed onto the pulley. These are 6008-series ABEC-1 bearings obtained from Bearing Enterprises Incorporated in Boston, and manufactured by Nachi America Incorporated. The bearing on the left hand side of the picture is axially fixed by means of a retaining ring that sits against the outside of the housing and is clamped in place by an external plate. This bearing is unshielded. The right hand bearing is shielded. Its axial position is defined by virtue of the pressed connection of both bearings to the pulley. This bearing is allowed to float in the axial direction relative to the pulley housing. This accommodates the different rates of thermal expansion of the steel pulley and bearings and the aluminum housing.

Due to an error in the machining specifications, the pulley was not made to press into the bearings, but rather to slip into the bearings. This is currently rectified by means of shims wedged between the pulley and the inner race of the bearings, until such time as

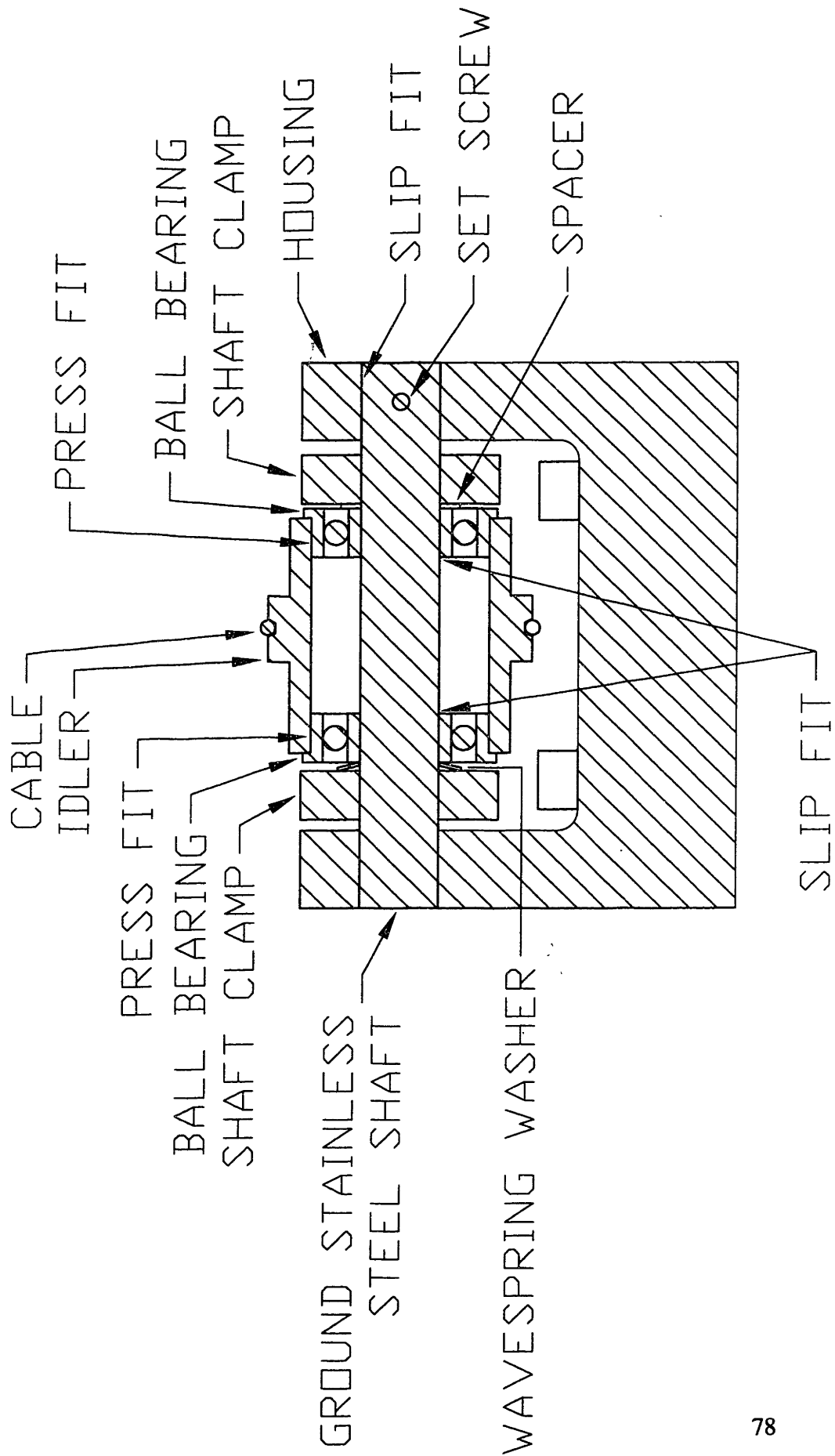


Figure 5.2. Idler pulley assembly

a new drive pulley is manufactured. The total runout on the current pulley is approximately 0.0008 inches (8 ten-thousandths of an inch).

A possible modification to improve the performance of the machine would be to make the pulley a constant diameter, that is, to make it without a stepped shaft. This may reduce eccentricity error.

### **5.3 IDLER PULLEY ASSEMBLY**

Figure 5.2 shows a cross-section of the idler pulley assembly. The pulley and associated components are supported on a ground stainless steel shaft that sits in the housing. The shaft is fixed in place by means of a set screw. A flanged ball bearing is pressed into each end of the idler pulley, and the whole unit slips onto the shaft. The idler pulley is axially located by means of squeeze-type shaft clamps. These clamps must exert axial force only on the inner races of the bearings. On one side, this is achieved by placing a spacer between the shaft clamp and the inner race. On the other side, a wavespring washer is used. This washer helps to ensure that no play is left in the assembly between the shaft clamps when they are tightened down.

### **5.4 MOTOR**

A direct current servo motor identical to that used in the M.I.T. production three dimensional printing machine was available for use in the observation station. This was a model JDTH-2250-FN-DC from Litton Special Devices Incorporated. The manufacturer's quoted ratings of this motor are presented in Table 5.1. The ratings of the

motor were checked against the required performance as presented by the following discussion.

Characteristic	Units	Tolerance	Value
Peak Current	Amps	Max.	28
Terminal Inductance	MilliHenries	Nom.	1.67
Terminal Resistance	Ohms	Nom.	1.4
Back EMF	Volts/kRPM	+/- 10%	6.43
Torque Sensitivity	Oz-in/Amp	+/- 10%	8.7
Thermal Resistance	Deg. C/Watt	Nom.	5.4
Winding Temperature	Deg. C	Max.	155
Weight	Oz	Nom.	37
Rotor Inertia	Oz-In-Sec <sup>2</sup>	Nom.	0.004
Damping Factor	Oz-In/kRPM	Nom.	0.1
Friction Torque	Oz-In	Max.	3.0
Continuous Torque	Oz-In	Max.	27
Peak Torque	Oz-In	Nom.	240

**Table 5.1.** Manufacturer's specifications for motor used.

The peak torque required of the motor occurs during acceleration of the carriage, and is the sum of the torque required to overcome the inertial load of the motor,

windings, pulleys, cable and carriage, the torque required to overcome damping and the torque required to overcome friction.

$$T_{peak} = J\alpha + K_D N + T_F \quad (5.6)$$

$J$  is the rotational inertia to be accelerated,  $\alpha$  is the rotational acceleration,  $K_D$  is the damping coefficient,  $N$  is the motor rotational speed and  $T_F$  is the friction torque.  $J$  is calculated as  $1.16 \times 10^{-3} \text{ kg}\cdot\text{m}^2$  (see Appendix C). With a pulley pitch radius of 0.835 in (0.0212m), the design linear acceleration of  $5 \text{ m/s}^2$  corresponds to an angular acceleration of

$$\alpha = \frac{a}{r} = \frac{5 \frac{m}{s^2}}{0.0212} = 236 \frac{rad}{s} \quad (5.7)$$

The top speed at which the motor is to be operated is

$$\omega = \frac{v}{r} = \frac{2.0 \frac{m}{s}}{0.0212} = 94.3 \frac{rad}{s} \quad (5.8)$$

$$N = \omega \times \frac{60s}{min} \times \frac{rev}{2\pi rad} = 901RPM$$

The quoted motor damping coefficient is 0.1 oz-in/kRPM ( $7.1 \times 10^{-7} \text{ N}\cdot\text{m/RPM}$ ), and the quoted maximum friction torque is 3.0 oz-in (0.021 N-m). The peak torque to be demanded of the motor is thus

$$T_{peak} = (1.16 \times 10^{-3} \text{ kg} \cdot \text{m}^2) \left( 236 \frac{\text{rad}}{\text{s}^2} \right) + \left( 7.1 \times 10^{-7} \frac{\text{N} \cdot \text{m}}{\text{RPM}} \right) (901 \text{ RPM}) + 0.021 \text{ N} \cdot \text{m} \quad (5.9)$$

$$= 0.295 \text{ N} \cdot \text{m} = 41.8 \text{ oz} \cdot \text{in}$$

This corresponds to a peak current of

$$I_{peak} = \frac{T_{peak}}{K_T} = \frac{41.8 \text{ oz} \cdot \text{in}}{8.7 \frac{\text{oz} \cdot \text{in}}{\text{A}}} = 4.8 \text{ A} \quad (5.10)$$

Both of these values are well below the rated maximum values of 240 oz-in and 28 A.

A pass consists of an acceleration phase, a constant speed phase, and a deceleration phase. The constant torque is evaluated by taking the root mean square of the three values that occur during a pass. During the constant speed phase there is no acceleration torque. During the deceleration phase, friction and damping do not load the motor, but instead assist it. For a pass at 2m/s, the three torques are thus:

$$T_{acc.} = 48.1 \text{ oz} \cdot \text{in}$$

$$T_{const.spd} = K_D N + T_F = \left( 7.1 \times 10^{-7} \frac{\text{N} \cdot \text{m}}{\text{RPM}} \right) (901 \text{ RPM}) + 0.021 \text{ N} \cdot \text{m}$$

$$= 0.022 \text{ N} \cdot \text{m} = 3.07 \text{ oz} \cdot \text{in} \quad (5.11)$$

$$T_{decel.} = J\alpha - K_D N - T_F$$

$$= (1.16 \times 10^{-3} \text{ kg} \cdot \text{m}^2) \left( 236 \frac{\text{rad}}{\text{s}^2} \right) - \left( 7.1 \times 10^{-7} \frac{\text{N} \cdot \text{m}}{\text{RPM}} \right) (901 \text{ RPM}) - 0.021 \text{ N} \cdot \text{m}$$

$$= 0.252 \text{ N} \cdot \text{m} = 35.7 \text{ oz} \cdot \text{in}$$

The times spent during each portion of such a pass are

$$t_{\text{accel}} = t_{\text{decel}} = \frac{v_f}{a} = \frac{2.0 \frac{m}{s}}{5.0 \frac{m}{s^2}} = 0.4s \quad (5.12)$$

$$t_{\text{const.}} = \frac{x_{\text{travel}} - at_{\text{acc}}^2}{v} = \frac{1.18m - 5 \frac{m}{s^2} (0.4s)^2}{2.0 \frac{m}{s}} = 0.19s \quad (5.13)$$

The root mean squared torque is thus

$$T_{\text{rms}} = \sqrt{\frac{\sum T_i^2 t_i}{\sum t_i}} = \sqrt{\frac{(48.1oz \cdot in)^2 (0.4s) + (3.07oz \cdot in)^2 (0.19s) + (35.7oz \cdot in)^2 (0.4s)}{(0.4s + 0.19s + 0.4s)}} \quad (5.14)$$

$$= 38.1oz \cdot in$$

It is noted that this torque is above the 27 oz-in continuous torque rating for the motor, and could therefore cause problems if the machine is operated for extended periods of time with maximum speed traverses. By comparison, if the machine is run at 1 m/s, the times spent in each part of the pass are:

$$t_{\text{acc.}} = t_{\text{dec.}} = \frac{1.0 \frac{m}{s}}{5.0 \frac{m}{s^2}} = 0.2s \quad (5.15)$$

$$t_{\text{const.}} = \frac{x_{\text{travel}} - at_{\text{acc.}}^2}{v} = \frac{1.18 - 5.0 \frac{m}{s^2} (0.2s)^2}{2.0 \frac{m}{s}} = 0.98s$$

This gives a root mean squared torque of:

$$T_{rms} = \sqrt{\frac{\sum T_i^2 t_i}{\sum t_i}} = \sqrt{\frac{(48.1oz \cdot in)^2(0.2s) + (3.07oz \cdot in)^2(0.98s) + (35.7oz \cdot in)^2(0.2s)}{(0.2s + 0.98s + 0.2s)}} \quad (5.16)$$

$$= 23.0oz \cdot in$$

The peak voltage required to drive the motor is

$$V_{peak} = K_b N + I_{peak} R \quad (5.17)$$

Where  $K_b$  is the motor back EMF and  $R$  is the motor terminal resistance.

$$V_{peak} = \left( 6.43 \frac{V}{kRPM} \right) (0.901kRPM) + (4.8A)(1.4\Omega) = 12.5V \quad (5.18)$$

This guides selection of a drive amplifier for the motor.

## 5.5 CONCLUSION

A working belt drive system using a round cable and a direct current servo motor is in place on the observation station. The importance of the cable stiffness and of pulley housing fits have been brought to light by tests of the motion, and deficiencies have been addressed. A possibility for the future is to try replacing the round cable with a flat belt of yet higher stiffness. The motor currently in use is generally adequate. Though



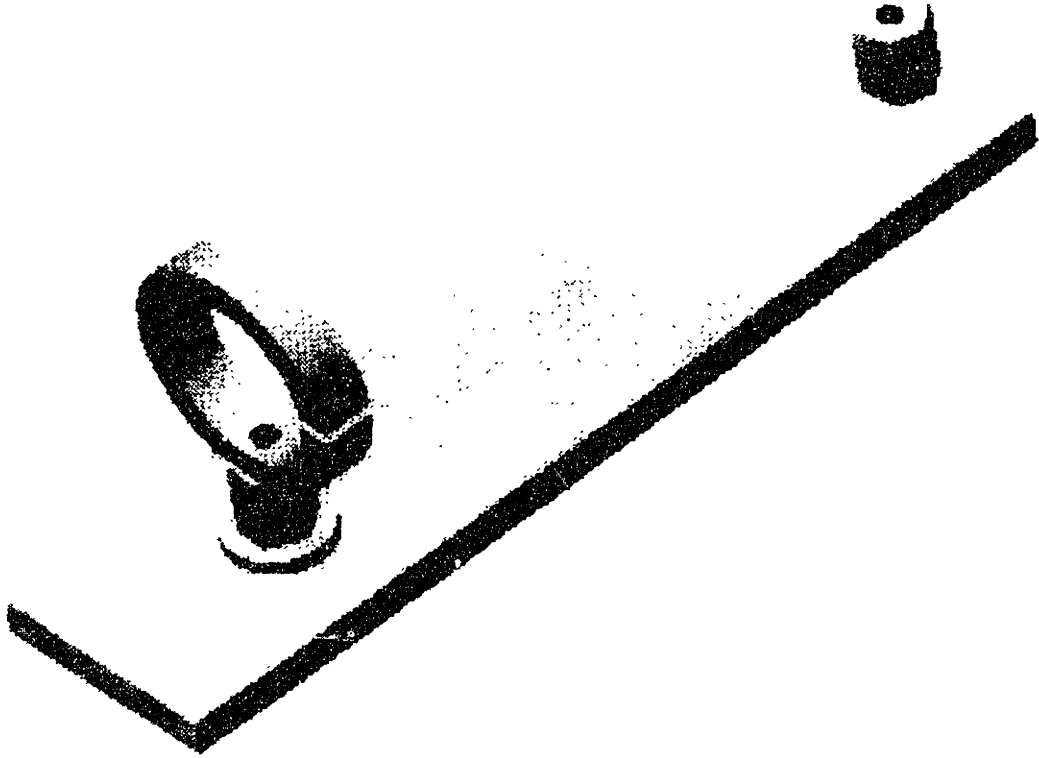
calculations suggest that it may have problems at extended high-speed operation, in practice it has proven to run without problems over all ranges of use.

## **6.0 OVERALL LAYOUT AND STRUCTURE**

Figure 1.6 shows the overall mechanical layout of the droplet impact observation station. Machine drawings for the various machined pieces are included in Appendix B. All components are mounted on a base that is a piece of aluminum jig plate, flat to within 0.015 inch over its entire area. The focal point of the layout is the axis of travel, in which lie the rails, carriage, pulley assemblies and encoder. The length of this entire axis is 62.1 inches, requiring a base plate of similar dimension. To provide adequate space for a camera, lighting and fluid supplies, the base plate was extended 16.5 inches beyond the rails on one side. To provide space for an encoder and a possible rolling umbilical, the base plate was extended 6.75 inches on the other side of the rails. The overall dimensions of the base plate are 62.3 x 30.0 inches. A piece of optical bench plate provides the means of mounting a printhead and a camera, and, if necessary, a strobe light source. A length of aluminum jig plate is used to mount the linear encoder scale. A powderbed mount, to be used in imaging applications in which the powderbed is stationary (see section 2.1.4), is provided beneath the printhead location. Several uncommitted tapped 1/4-20 holes are machined in the base plate to accommodate possible unforeseen needs.

### **6.1 CAMERA AND PRINTHEAD MOUNTING**

A 12-inch by 13-inch piece of optical bench plate covered with a 1 inch grid of 1/4-20 tapped holes and having a 4-inch by 4-inch section overhanging the travel of the powderbed provides a platform for flexible mounting of a printhead and a camera. This mounting plate is secured to the base plate by means of two triangular corner braces.



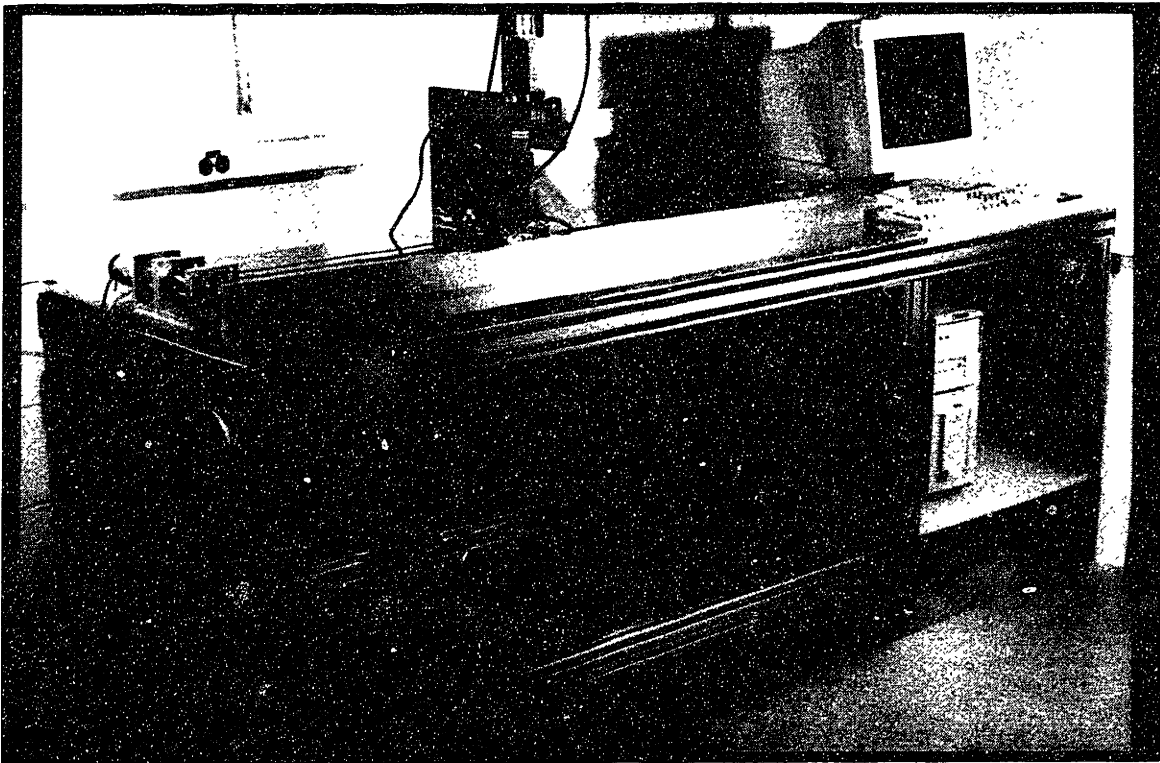
**Figure 6.1.** Camera mounting assembly.

Figure 6.1 shows the assembly by which a typical CCD video camera is affixed to the mount plate. The camera is held to this assembly by means of a 1/4-20 screw, a hole for which is typically provided on the base of the camera, and by means of a ring clamp that grips the lens tube to be used with the camera. The entire assembly is clamped to the mountplate by means of a steel crosspiece with two slots for 1/4-20 bolts. This scheme provides rigid mounting that is easily adjustable through nearly 90° from a near top view of the powderbed to a horizontal profile view.

## 6.2 ENCODER PLATE

The linear encoder scale as obtained from the manufacturer was a flexible strip that had to be mounted on a flat surface, the manufacturer's specification calling for a parallelism to the travel axis of 0.002 inch and a surface finish of 0.125 microinches maximum average roughness. A suitable mounting surface was achieved using a length of 3/4-inch thick aluminum jig plate. The central portion of the bottom edge of this plate was machined away, leaving a 0.060-inch-thick strip on each side, to improve the seating of the plate.

## 6.3 FRAME



**Figure 6.2.** Photograph of machine on frame.

Figure 6.2 shows the frame by which the entire machine is set on the floor. It carries both the base plate, on which the entire mechanical assembly is set, and the electronics, including a computer with its keyboard, mouse and monitor. It is assembled from modular interlocking pieces of extruded aluminum obtained from 80/20 Incorporated, who dub their product “The Industrial Erector Set®”. This approach has several advantages over alternatives: It is easy to create the exact form required, additional features can be added at a later date should they be needed and it is less expensive than any pre-made alternative that is comparably suited to the application.

Between the base plate and the frame is a layer of Sorbothane™ vibration isolation padding. The computer shelves are of 3/4-inch thick polypropylene panel. The electronics external to the computer, apart from the camera and light source, are to be mounted against a framework of horizontal bars. This mounting had yet to be done at the time that this thesis was written.

## **7.0 ELECTRONIC SYSTEM OVERVIEW**

This chapter gives an overall view of the electronic system. The first four sections present, in order, the tasks performed by the electronic system, the parts of the system, the flow of information in the system and the timing of signals in the system. The fifth section describes *synchronous operation*, the requirements that it imposes on the encoder used, and its implications for drop breakoff timing. The final two sections briefly describe the computer and software used.

### **7.1 TASKS PERFORMED BY THE SYSTEM**

The electronic system performs the following tasks:

1. Motion control
2. Excitation of droplet formation at a desired frequency, ranging from 10 Hz to 100 kHz.
3. Application of voltages to a charging cell, synchronously with droplet formation.
4. Triggering of a strobe flash at the appropriate instant, with timing synchronized with droplet formation, and with adjustable phase delay.
5. Acquire a video frame or a series of video frames from a video camera, at the right moment.

### **7.2 PARTS OF THE SYSTEM**

Figure 7.1 is a diagram of the electronic system showing all the discrete pieces of hardware.

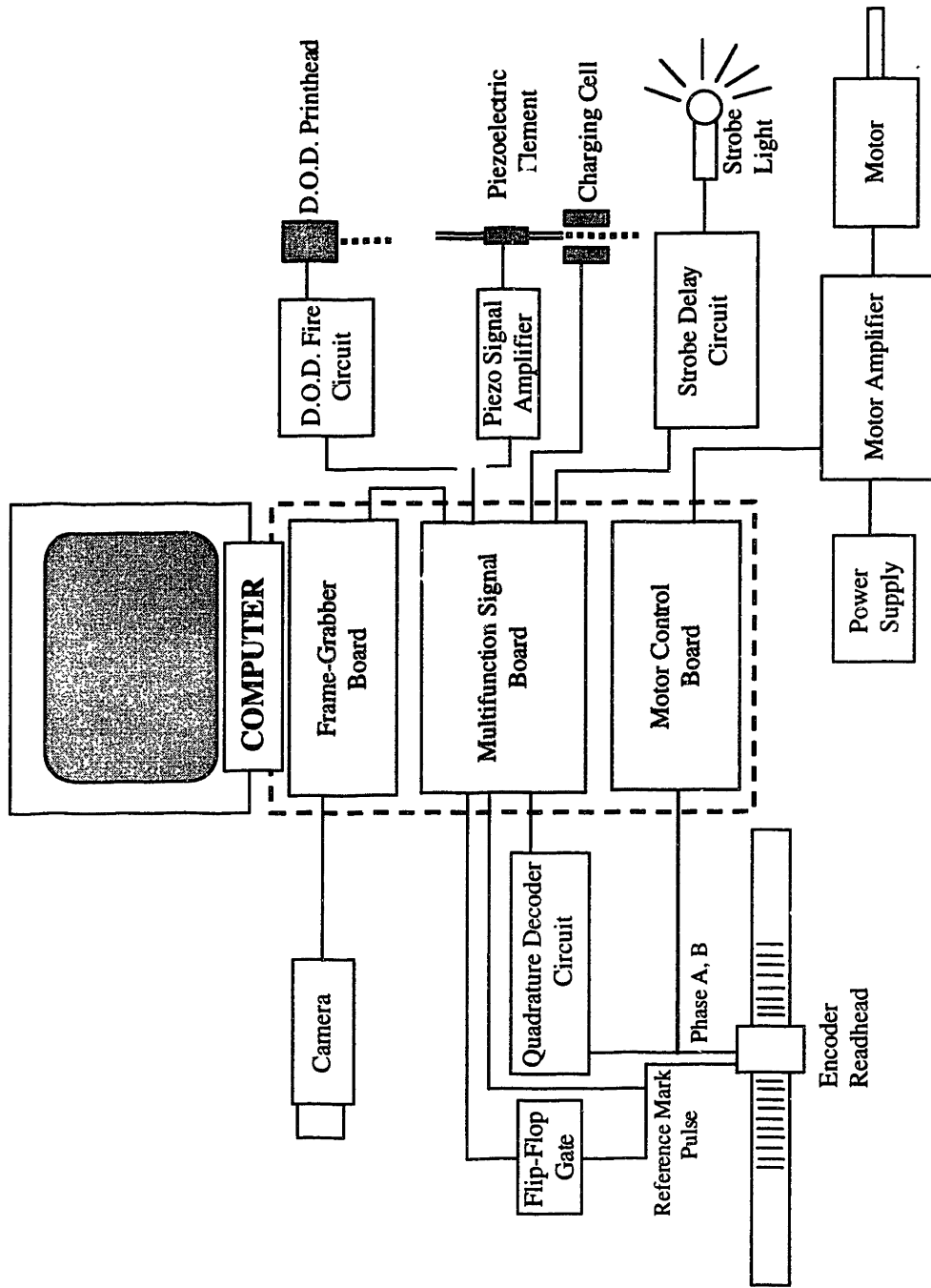


Figure 7.1. Overall electronic system

The encoder readhead puts out two square wave signals which are in quadrature, that is, 90 degrees out of phase, so that they can be combined to give a single signal with a frequency a factor of four higher. The encoder output is sent to the motor controller and to the multifunction card via a quadrature decoder circuit. The encoder readhead also puts out a reference mark pulse, which is sent to the multifunction signal board to gate output signals.

The motion control board sends voltage commands to a motor amplifier , according to the commanded motion and the encoder feedback received.

The motor amplifier converts the motion control voltage commands into the appropriate current and voltage levels for the motor being used.

The power supply provides power to the motor amplifier.

The quadrature decoder circuit converts the two encoder output phases into a single signal of four times the frequency, and sends this signal to the multifunction signal card.

The flip-flop gate circuit gates the counter on the multifunction signal card (starts it at the right moment.)

The multifunction signal card generates signals to excite droplet formation, charge droplets, trigger a strobe flash and trigger acquisition of a video frame.

The strobe delay circuit controls the point in droplet phase at which the strobe flash occurs.

The D.O.D. fire circuit converts the droplet excitation signal from the multifunction signal card into a form appropriate for driving a drop-on-demand printhead.



The piezo amplifier converts the droplet excitation signal from the multifunction signal card into a form appropriate for driving a piezoelectric element.

The frame grabber card acquires a video image or series of images upon receipt of a trigger signal.

### 7.3 FLOW OF INFORMATION

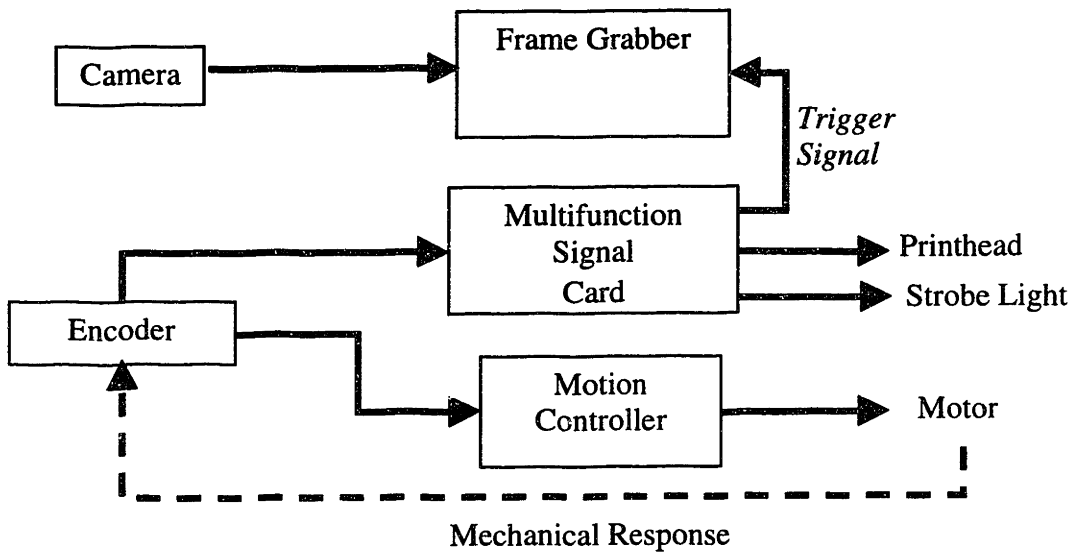


**Figure 7.2.** Flow of information. Broad view.

Figure 7.2 illustrates in broad strokes the flow of information in the system. The encoder output goes to the motion controller and to the multifunction signal card. The motion control output goes to the motor. The multifunction signal card sends outputs to a printhead, a strobe light and a frame grabber. The frame grabber receives input signals from a camera and the multifunction signal card.

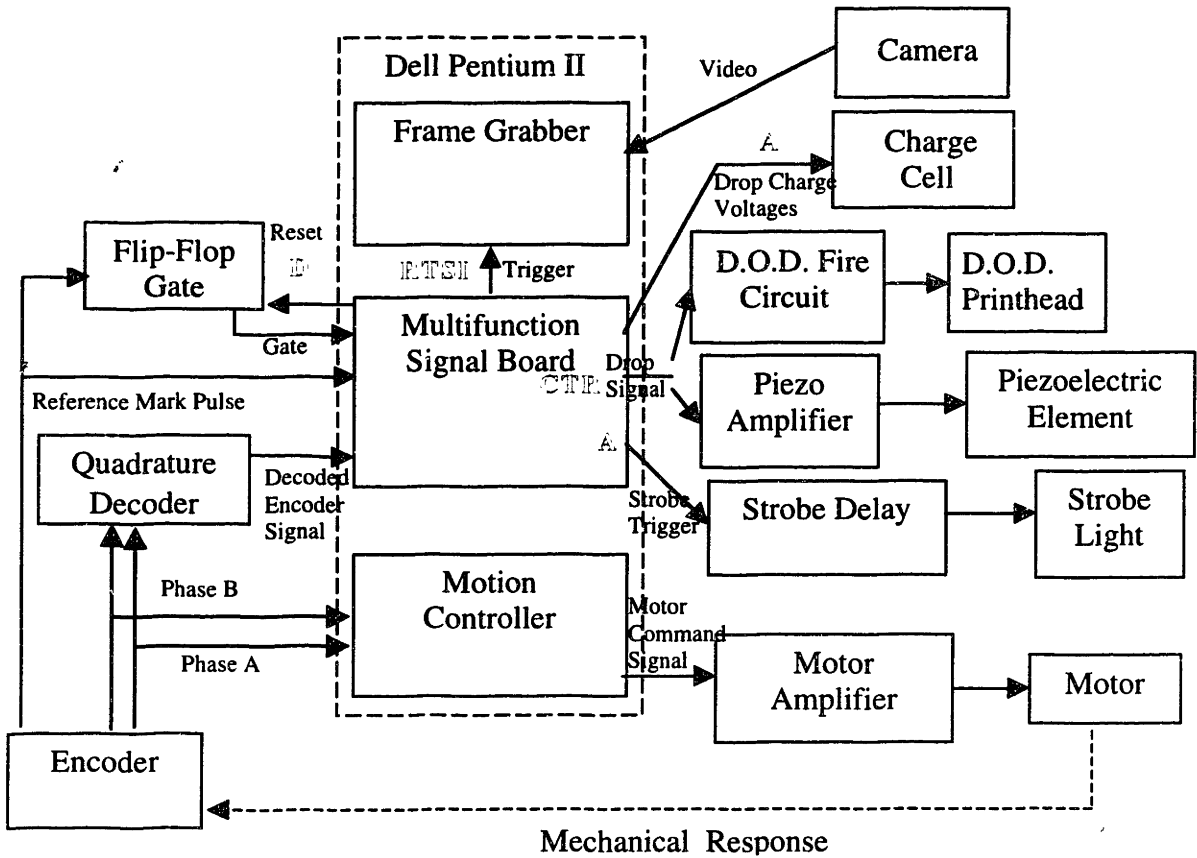


**Figure 7.3.** Flow of Information. Detailed view.

Figure 7.3 presents the finer detail of the flow of information. There are three principal outputs from the linear encoder – the two phases of the encoder output and a pulse output that occurs whenever a reference mark at a specific location along the encoder scale is passed. These three signals are sent to the multifunction signal card. The two encoder output phases are not wired directly to the multifunction signal card, but to a quadrature decoder circuit. This circuit sends a single quadrature decoded signal (four times higher in frequency than either phase) to the multifunction signal card.

The two phases of the encoder output are also routed to the motion controller, which performs quadrature decoding internally. The motion controller also internally determines the count direction according to the order of the two encoder phases.

In addition to being sent directly to the multifunction signal card, the reference pulse signal is sent to a flip-flop gate circuit. This circuit is necessary to provide a gating signal for the droplet generation output of the multifunction signal card, because the reference pulse itself is very short (4 microns). This droplet generation signal serves as a clock signal for the droplet charge signal, strobe trigger signal and frame grabber trigger signal.

The direct input of the reference pulse signal to the multifunction signal card controls the start of the droplet charge signals and the strobe trigger signal. In other words, as soon as the reference mark is passed, the streaming out of an array of voltages from each analog output channel begins. These analog outputs are timed by the drop generation signal, a new value being put out for each drop. The arrays are generated before the pass and stored in computer RAM. The values are retrieved from RAM by the multifunction signal card using Direct Memory Access (DMA) during a pass. The maximum analog output rate of the card is several hundred kilo-samples per second, so the length of the arrays to be streamed out is not a concern. In this case the brief reference pulse is sufficient for initiating the output, as only a triggering edge is required, rather than gating of the entire signal.

The strobe trigger signal does not directly activate a strobe flash, but goes to a strobe delay circuit which interposes a delay of up to 20 microseconds before activating the flash. The duration of the delay is controlled by the voltage level of the strobe trigger pulse.

The outputs of the multifunction signal card are labeled according to their type on Figure 7.3 - **A** for analog, **D** for digital, **CTR** for counter (which is a digital signal), and **RTSI** for RTSI bus signal (which is a digital signal).

#### **7.4 SIGNAL TIMING**

Figure 7.4 illustrates the timing of the signals in the system.

#### **7.5 SYNCHRONOUS OPERATION**

The synchronous/asynchronous distinction applies only to continuous-jet printing. In continuous-jet printing there is a droplet generator and a charging cell, and the operation of these can be synchronized. Synchronous operation means that the same signal causes drops to be released and “clocks” new voltages onto the charging cell. Thus the two operations are synchronized. In drop-on-demand printing there is no charging cell. Essentially, drop-on-demand printing is by definition always synchronized.

The voltages to be applied to the charging cell are stored in memory before a print pass. On each period of a clocking signal, the next voltage in memory is loaded to the charging cell. In synchronous operation, this clocking signal also causes one drop to be released each period. Thus *each charging voltage in memory corresponds to one drop*. In the present implementation, the clocking signal is the droplet excitation signal.

The alternative to synchronous operation, asynchronous operation, is the case in which the droplets are generated at a rate determined by one signal source and new

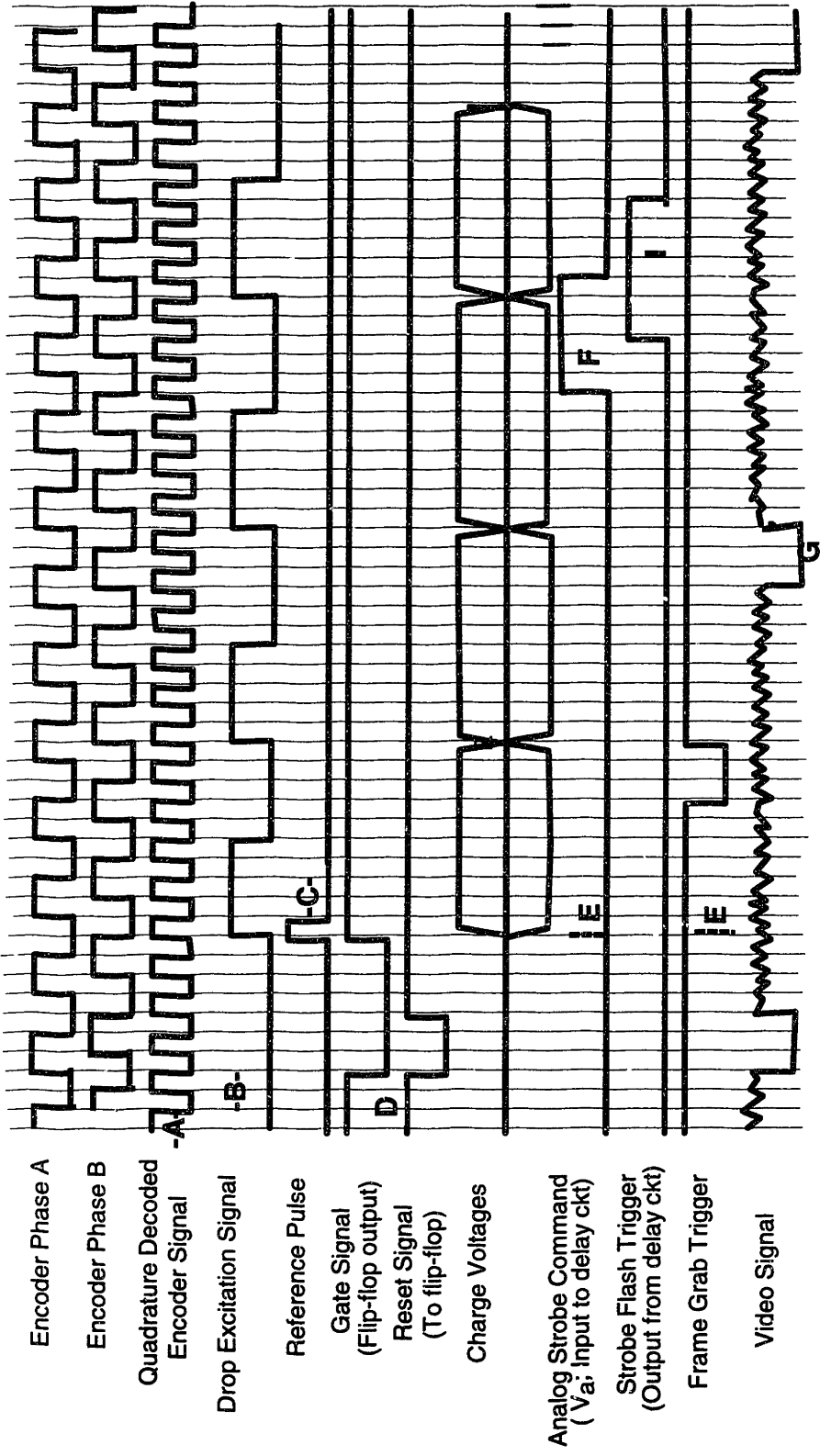


Figure 7.4. Signal timing diagram.

voltages are applied to the charging cell at a rate determined by another signal source.

There is *no one-to-one correspondence between droplets and charging cell voltages*.

The primary advantages of synchronous operation are that the one-to-one correspondence between charging voltages and droplets makes it easier to assure that droplets do not acquire incorrect charges via partial charging, and that no voltage values are lost. With asynchronous printing, a voltage value is lost if it is replaced by a new one before a drop has been released. For example, a system with an encoder resolution of 10 microns travelling at 1.5 meters per second updates the charging cell 150,000 times per second, if updating is directly clocked by the encoder output. However typical continuous-jet droplet frequencies are in the range of 30 kHz to 80 kHz. In this example, if the droplet frequency is 50 kHz, there are three consecutive charging voltage values in memory for each droplet. Voltages applied to the charging cell and removed after less than three memory locations may not charge any drop.

### **7.5.1. Synchronous Operation and Encoder Resolution**

The signal source for synchronous operation is the linear encoder on the fast axis. The encoder used puts out a signal (after quadrature decoding) with a period equal to the time that it takes the readhead to move 1 micron. The frequency of this output signal thus depends on the speed at which the carriage is travelling according to

$$f = \frac{\text{speed}}{10^{-6} \text{ m}} \quad (7.1)$$

Thus, at a speed of 1 meter per second, this frequency is 1 MHz. The droplet and charge voltage timing signal is obtained by dividing this encoder output signal by the desired factor. For example, for a 50 kHz droplet frequency at a speed of 1 meter per second, the 1 MHz encoder output signal would have to be divided by a factor of 20.

In order to have a high resolution of available droplet frequencies at a given speed of no more than a few kHz, it is necessary that the output of the encoder be of many times higher frequency than the desired droplet frequency. Table 7.1 shows the available droplet frequencies at speeds of 0.001 m/s, 1 m/s, 1.5 m/s and 2 m/s using a 1 micron resolution encoder. Table 7.2 presents options available in terms of velocities available for a given frequency, for frequencies of 500Hz, 1kHz, 40 kHz and 50kHz.

As noted on Figure 7.4, the droplet excitation output from the multifunction signal card, generated by dividing the encoder signal, can be either a toggle mode output or a pulse mode output. A toggle mode output is always a square wave, which is preferable for driving a continuous-jet printhead. However, only even divisors (2, 4, 6, etc.) of the encoder signal are available with toggle mode output. With pulse mode output, all divisors are available, but the duration of the high portion of the cycle is equal to the time it takes the encoder to travel 1 micron, regardless of the output frequency. Thus, at a speed of 1 m/s (encoder signal frequency of 1 MHz) and an output frequency of 100 kHz, the duty cycle of the output would be 10 %. To achieve ~50% duty cycle with pulse mode output and a divisor other than 2, it will be necessary to drive a monostable multivibrator ("one-shot") or a similar circuit from the output signal. At the time of writing of this thesis, such a circuit had not been implemented.

Divisor	0.001 m/s	1 m/s	1.5 m/s	2 m/s
1	1000	1000000	1500000	2000000
2	500	500000	750000	1000000
3	333	333333	500000	666667
4	250	250000	375000	500000
10	100	100000	150000	200000
11	91.0	90909	136364	181818
12	83.0	83333	125000	166667
13	77.0	76923	115385	153846
14	72.0	71429	107143	142857
15	67.0	66667	100000	133333
16	62.5	62500	93750	125000
17	58.8	58824	88235	117647
18	55.6	55556	83333	111111
19	52.6	52632	78947	105263
20	50.0	50000	75000	100000
21	47.6	47619	71429	95238
22	45.5	45455	68182	90909
23	43.5	43478	65217	86957
24	41.7	41667	62500	83333
25	40.0	40000	60000	80000
26	38.5	38462	57692	76923
27	37.0	37037	55556	74074
28	35.7	35714	53571	71429
29	34.5	34483	51724	68966
30	33.3	33333	50000	66667
31	32.3	32258	48387	64516
32	31.3	31250	46875	62500
33	30.3	30303	45455	60606
34	29.4	29412	44118	58824
35	28.6	28571	42857	57143
36	27.8	27778	41667	55556
37	27.0	27027	40541	54054
38	26.3	26316	39474	52632
39	25.6	25641	38462	51282
40	25.0	25000	37500	50000

**Table 7.1** Frequencies in Hz available at given speeds. Note that at the time of writing of this thesis, odd divisors can only be obtained with pulse mode output (non-50% duty cycle). This is due to the multifunction signal card design. The card achieves a 50% duty cycle via "toggle mode" output, in which there is a transition of the output signal on each N periods of the input signal. This effectively multiplies divisor N by 2.



Divisor	500 Hz	50000 Hz	40000 Hz	30000 Hz
1	0.0005	0.05	0.04	0.03
2	0.001	0.1	0.08	0.06
3	0.0015	0.15	0.12	0.09
4	0.002	0.2	0.16	0.12
11	0.0055	0.55	0.44	0.33
12	0.006	0.6	0.48	0.36
13	0.0065	0.65	0.52	0.39
14	0.007	0.7	0.56	0.42
15	0.0075	0.75	0.6	0.45
16	0.008	0.8	0.64	0.48
17	0.0085	0.85	0.68	0.51
18	0.009	0.9	0.72	0.54
19	0.0095	0.95	0.76	0.57
20	0.01	1	0.8	0.6
21	0.0105	1.05	0.84	0.63
22	0.011	1.1	0.88	0.66
23	0.0115	1.15	0.92	0.69
24	0.012	1.2	0.96	0.72
25	0.0125	1.25	1	0.75
26	0.013	1.3	1.04	0.78
27	0.0135	1.35	1.08	0.81
28	0.014	1.4	1.12	0.84
29	0.0145	1.45	1.16	0.87
30	0.015	1.5	1.2	0.9
31	0.0155	1.55	1.24	0.93
32	0.016	1.6	1.28	0.96
33	0.0165	1.65	1.32	0.99
34	0.017	1.7	1.36	1.02
35	0.0175	1.75	1.4	1.05
36	0.018	1.8	1.44	1.08
37	0.0185	1.85	1.48	1.11
38	0.019	1.9	1.52	1.14
39	0.0195	1.95	1.56	1.17
40	0.02	2	1.6	1.2
41	0.0205		1.64	1.23
42	0.021		1.68	1.26
43	0.0215		1.72	1.29
44	0.022		1.76	1.32
45	0.0225		1.8	1.35
46	0.023		1.84	1.38
47	0.0235		1.88	1.41
48	0.024		1.92	1.44
49	0.0245		1.96	1.47
50	0.025		2	1.5

**Table 7.2.** Speeds in m/s available at given frequencies

### **7.5.2 Synchronous Operation and Droplet Breakoff Timing**

The timing of droplet breakoff relative to the timing of voltage application to the charging cell is important, as the wrong timing leads to drops with the wrong charge, which are then deflected incorrectly. With synchronous operation, this timing does not change from one drop to the next. Assuring correct droplet breakoff timing therefore involves at most the insertion of a fixed delay between the rising edge of the droplet excitation signal and the transition of the charging cell voltage signal.

The breakoff timing could be tested by applying a square wave to the charging cell, at half the droplet frequency. This will result in two sharply separated streams, unless, possibly, if the breakoff timing is wrong. The delay should be varied until the maximum separation of the streams is obtained, indicating complete charging of droplets.

## **7.6 COMPUTER**

The motion controller, multifunction signal board and frame grabber are all computer plug-in boards, used with a Microsoft Windows®-based personal computer. The computer also provides storage for image data acquired. A 233 MHz Dell Dimension XPS™ model based on the Intel Pentium II processor is used.

## **7.7 SOFTWARE**

Software to provide a user interface to the machine is created using the Labview™ software package sold by National Instruments Corporation. Labview™ is a graphical programming environment, in which applications are built by connecting together icons representing underlying functions written in the C programming language.

Data values and program flow structures such as loops and case structures are likewise assembled graphically. In addition to utility Labview™ functions used in Labview™ applications in general, several families of functions specialized to the tasks being performed are used. The first such family is the set of Data Acquisition functions, used to control the multifunction signal card. These include functions to control the counters, analog outputs and digital outputs, as well as analog input functions that were not used. The C-code underlying these data acquisition functions is named NI-DAQ by National Instruments. The second family of specialized functions used were the family of Image Acquisition functions used to control the operation of the frame grabber. The C-code underlying these routines is named NI-IMAQ by National Instruments. The third family of specialized functions handles image storage, display and analysis, and are called the IMAQ Vision functions. The final family of specialized functions used were a simple set of functions to download commands to the motion controller.

Two primary application programs have been created for the impact observation station using these Labview™ functions. The first is the application that handles normal operation of the machine - a series of traverses with printing and strobing. User-defined parameters include speed, acceleration, motion control gains, drop frequency or spacing, and strobe delay. The second is an application used to perform measurement of velocity fluctuation, position error and torque values over a traverse.

## **8.0 MOTION CONTROL**

Figure 8.1 highlights the part of the electronic system that deals with motion control. The motor is run under closed loop control via linear encoder feedback to the motor controller. The electronic parts of the system are the encoder, the motion controller and the motor amplifier.

### **8.1 ENCODER**

#### **8.1.1 Signals**

The linear encoder used is the RG2 series manufactured by Renishaw plc., with a digital readhead with the model number RGH22 X. The encoder scale has a 20-micron-pitch grating. The readhead performs 5 x interpolation of the scale pitch, putting out square wave signals with a period equal to the time it takes the encoder to travel 4 microns. It puts out two such signals, 90 degrees out of phase, both differential for improved noise immunity. Quadrature decoding of the signals results in a signal with a period equal to the time it takes the encoder readhead to travel 1 micron.

A home switch is mounted at each end of the travel axis, and a limit switch output provided from the encoder readhead. The home switches are 10 mm-long magnets that drive the limit switch output line low when reached. These home switches are not "hard" limits, in that reaching them does not automatically turn off the motor.

A reference mark pulse output is also provided. This pulse is output every time the readhead passes a reference pulse actuator, another magnet mounted along the travel axis.

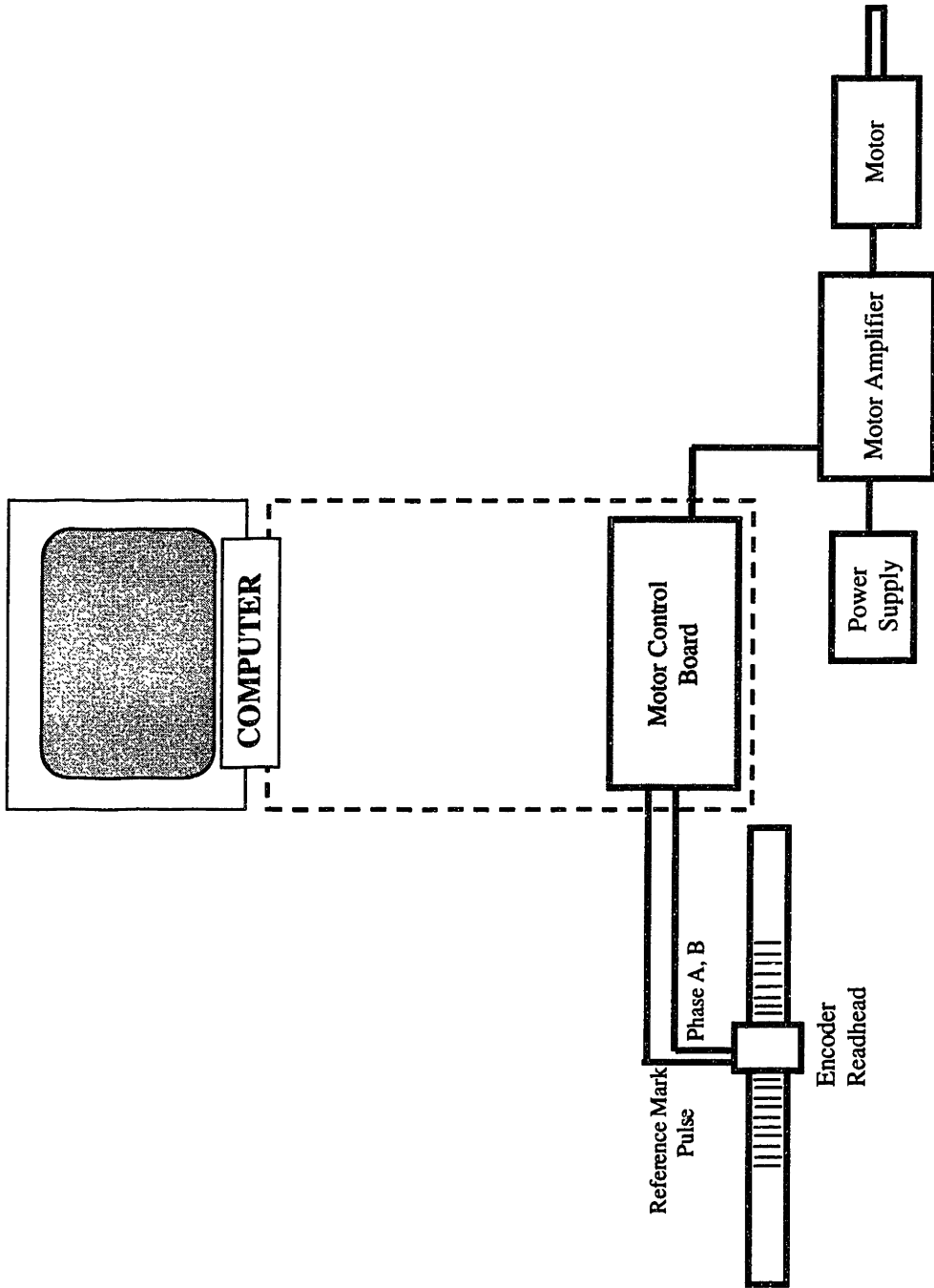


**Figure 8.1.1.** Parts of electronic system concerned with motion control

The duration of the output pulse is the time it takes the readhead to travel 4 microns, and its repeatability is 1 micron. Complete documentation of the readhead signals can be found in the Renishaw RG22 readhead installation.

### **8.1.2 Scale and Limit Switch Mounting**

The encoder scale is supplied as a flat steel tape that must be affixed to a surface parallel to the travel axis of the readhead. As mentioned before, the required parallelism of the mount surface to the travel axis is 0.002 inch ( $\pm 0.001$  inch), and the required surface finish is 125 microinches. The underside of the encoder tape is coated with an adhesive, and then covered by a paper backing. This paper backing must be removed, and the encoder tape pressed onto its mount surface. An end-plate at each end of the tape straddles the tape and is affixed to the mount surface with epoxy. The home switches and reference pulse actuator are also mounted with epoxy.

The mounting of the scale was done using the Renishaw scale applicator. This piece of equipment is mounted in the same position as a readhead would be, on the moving carriage. The carriage is then moved slowly and steadily along its travel as the tape is fed into the scale applicator. The applicator strips the paper backing from the tape and presses the tape onto the mounting surface. The limit switches and the reference mark actuator are positioned using the Renishaw readhead height-setting gauge, a small piece of plastic with slots that position the magnets correctly relative to the scale. The reference mark actuator is provided with an adjustment screw to orient the magnet properly with respect to the readhead. The scale mounting procedure is set forward in a step-by-step manner in the Renishaw RG2 scale installation guide.

### 8.1.3 Readhead Mounting

The readhead is mounted to the carriage via a two-bracket mount that allows adjustment of standoff, pitch, yaw, and roll. This mounting scheme is shown in Figure 8.2. The specified readhead standoff from the scale is 0.032 inches,  $\pm 0.004$  inches. A set-up L.E.D. and output signal is provided to indicate proper standoff and alignment. Initial mechanical setting of the offset is done using the readhead height setting gauge. From this starting point, adjustments are made while looking at the set-up indicator L.E.D. or output signal.

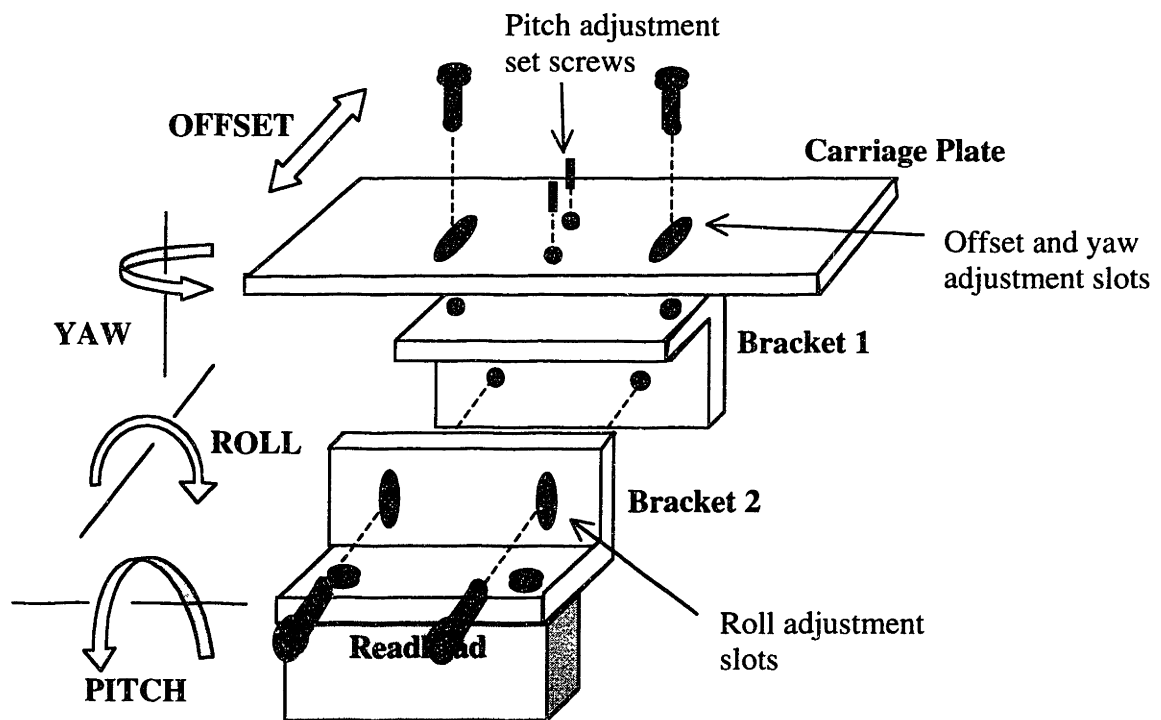


Figure 8.2. Readhead mounting scheme.

## **8.2 MOTION CONTROLLER**

The motion control board used is the DMC 1030 manufactured by Galil Motion Control Incorporated. This controller performs internal quadrature decoding of encoder inputs, and accepts either differential or single-ended inputs at up to 8 million quadrature counts per second. The output command resolution is 16 bits. It performs data gathering of position, position error, torque and other quantities, which is very useful for applications such as velocity fluctuation measurement. It will accept input from an auxiliary encoder, which in the present application could be relevant if at some point it was desired to use a rotary encoder on the motor to control the motion, while using the linear encoder to get an accurate measurement of the velocity fluctuation. It can control up to 3 motors, which can be any combination of servomotors and step motors.

The controller implements full proportional-integral-derivative control, with settable proportional, integral and derivative gains. Motion profile smoothing and torque limiting are also provided. The servo loop time of the encoder has a minimum value of 500 microseconds, and can be increased in increments of 125 microseconds up to a maximum of 20,000 microseconds.

Complete documentation of the motion controller can be found in the Galil DMC 1000 manual.

## **8.3 AMPLIFIER**

The amplifier used is the AMP 1120 from Galil Motion Control and is a twin amplifier (two amplifiers in a single package, for two motors). It is a pulse-width-modulated amplifier for brush-type servomotors. Its PWM frequency is 30 KHz, and it



has a gain of 1 amp/volt. It has an output voltage range of up to 24 volts and current rating of 6 amps continuous and 10 amps peak.

## **9.0 PRINTING AND IMAGING**

Figure 9.1 highlights the parts of the electronic system that deal with the generation of printing and imaging signals. The centerpiece of the system is a flexible PC-based multifunction signal card purchased from National Instruments Incorporated, the PCI-MIO-16E-1. The system can be looked at in terms of five sets of signals: the encoder inputs to the multifunction signal card, the drop excitation output from the card, the drop charge output, the frame grabber trigger output and the strobe trigger output.

### **9.1 ENCODER SIGNALS FOR PRINTING AND IMAGING**

The encoder output is the timing signal for the multifunction board and all of its outputs. The use of the encoder signal to derive the droplet generation signal places a requirement on the resolution of the encoder, discussed earlier in section 7.5. A quadrature decoder chip is used to get the full encoder system resolution from the two encoder phases put out by the encoder readhead. A third encoder output, a pulse that occurs when the readhead passes a reference mark at a specific location in its travel, is used to gate the output signal from the multifunction signal card.

#### **9.1.1 Quadrature Decoder Chip**

Figure 9.2 shows the circuit used to combine the two phases of the encoder output signal into a single signal four times higher in frequency. The decoding is done by a single chip, the LS 7084 from LSI Computer Systems Incorporated, which puts out four pulses for each period of either encoder input phase. The output pulse width is set by resistor R1 and capacitor C1 according to Figure 9.3.

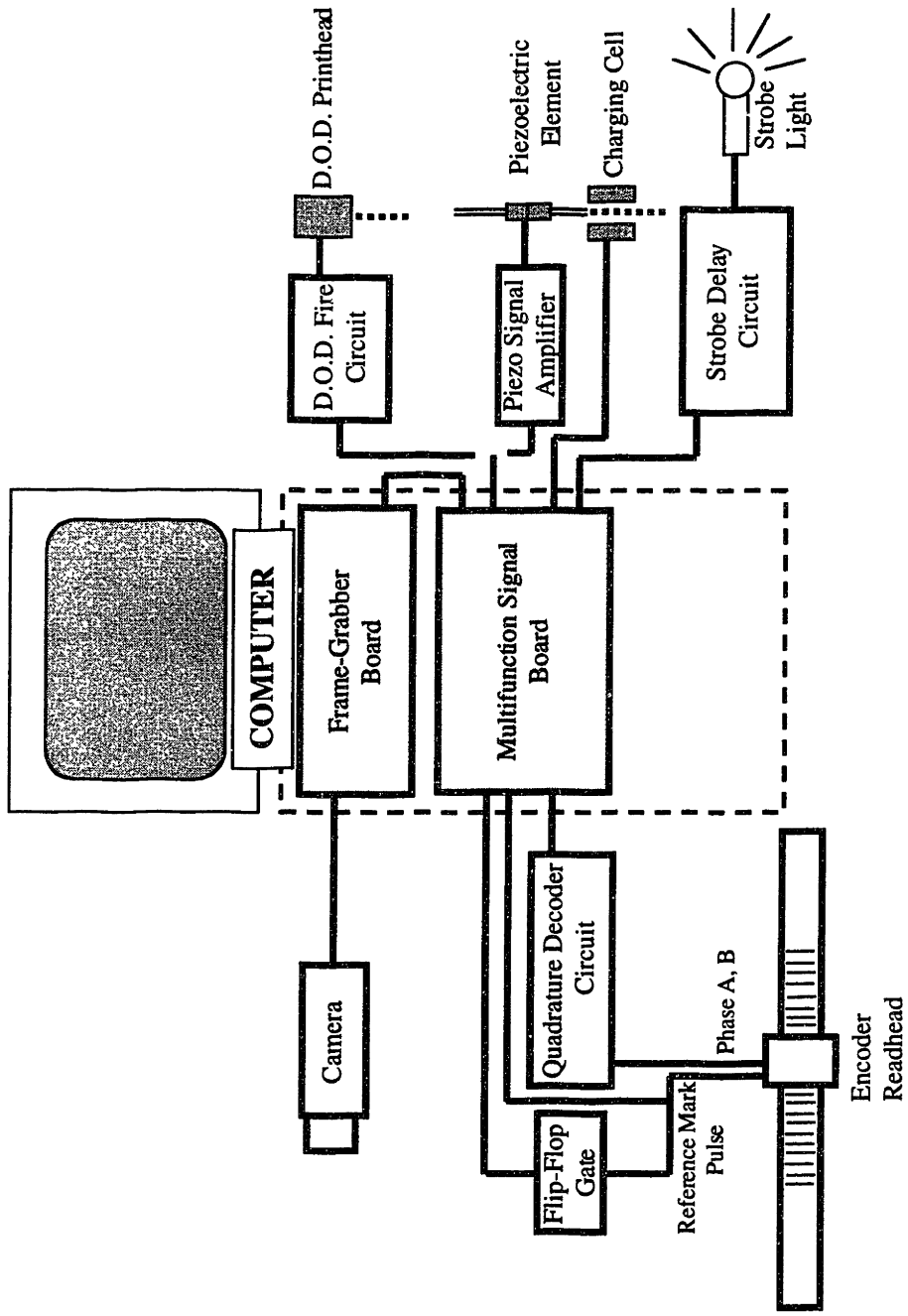


**Figure 9.1.** Parts of the electronic system related to printing and imaging

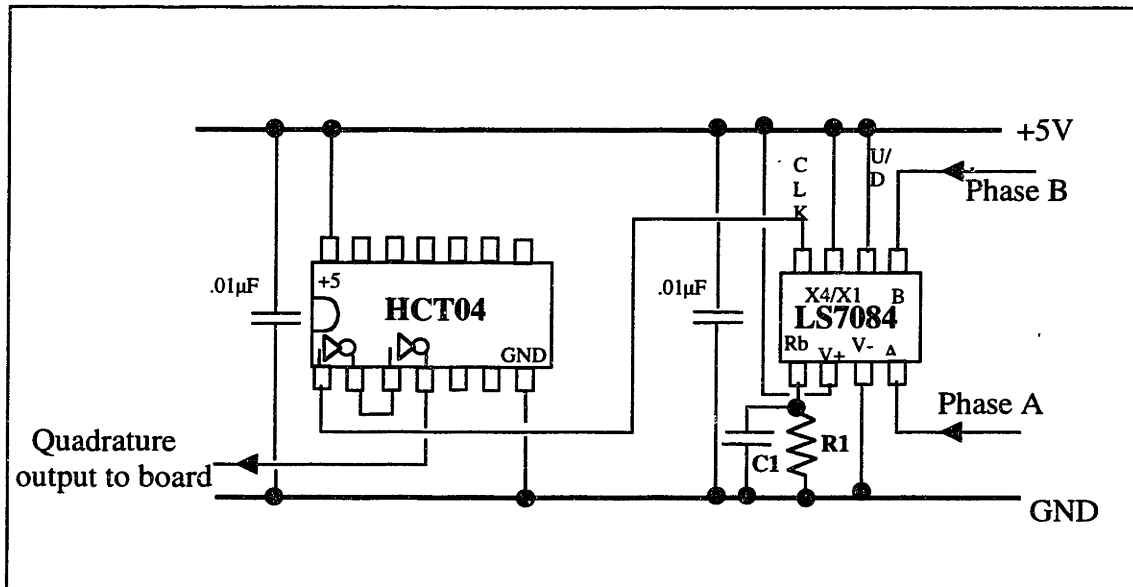


Figure 9.2. Quadrature decoding circuit

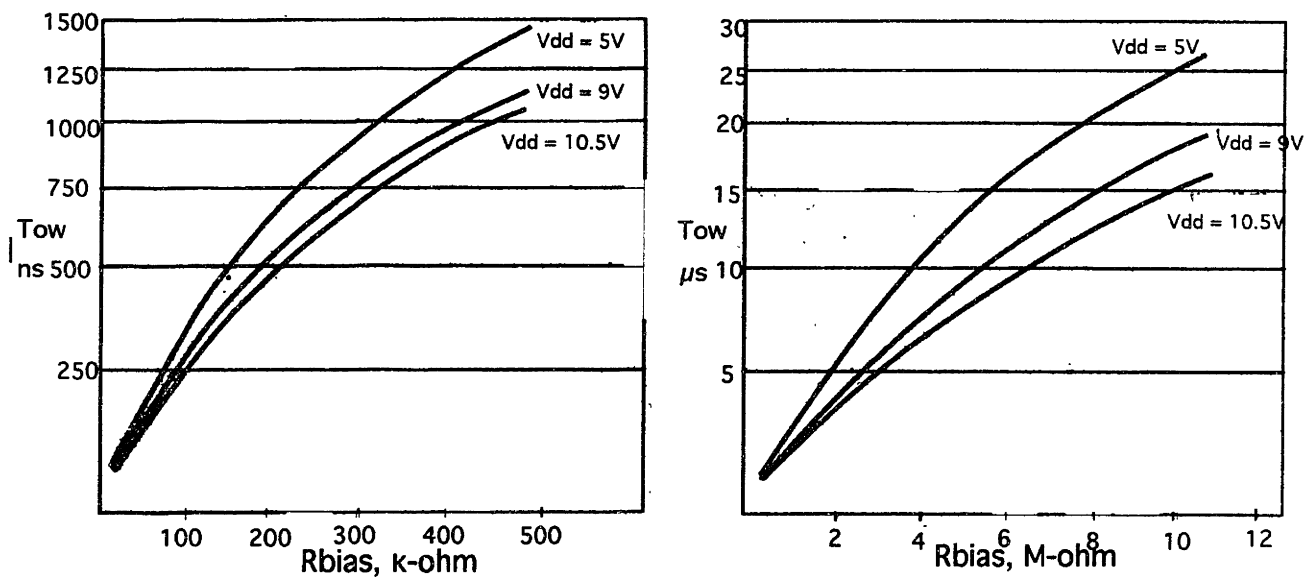


Figure 9.3. Output pulse width (Tow) versus R1 (Rbias).

The output from the 7084 is inverted twice by CMOS inverters before being sent to the multifunction card. This was found to be necessary for reliable operation of the multifunction signal card, perhaps due to the elimination of some noise, though this was not clear.

## **9.2 DROP EXCITATION**

A counter on the multifunction signal board is used to divide the incoming encoder signal to produce a droplet excitation signal of the desired frequency. The divisor is software-determined, according to the droplet frequency specified by the user. For example, suppose that the carriage is moving at 0.5 meters per second and thus sending a 500 kHz signal to the multifunction board. If the user selects a droplet frequency of 50 kHz, a divisor of 10 is used. As explained in section 7.5, the available divisors depend on the output mode chosen for the droplet excitation signal. For a toggle mode output only even divisors are available, while all divisors are available for pulse mode output. For accurate droplet registration from pass to pass, it is necessary that the counter that does this dividing start counting at the same exact point on each pass. This is achieved by using software commands to set the counter to start counting when a gate input signal goes high. The gate signal is derived from the encoder reference pulse using a bistable multivibrator, commonly referred to as a “flip-flop”. The counter is stopped at the end of each pass via a software command.

## 9.2.1 Flip-Flop Gate

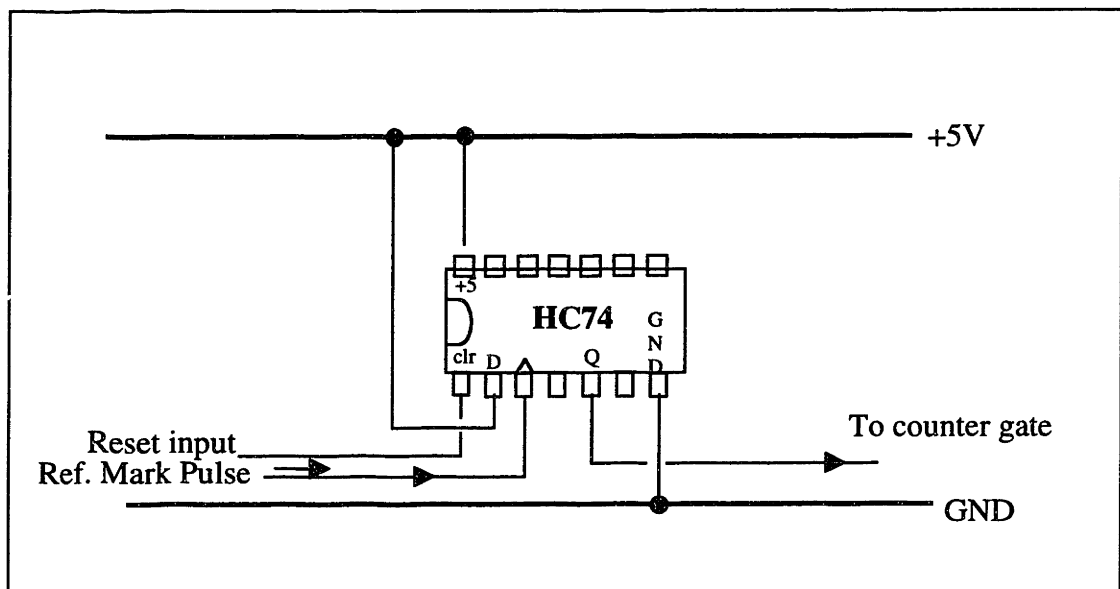


Figure 9.4. Flip-flop gate circuit.

Figure 9.4 shows the circuit used to provide the gate signal to the counter. When a transition from low to high is received on the **clock** pin, the voltage on the **D** pin (+5 Volts) is transferred to the **Q** output. This transition occurs when the reference mark is passed on the encoder scale and a pulse put out by the readhead. The location of this rising edge is quoted to be repeatable to within 1 micron. Output **Q** of the flip-flop remains high, allowing the counter to continue counting, until a low-going pulse is applied to the **reset** pin. This is done by a digital output from the multi-function card in-between passes.

### **9.3 DROP CHARGING**

For continuous-jet printing, before each pass an array with the same number of elements as there are drops in a pass is loaded with the voltage values that are to be applied to the charging cell of the printhead. These analog voltages are put out during the pass from an analog output channel of the multifunction card, a new voltage being clocked out for each high-going edge of the droplet excitation signal. The drop-charging signal is set via software to begin on receipt of the reference mark pulse by the multifunction card, which is the same time that the droplet excitation signal begins.

### **9.4 STROBE TRIGGERING**

Like the drop charging signal, the strobe triggering signal is put out on an analog output channel of the multifunction signal card. The voltage level of the triggering pulse controls the magnitude of the delay that occurs between the time when the trigger pulse is put out and when the strobe flashes, as will be explained in subsection 9.4.1. The array of voltage values put out on this analog channel is loaded before the pass such that the strobe flash occurs for the desired droplet. As with the drop-charging signal, the analog output is set to begin on receipt of the reference mark pulse from the encoder.

#### **9.4.1. Strobe Delay Circuit**

Figure 9.5 shows a diagram of the circuit used to interpose a controllable delay of several microseconds between the rising edge of the strobe trigger signal and the occurrence of a strobe flash. The two inputs to this circuit are the drop excitation signal ("Piezo") and the strobe trigger pulse. Whenever the drop excitation signal goes high, the

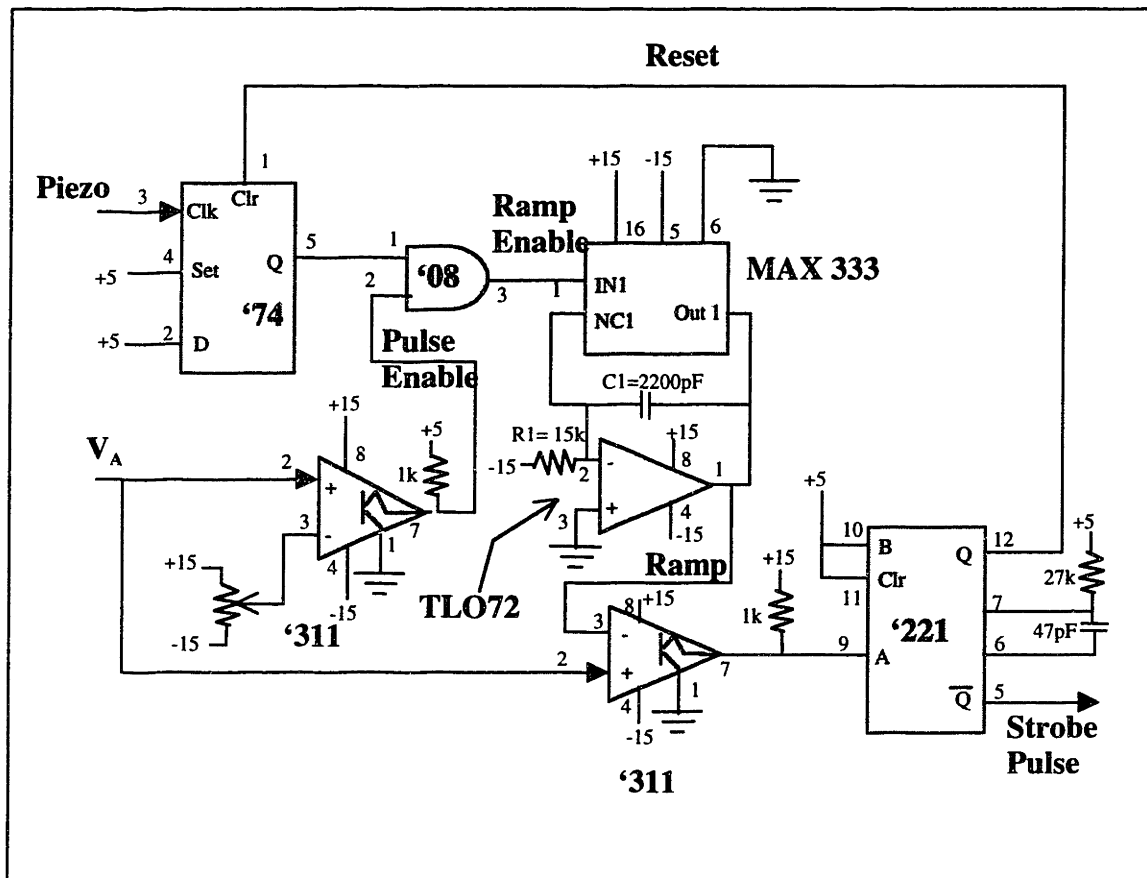


Figure 9.5. Strobe delay circuit.

output of the flip-flop goes high. If the level of the strobe trigger input ( $V_A$ ) is above the voltage at the inverting input of the pulse enabling comparator (currently set to zero volts using a potentiometer), the high output of the flip-flop enables the ramp generator to start. The voltage output of the ramp generator increases until it is equal to the strobe trigger voltage ( $V_A$ ) level. The current ramp rate is 0.5 volts per microsecond, giving a 10-volt rise over 20 microseconds. Ten volts is the maximum voltage of the strobe trigger pulse



that can be put out by the multifunction signal card. When the ramp voltage reaches the strobe trigger voltage level, a pulse is put out which fires the strobe. At the same time a low-going reset pulse is sent to clear the flip-flop. Thus, a strobe flash occurs only when the strobe trigger line goes above zero and occurs after a delay after droplet excitation that depends on the voltage level of the strobe trigger pulse. Note that if the droplet period is greater than 20 microseconds, the ramp rate must be changed (by changing R1 and/or C1) for all phases in the droplet cycle to be available for imaging.

## **9.5 FRAME GRABBER TRIGGERING**

The frame grabber used is a black-and-white PC-based board, the PCI-IMAQ-1408 from National Instruments. Whenever this receives a trigger pulse, it grabs the next incoming video frame (or series of frames, if programmed to do so) from the camera.

The trigger signal is generated by a second counter on the multifunction signal card. It is timed to occur so that each frame grabbed from the camera contains a strobe flash. The camera currently used has a frame period of 33 milliseconds. Each frame consists of two fields, each 16.6 milliseconds long. When triggered, the frame grabber grabs the next two fields that it sees. The frame grab trigger is therefore timed to occur between 17 and 33 milliseconds before the strobe flash, to assure that the strobe flash occurs during one of the two grabbed fields. Because the camera being used cannot be synchronized with the rest of the system, there is a chance that the strobe flash will occur during the short period in each frame when the camera is not collecting video information. The horizontal blanking period after each line is 11.7  $\mu\text{s}$  out of a total line period of 62.2  $\mu\text{s}$ , and the vertical blanking time at the end of each field is 1.35 ms out of

a total field period of 16.6 ms. The probability of the strobe flash occurring when the camera is actively grabbing video is thus:

$$\text{Pr.} = 100\% \times \left[ \left( 1 - \frac{1.35}{16.6} \right) \left( 1 - \frac{11.7}{62.2} \right) \right] = 74.6\% \quad (9.1).$$

It has indeed been found that the frame grabber occasionally grabs a blank image, but systematic data for the percentage of time that this occurs have not been gathered. It is worth noting that this problem is not related to the fact that the camera is an interlace camera: any video camera that cannot be synchronized with the rest of the system will suffer from this problem.

## **9.6 CAMERA**

The camera being used is the MicroMac-VA by Techni-Quip Corporation. It is a CCD camera with a 610-by-488 pixel array. It puts out interlaced analog video in the NTSC format, with a frame duration of 33 milliseconds. However, it has been found to produce clearer pictures when run with a CCIR camera interface, rather than with the NTSC interface.

The interlaced nature of the camera has significant implications for strobe-illuminated images. The strobe flash falls in just one of the two fields of a frame, so only every other line in a frame is illuminated, the remainder being black.

## **9.7 FRAME GRABBER**

The frame grabber being used is the PCI-IMAQ-1408 from National Instruments. It is an 8-bit monochrome frame grabber for analog cameras. It is reported by National

Instruments to operate at up to 20 frames per second (640 pixels x 480 pixels) while being run from the Labview™ environment. It is specified to perform at 30 frames per second for NTSC and RS-170 video formats and at 25 frames per second for CCIR-601 and PAL video formats, but this full performance is not achieved while running under Labview™. In its present application, it is being used at low imaging rates, such as for snapping a single image per pass. The frame grabber can accept up to four video inputs and has seven trigger lines.

## 10.0 TESTS OF OPERATION

This chapter presents the results of the various tests of operation of the observation station. These tests include tuning of the motion controller gains, measurement of velocity ripple, a test to assure that the encoder was not losing counts, a test on the repeatability of strobing, a test on the operation of the strobe delay circuit, and a test on driving a continuous-jet printhead.

### 10.1 GAINS TESTING

The motion controller offers proportional, integral and derivative gain control. The values of these parameters used were selected in accordance with the procedure prescribed by the manufacturer: with the carriage stationary, and with KI and KP 0, KD was increased until the motor began to vibrate, and then reduced slightly. KP was then increased likewise, and finally KI was increased. The motion of the carriage was then tested, and the gains adjusted accordingly. In this way, the standard operating gains were selected to be:

$$KD = 50; KP = 1; KI = 0; \quad (10.1)$$

At high speed (2 m/s) these are the optimum gains. A KI as small as 0.1 results in oscillation of the carriage during a pass. Increasing KP prevents the carriage from reaching full speed quickly enough. Setting KP to zero results in runaway following error. Increasing KD is observed to prevent the motion from getting up to speed quickly

enough, and at  $KD = 65$  the motor starts to vibrate. Decreasing  $KD$  increases velocity overshoot and thus velocity ripple.

At 0.5 m/s, the best performance is achieved with the same  $KD$  and  $KI$ , but with  $KP$  equal to 15. At this lower speed, the increased time to full speed due to the increased value of  $KP$  is not a concern. As  $KP$  is increased from 1, velocity ripple drops gradually, dropping by 30-40% at  $KP = 15$ . As  $KP$  is increased further, velocity ripple creeps back up. At  $KP = 30$ , the motor begins to vibrate. The results of the gains testing are summarized in Table 10.1.

Speed	Optimum $KD$	Optimum $KP$	Optimum $KI$
2.0 m/s	50	1	0
0.5 m/s	50	15	0

**Table 10.1.** Result of gains testing.

The selection of gains described above was done with acceleration set to  $5 \text{ m/s}^2$ , the torque limit at the maximum value of 9.998 V, the servo loop time at the minimum value of  $500 \mu\text{s}$ , and motion smoothing factor  $IT = 0.02$ .

Gains are set by the user on the Labview™ "front panel" that constitutes the user interface for the machine. These are set independently of velocity, acceleration, torque limit, etc., to allow for alterations to the machine that may change the optimum gains.

## 10.2 VELOCITY RIPPLE

Velocity fluctuations or 'ripple' lead to drop placement errors. The velocity ripple during the central, flat portion of a pass was measured at four different speeds. The results are presented in Table 10.2. Also presented in Table 10.2 are the corresponding position errors that would result from a droplet time-of-flight of 3 milliseconds. All of these measurements were done with gains of  $KD = 50$ ,  $KP = 1$  and  $KI = 0$ , acceleration of  $5 \text{ m/s}^2$ , a servo loop time of  $500 \mu\text{s}$ , and torque limit at the maximum. For operation at 2 m/s, motion profile smoothing factor IT was set equal to 0.017, while for all lower speeds it was set equal to 0.02.

Speed (m/s)	Ripple (m/s) [max. - min.]	Drop Placement Error ( $\mu\text{m}$ ) For TOF of 3 ms
0.1	.002	6
0.5	.006	18
1.0	.007	21
1.5	.007	21
2.0	.005	15

**Table 10.2.** Measured velocity ripple

The ripple was observed to have a wavelength of approximately 7 cm, independent of velocity. The circumference of the drive pulley at the cable centerline is 5.2 cm, suggesting that this is not the primary source of ripple. Furthermore, the runout on the drive pulley is only 0.0008 inches, 0.048% of the cable wrap diameter of 1.67 inches. At 2 m/s, for example, this would result in a velocity ripple of 0.001 m/s.

### 10.3 TEST OF ENCODER COUNTING: REPOSITIONING TEST

It was important to determine that the encoder was neither losing counts nor getting extra counts (due to vibration). To make this determination, the following test was conducted: A set of crosshairs was mounted on the moving carriage. The crosshairs consisted of two 20-micron-thick fibers glued (potted) onto a glass slide. These were brought into focus under the camera, and the position of the center of the crosshairs in the frame determined by image analysis. Each pixel corresponded to approximately 1.25 microns. The position of the carriage along the travel axis was recorded. The carriage was then moved away from the focus position and back. The crosshair center within the frame and the position of the carriage were again recorded. This procedure was repeated 5 times. An acceleration and deceleration of  $5\text{m/s}^2$  were used. The commanded top velocity for the moves was 2 m/s, but each move was only about 0.5m long, so this top velocity was not reached. The data recorded are presented in Table 10.3.

Crosshair position (microns)	Crosshair position variation (microns)	Reported carriage position (microns)	Carriage position variation (microns)
383.75		601313	
390.0	+6.25	601321	+8
348.75	-35	601286	-27
373.75	-10	601304	-9
393.75	+10	601320	+7

**Table 10.3.** Repositioning test #1 data.

The image analysis routine used determined the crosshair center position as follows: A line in the image parallel to the travel axis was selected. In such a line, all the pixels are light except for those located where the line crosses the crosshair. A user-

selected intensity threshold was used to determine where the edges of the crosshair were. The average of these two values was taken as the crosshair center position. This routine, with improvements that have been made since the time of this test, is documented more thoroughly in Appendix D.

It is seen from the data that

- There is a correspondence between the carriage position variation and the crosshair position variation.
- There is no trend in the crosshair position data.

These two observations indicate that the encoder is not losing counts or taking extra counts.

The repositioning test was repeated with modification of the motion such that there would be zero reported carriage position variation. This was done by inserting a wait of a few seconds with a finite integral gain between the end of each pass and the taking of a picture. The crosshair used for this and further tests was a microscope crosshair reticle from Edmund Scientific, with a line width of 20 microns, and the camera resolution for this and further tests was 1.03 microns per pixel. The commanded maximum velocity used this time was 0.5 m/s and thirty data points were taken. The recorded data are shown below in Table 10.4. The reported variation in the *transverse* crosshair position is also presented. The data confirm that counts are not being lost, and demonstrate the ability of the machine to precisely position an object carried on the moving carriage. The resolution demonstrated is about 4 microns, but if the first four data points are neglected, the resolution demonstrated is essentially the resolution of the



encoder. It has been observed in such tests of the machine that it is often the case that the first few data points deviate from the remainder, but the reason for this is not known.

Trial	Travel Axis Crosshair Center (microns)	Transverse Axis Crosshair Center (microns)
1	327.9	102.6
2	328.4	105.0
3	330.1	106.2
4	330.1	106.0
5	331.6	106.4
6	331.3	107.2
7	331.5	107.1
8	331.1	107.2
9	331.3	106.4
10	331.9	106.7
11	331.7	106.9
12	331.6	106.9
13	331.2	106.7
14	331.5	107.1
15	331.5	106.5
16	331.4	106.9
17	331.5	106.9
18	331.5	106.2
19	331.3	106.4
20	331.4	106.9
21	331.3	106.7
22	331.6	106.3
23	331.4	106.8
24	331.2	106.5
25	331.6	106.3
26	331.4	106.8
27	331.7	106.9
28	331.8	107.0
29	331.6	106.3
30	331.4	106.7
<b>Max. - Min.</b>	4.0	4.6
<b>Max. - Min., neglecting first four data points</b>	0.8	1.0
<b>Standard Deviation</b>	0.89	0.84

**Table 10.4** Repositioning test #2 data.

The observed repeatability in the transverse direction is the same as in the travel direction, suggesting that variations may be due to variation in the image quality and image analysis, rather than to position error of the carriage. The magnitude of transverse direction error also indicates that the air bearings are performing well in this regard.

To determine the magnitude of the errors stemming from variation in the image quality and image analysis, a series of strobed images of crosshairs with the carriage sitting in place, held at a constant location by the motor (integral gain applied) was taken and analyzed. Fifteen images were snapped and analyzed. The reported crosshair centers are shown in Table 10.5.

Trial	Travel Axis Crosshair Center (microns)	Transverse Axis Crosshair Center (microns)
1	106.8	331.3
2	106.7	330.3
3	106.9	330.2
4	106.7	330.1
5	106.4	328.4
6	106.4	329.6
7	106.4	330.1
8	106.6	328.4
9	106.8	329.9
10	106.6	330.0
11	106.2	329.5
12	106.2	328.4
13	106.5	329.5
14	106.0	329.8
15	106.5	331.4
<b>Max. - Min.</b>	0.9	3.0
<b>Standard Deviation</b>	0.25	0.88

**Table 10.5.** Repeatability of image analysis.

It is seen from the data that the reported variation in crosshair position in the test reported in Table 10.4 is within the range of variation due to image quality and analysis reported in Table 10.5.

**10.4. STROBING MOVING CROSSHAIRS: REPEATABILITY OF STROBE FLASH TIMING**

The next test of the machine's operation done was to strobe the crosshairs while they were in motion. This measured the repeatability of the location of a strobe flash within a pass. Tests were done at 0.02 m/s, 0.5 m/s and 2.0 m/s. The data gathered are presented in Tables 10.6, 10.7 and 10.8. It is seen that the repeatability is around 2-3 microns.

Trial	Travel Axis Crosshair Center (microns)	Transverse Axis Crosshair Center (microns)
1	117.6	376.2
2	117.4	376.2
3	117.2	376.2
4	117.5	376.0
5	117.0	376.2
6	117.1	378.0*
7	117.7	376.2
8	117.6	376.1
<b>Max. - Min.</b>	0.6	2.0
<b>Standard Deviation</b>	0.24	0.61

\* Investigation of the strobed image and its treatment by the image analysis routine traced the cause of this outlying data point to the image quality and analysis.

**Table 10.6.** Strobing crosshairs moving at 0.02 m/s.

Trial	Travel Axis Crosshair Center (microns)	Transverse Axis Crosshair Center (microns)
1	124.3	371.0
2	123.8	371.1
3	124.6	371.0
4	124.1	371.1
5	123.6	371.1
6	124.6	370.9
7	124.1	371.1
8	124.0	371.0
9	123.7	371.0
10	124.1	371.1
<b>Max. - Min.</b>	1.0	0.2
<b>Standard Deviation</b>	0.32	0.07

**Table 10.7.** Strobing crosshairs moving at 0.5 m/s.

Trial	Travel Axis Crosshair Center (microns)	Transverse Axis Crosshair Center (microns)
1	124.1	377.9
2	126.9	376.3
3	126.1	375.9
4	125.2	376.3
5	125.9	376.1
6	125.3	376.2
7	125.8	376.5
8	124.9	376.1
9	125.3	376.1
10	126.6	375.9
<b>Max. - Min.</b>	2.8	2.0
<b>Standard Deviation</b>	0.78	0.55

**Table 10.8.** Strobing crosshairs moving at 2.0 m/s.

There is some variation in the delay between the application of a trigger pulse to the strobe light and the occurrence of the strobe flash. This variation is called *jitter*.

Prolonged observation of the behavior of the stroboscope, using a photodetector and an oscilloscope revealed a jitter of 1.8  $\mu\text{s}$ . This corresponds to a variation in travel axis crosshair position of 0.036  $\mu\text{m}$  at 0.02 m/s, 0.9  $\mu\text{m}$  at 0.5 m/s and 3.6  $\mu\text{m}$  at 2.0 m/s. Jitter

is a probable source of source of some of the position variation observed, and the increase of variation with speed may be due to this. However the observed crosshair position variation at 0.02 m/s is more than can be explained by strobe jitter, so this is not the only source of variation.

### 10.5 STROBING MOVING CROSSHAIRS: TEST OF STROBE DELAY

The next test done was on the operation of the strobe delay scheme. For a given voltage input to the strobe delay circuit, a set of ten passes was done at 1.0 m/s. Seven different delay voltages were tested. The recorded data are shown in Table 10.9. It is seen that the strobe delay scheme does indeed function as intended, with a delay of between 2 and 3 microseconds per volt. At 1.0 m/s, strobe jitter results in a maximum crosshair position variation of 1.8  $\mu\text{m}$ , which could be a significant portion of the observed variation.

Delay Voltage (Volts)	Average Crosshair Travel Axis Center (microns)	Max. - Min. (microns)	Standard Deviation (microns)
2.5 [0]	308.2 [0]	3.65	0.95
3.0 [+0.5]	309.0 [+0.8]	2.79	0.84
3.5 [+1.0]	310.6 [+2.4]	2.72	0.97
4.5 [+2.0]	312.9 [+4.7]	2.43	0.81
5.0 [+2.5]	315.5 [+7.3]	3.83	1.10
5.5 [+3.0]	316.9 [+8.7]	2.00	0.72
6.6 [+4.1]	321.6 [+13.4]	1.99	0.57

**Table 10.9.** Testing of strobe delay.

### 10.6 SYNCHRONOUS GENERATION OF DROPLETS

The use of the encoder output to generate the droplet excitation signal was tested on a continuous jet of water. The droplet excitation signal was amplified to 20-35 V

peak-to-peak by a Krohn-Hite model 7500 amplifier, and applied to the piezoelectric element exciting breakoff. A pressure of 25 psi was used to force the water through a 5-micron (pore-size) filter and a 50-micron-diameter nozzle. The shortest breakoff length was found to occur at an excitation frequency between 30 kHz and 40 kHz.

The first test done was the excitation of droplets with square waves of various duty cycles, using a function generator to generate the square waves. This was done to investigate the feasibility of using pulse mode output from the multifunction signal card, which makes all divisors available but gives a non-50% duty cycle. It was found the cleanest and shortest breakoff was obtained with a 50% duty cycle, the condition of the breakoff worsening as the waveform asymmetry increased.

Next, toggle mode output from the multifunction signal card was used to drive the piezo (via the amplifier). The droplet excitation signal had a frequency of 40 kHz. The first observation made was that velocity ripple showed up as a roughly 300 Hz variation of the droplet excitation frequency. This caused oscillation of the drop position observed on a television monitor, apparently due to breakoff length variation. The second observation made was that ghost images of droplets were observed on the screen. The droplet excitation signal was observed to have jitter corresponding to the appearance of ghost images. This jitter was worse at 0.16 m/s, where the 40 kHz signal was obtained using a divisor of 4, than at 1.2 m/s where the divisor was 30. Using a function generator to take the place of the encoder input to the multifunction signal card resulted in a droplet excitation signal with no jitter and an absence of ghost images. Observation of the encoder output (both phases) on an oscilloscope confirmed that this was the source of the jitter. It was also determined that the jitter was worst where the readhead was most poorly

aligned, and that the jitter could be reduced by improved alignment. At present, the jitter causes ghost images displaced from the dominant droplet location by about 1 droplet diameter at a speed of 0.16 m/s. As the speed is increased, the deviation of the ghost images from the dominant droplet location is reduced.

## 10.7 STROBING DROPS

The capability of the station to grab strobe-illuminated images of generated droplets was tested, and confirmed to be operational. A grabbed image is presented as Figure 10.1.

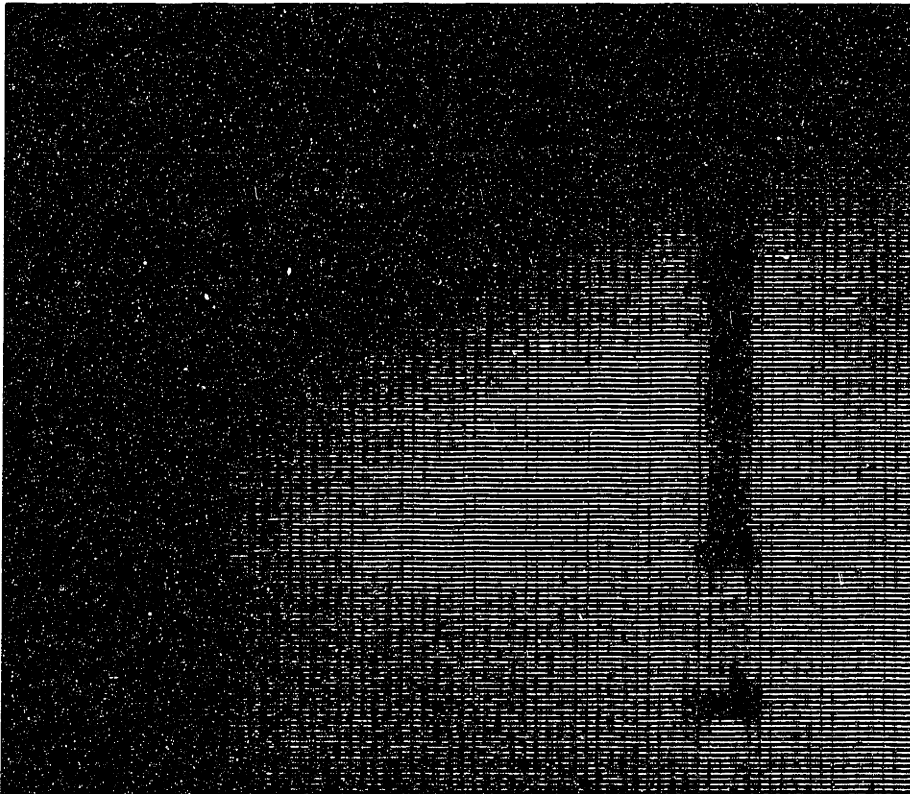


**Figure 10.1.** Grabbed image of droplet breakoff, illuminated by single strobe flash.

## **11.0 FURTHER WORK AND IMPROVEMENTS**

This chapter briefly outlines the further work that must be done to make the droplet impact observation station fully functional, and discusses improvements that may be made to parts of the station.

### **11.1 STROBING DROPS WITH PHASE DELAY**

The testing of the operation of the machine has been taken to the point of strobing and imaging drops being ejected from a continuous-jet nozzle. The next step in testing is to use the strobe delay circuit to control the phase advance between frames. The station is currently equipped to perform this task.

### **11.2 PRINTING LINES**

An aspect of the machine yet to be satisfactorily tested is printing. A few drop-on-demand lines were printed on paper before the motion and strobing aspects of the carriage had been well developed. This testing must now be repeated and completed. Continuous-jet printing must also be tested. This requires installation of a continuous-jet printhead (see next section).

### **11.3 ADDING CHARGING, DEFLECTION AND CATCHING**

Jetting has thus far been done using a continuous-jet nozzle without charging, deflection or catching (CDC). A CDC printhead must be added to the machine to make it fully functional.



## 11.4 HIGH-SPEED FRAME GRABBING

In order to perform multiple-image-per-pass imaging as described in section 2.1.2., the frame grabber currently in use must be replaced by a higher-speed model.

## 11.5 ELECTRONICS MOUNTING

The electronic components external to the computer have not yet been mounted in their permanent location on the machine frame.

## 11.6 STEEL BAND

The current drive cable in use appears thus far to be stiff enough, but only barely so. A steel band could offer higher stiffness, and it may therefore be of interest to install and test one. A 10 inch long steel band .004 inch thick and 1 inch wide would have a stiffness of

$$\frac{F}{\delta} = \frac{AE}{L} = \frac{\left(0.004in \times 1in \times 30 \times 10^6 \frac{lb}{in^2}\right)}{10in} = 12,000 \frac{lb}{in} \quad (11.1)$$

which is 4.3 times the nominal stiffness of the cable currently in use. Some form of crowning of the pulleys may have to be implemented in order to use a flat band.

## **11.7 PULLEY AND IDLER FITS**

As noted in chapter 5, the pulley and idler fits currently in place are not all correct. Correcting them requires the machining of a new drive pulley and idler. An additional fit which is not ideal is the motor mounting fit on the pulley housing. This currently has several tens of mils of clearance, whereas a fit with minimal clearance could be used to assist in accurately locating the motor. Rectifying this would require a new pulley housing.

## **11.8 PHASE DELAY CIRCUIT**

As noted in chapter 9, the phase delay circuit does not permit imaging of the full range of droplet phases if the droplet period is longer than 20 microseconds, without changing the values of R1 and C1. Conversely, for droplet periods shorter than 20 microseconds, the phase resolution (degrees per volt) decreases. Also, delays of less than a half microsecond or so do not work, as there must be a finite initial voltage difference between the terminals of the trigger pulse generating comparator for it to operate properly.

An alternate scheme that would circumvent the second of these shortcomings is shown schematically in Figure 11.1. The voltage ramp is in this case replaced by a counter, which counts down from (or up to) a value set by the voltage  $V_a$ , at a rate set by an external clock, and triggers the strobing pulse at the end of the count. If a variable clocking frequency source is used, such as a function generator, the first of the two problems with the current strobe delay circuit would also be avoided.

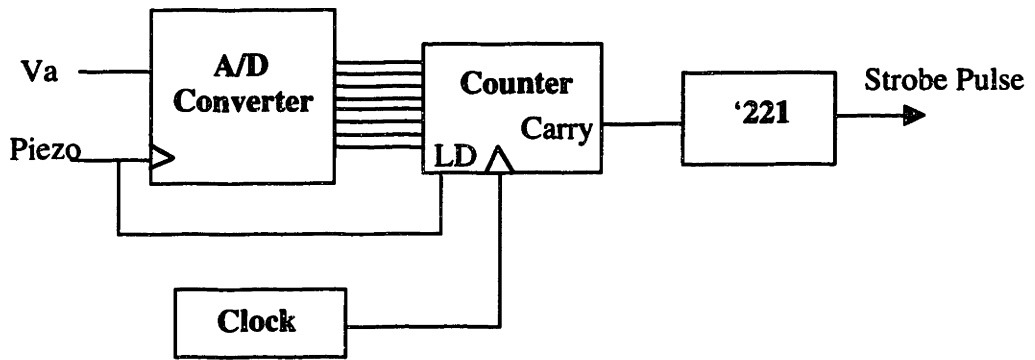


**Figure 11.1.** Alternate strobe delay scheme.

## References

Arthur, Tara L. "Factors Limiting the Surface Finish of Three Dimensional Printed Parts", MSME Thesis, MIT, June 1996.

Fan, Tailin. "Droplet-Powder Impact Interaction in Three-Dimensional Printing", Ph.D. Thesis, MIT, September 1995.

Sachs, E., Haggerty, J., Cima, M., & Williams, P., "Three Dimensional Printing Techniques", U.S. Patent #5,204,055 4/28/93.

Young, Warren C., Roark's Formulas for Stress and Strain, McGraw-Hill Book Co., New York (1989).

## Manuals

Galil Motion Control, Inc., DMC-1000 Manual, Rev. 2.0xa, Galil Motion Control Inc., Mountain View, CA (1987).

National Instruments Corp., Labview® Data Acquisition VI Reference Manual, National Instruments Corp., Austin, TX (1995).

National Instruments Corp., BridgeView™ and Labview® IMAQ™ Vision for G Reference Manual, National Instruments Corp., Austin, TX (1995).

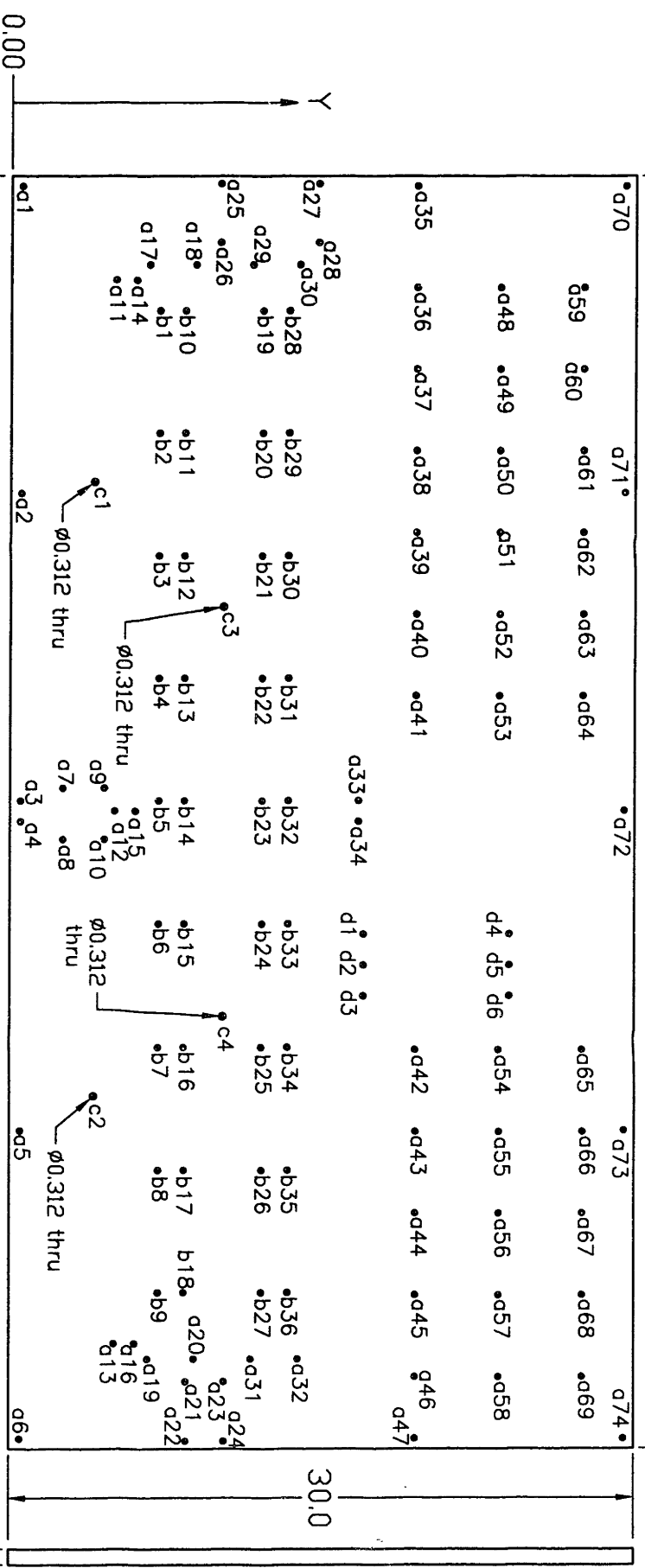
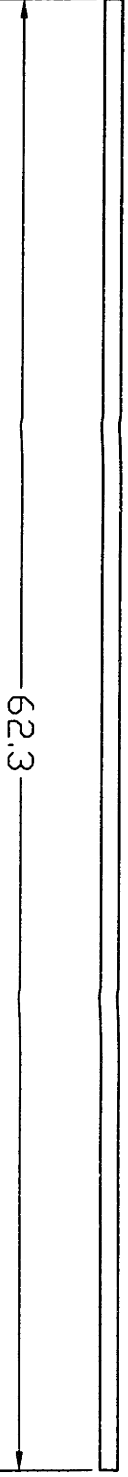
National Instruments Corp., Labview® Function and VI Reference Manual Reference Manual, National Instruments Corp., Austin, TX (1995).

National Instruments Corp., Labview® NI-IMAQ for G Reference Manual, National Instruments Corp., Austin, TX (1995).

Renishaw PLC., RG2 Encoder System Readhead RGH22 Series Installation Guide, Renishaw PLC., Gloucestershire U.K. (1997).

Renishaw PLC., RG2 Encoder System RGS-S Scale RGH22 Series Installation Guide, Renishaw PLC., Schaumburg, IL (1997).

## **APPENDIX A: MACHINE DRAWINGS**



ALL HOLES THRU

type a holes: 1/4-20 thread

type b holes: 10-32 thread

type c holes: 0.312 reamed

type d holes: drill letter l through

location of hole centers on attached table

MIT THREE-DIMENSIONAL PRINTING PROJECT  
 Ako Chijioko  
 PH: 617-253-5028 FAX: 617-253-0209  
 BASE  
 DIMENSIONS: INCHES  
 SCALE: 1:8  
 MAT'L: 3/4" ALUMINUM JIG PLATE  
 QTY: 1

TOLERANCES:  
 x.x +/- 0.100  
 x.xx +/- 0.010  
 x.xxx +/- 0.002

Rev. 3  
 8-19-97

**Table 1: 1/4-20 holes**

Hole	X	Y
a1	0.50	0.50
a2	15.56	0.50
a3	30.63	0.50
a4	31.63	0.50
a5	46.69	0.50
a6	61.75	0.50
a7	30.00	2.50
a8	32.50	2.50
a9	30.00	4.50
a10	32.50	4.50
a11	5.13	5.00
a12	31.13	5.00
a13	57.13	5.00
a14	5.13	6.00
a15	31.13	6.00
a16	57.13	6.00
a17	4.38	6.63
a18	4.38	8.88
a19	57.88	6.63
a20	57.88	8.88
a21	58.98	8.48
a22	61.88	8.48
a23	58.98	10.33
a24	61.88	10.33
a25	0.38	10.06
a26	3.28	10.06

**Table 1: 1/4-20 holes**

Hole	X	Y
a27	0.38	14.79
a28	3.28	14.79
a29	4.38	11.63
a30	4.38	13.88
a31	57.88	11.63
a32	57.88	13.88
a33	30.63	16.75
a34	31.63	16.75
a35	0.50	19.50
a36	5.50	19.50
a37	9.50	19.50
a38	13.50	19.50
a39	17.50	19.50
a40	21.50	19.50
a41	25.50	19.50
a42	42.75	19.50
a43	46.75	19.50
a44	50.75	19.50
a45	54.75	19.50
a46	58.75	19.50
a47	61.75	19.50
a48	5.50	23.50
a49	9.50	23.50
a50	13.50	23.50
a51	17.50	23.50
a52	21.50	23.50
a53	25.50	23.50



**Table 1: 1/4-20 holes**

Hole	X	Y
a54	42.75	23.50
a55	46.75	23.50
a56	50.75	23.50
a57	54.75	23.50
a58	58.75	23.50
a59	5.50	27.50
a60	9.50	27.50
a61	13.50	27.50
a62	17.50	27.50
a63	21.50	27.50
a64	25.50	27.50
a65	42.75	27.50
a66	46.75	27.50
a67	50.75	27.50
a68	54.75	27.50
a69	58.75	27.50
a70	0.50	29.50
a71	15.56	29.50
a72	31.13	29.50
a73	46.69	29.50
a74	61.75	29.50

**Table 2: # 10-32 holes**

Hole	X	Y
b1	6.63	7.13
b2	12.63	7.13
b3	18.63	7.13
b4	24.63	7.13
b5	30.63	7.13
b6	36.63	7.13
b7	42.63	7.13
b8	48.63	7.13
b9	54.63	7.13
b10	6.63	8.38
b11	12.63	8.38
b12	18.63	8.38
b13	24.63	8.38
b14	30.63	8.38
b15	36.63	8.38
b16	42.63	8.38
b17	48.63	8.38
b18	54.63	8.38
b19	6.63	12.13
b20	12.63	12.13
b21	18.63	12.13
b22	24.63	12.13
b23	30.63	12.13
b24	36.63	12.13
b25	42.63	12.13
b26	48.63	12.13

**Table 2: # 10-32 holes**

Hole	X	Y
b27	54.63	12.13
b28	6.63	13.38
b29	12.63	13.38
b30	18.63	13.38
b31	24.63	13.38
b32	30.63	13.38
b33	36.63	13.38
b34	42.63	13.38
b35	48.63	13.38
b36	54.63	13.38

**Table 3: 0.312Reamed Holes**

Hole	X	Y
c1	15.000	4.000
c2	45.000	4.000
c3	21.125	10.250
c4	41.125	10.250

**Table 4: Drill Letter Size I Holes**

Hole	X	Y
d1	37.13	17.00
d2	38.63	17.00
d3	40.13	17.00
d4	37.13	24.00
d5	38.63	24.00
d6	40.13	24.00



**Table 1: Carriage Plate Holes**

Hole #	Hole Type	X	Y
a1	#10-24 UNC-2B THRU	1.360	0.625
a2	#10-24 UNC-2B THRU	2.141	1.375
a3	#10-24 UNC-2B THRU	1.360	5.125
a4	#10-24 UNC-2B THRU	2.141	5.875
a5	#10-24 UNC-2B THRU	6.360	2.875
a6	#10-24 UNC-2B THRU	7.141	3.625
a7	#10-24 UNC-2B THRU	1.360	5.875
a8	#10-24 UNC-2B THRU	2.141	5.125
a9	#10-24 UNC-2B THRU	2.141	3.625
a10	#10-24 UNC-2B THRU	2.141	2.875
a11	#10-24 UNC-2B THRU	2.141	2.125
a12	#10-24 UNC-2B THRU	2.141	0.625
a13	#10-24 UNC-2B THRU	1.360	1.375
a14	#10-24 UNC-2B THRU	1.360	2.125
a15	#10-24 UNC-2B THRU	1.360	2.875
a16	#10-24 UNC-2B THRU	1.360	3.625
a17	#10-24 UNC-2B THRU	1.360	4.375
a18	#10-24 UNC-2B THRU	2.141	4.375
b1	#8-32 UNC-2B THRU	- 2.500	2.500
b2	#8-32 UNC-2B THRU	- 2.500	3.000
b3	#8-32 UNC-2B THRU	- 2.500	3.500
b4	#8-32 UNC-2B THRU	- 2.500	4.000
b5	#8-32 UNC-2B THRU	- 1.000	2.500
b6	#8-32 UNC-2B THRU	- 1.000	3.000
b7	#8-32 UNC-2B THRU	- 1.000	3.500
b8	#8-32 UNC-2B THRU	- 1.000	4.000

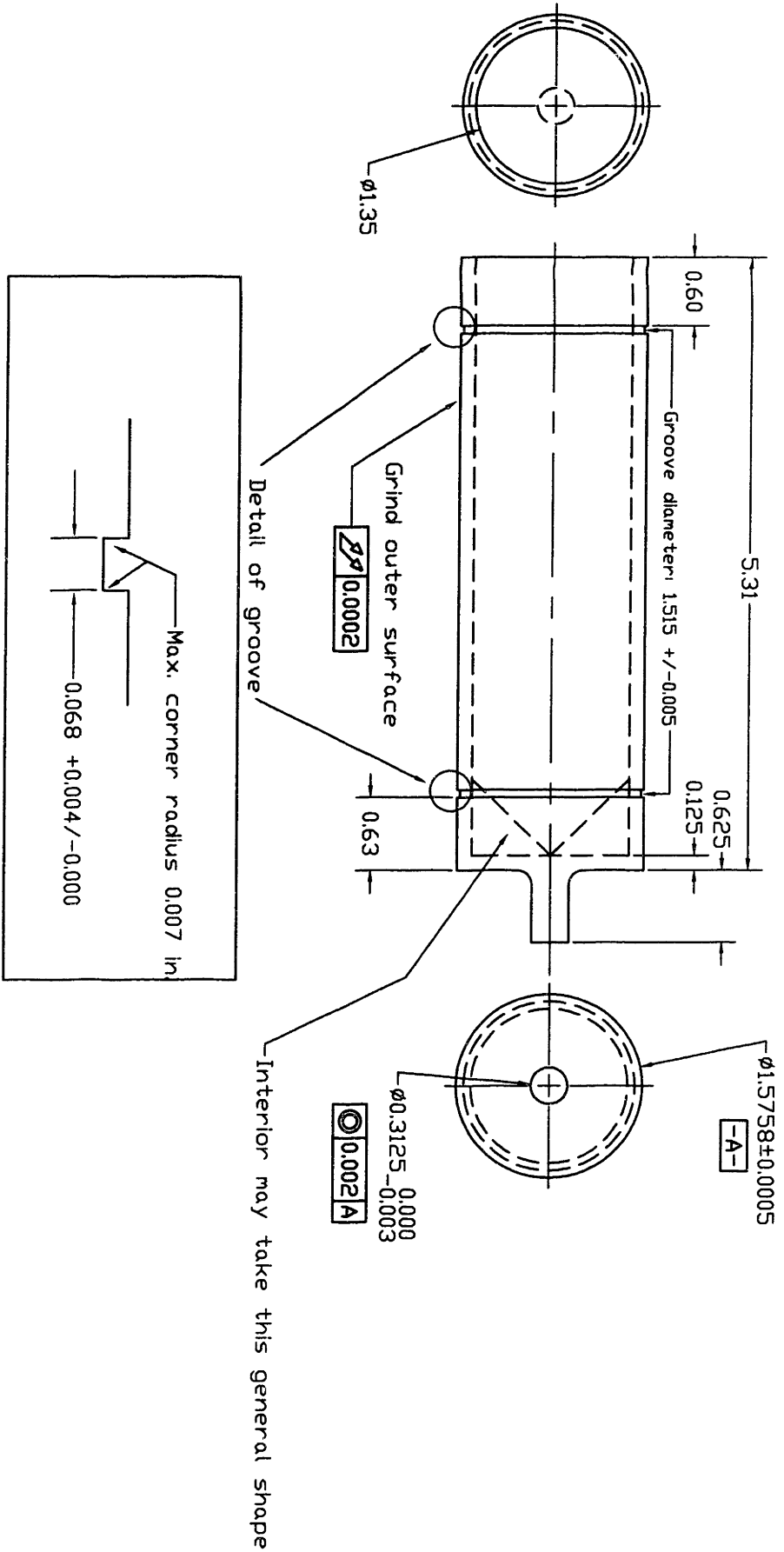
**Table 1: Carriage Plate Holes**

Hole #	Hole Type	X	Y
c1	DRILL #16 THRU	0.272	2.792
c2	DRILL #16 THRU	0.272	3.710
c3	DRILL #16 THRU	3.303	5.625
c4	DRILL #16 THRU	3.803	5.625
c5	DRILL #16 THRU	3.303	6.375
c6	DRILL #16 THRU	3.803	6.375
d1	DRILL LETTER H THRU	2.875	2.750
d2	DRILL LETTER H THRU	2.875	3.750
d3	DRILL LETTER H THRU	7.250	2.250
d4	DRILL LETTER H THRU	7.250	4.250
d5	DRILL LETTER H THRU	0.500	4.500
d6	DRILL LETTER H THRU	0.500	2.000
d7	DRILL LETTER H THRU	2.750	5.500
d8	DRILL LETTER H THRU	2.750	3.250
d9	DRILL LETTER H THRU	2.750	1.000
d10	DRILL LETTER H THRU	4.000	2.000
d11	DRILL LETTER H THRU	5.250	2.000
d12	DRILL LETTER H THRU	5.250	4.500
d13	DRILL LETTER H THRU	4.000	4.500
d14	DRILL LETTER H THRU	5.250	6.000
d15	DRILL LETTER H THRU	5.250	0.500
d16	DRILL LETTER H THRU	5.750	4.250
d17	DRILL LETTER H THRU	5.750	2.250
d18	DRILL LETTER H THRU	5.250	3.250
e1	#4-40 UNC-2B THRU	3.125	0.250
e2	#4-40 UNC-2B THRU	3.125	0.813
e3	#4-40 UNC-2B THRU	3.875	0.250

**Table 1: Carriage Plate Holes**

Hole #	Hole Type	X	Y
e4	#4-40 UNC-2B THRU	3.875	0.813
e5	#4-40 UNC-2B THRU	0.917	3.251
e6	#4-40 UNC-2B THRU	0.567	3.251
f1	Slot 9/64" wide, 0.315" long	0.567	2.503
f2	Slot 9/64" wide, 0.315" long	0.567	3.999
g1	Slot 3/16" wide, 1/4" long	3.125	2.500
g2	Slot 3/16" wide, 1/4" long	3.875	2.500
g3	Slot 3/16" wide, 1/4" long	3.125	4.000
g4	Slot 3/16" wide, 1/4" long	3.875	4.000





MIT THREE-DIMENSIONAL PRINTING PROJECT

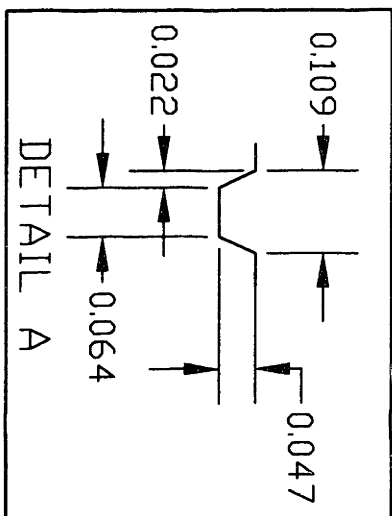
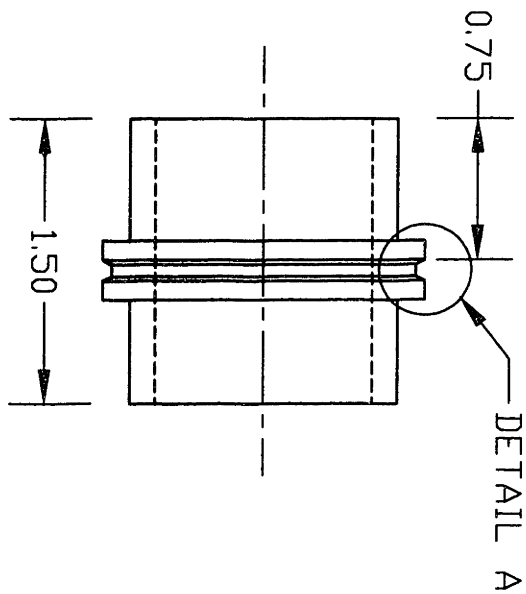
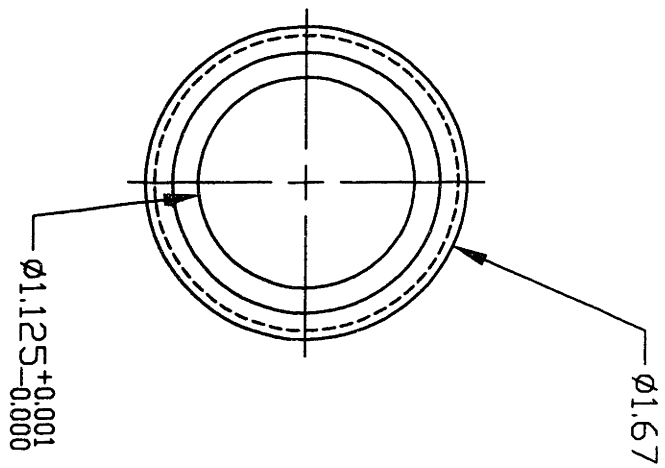
Ako Chijioke  
NEW PULLEY

PH: 617-253-2606 FAX: 617-253-0209  
Rev. 1  
5-14-98

DIMENSIONS: INCHES  
TOLERANCES:

SCALE: NDT TD SCALE  
+/- 0.010

MT'L: 303 STAINLESS STEEL  
QTY: 1  
unless otherwise specified



MIT THREE-DIMENSIONAL PRINTING PROJECT

Ako Chijloke

IDLER

PH: 617-253-5028

FAX: 617-253-0209

Rev. 1  
8-2-97

DIMENSIONS: INCHES

TOLERANCES:

SCALE: 1:1

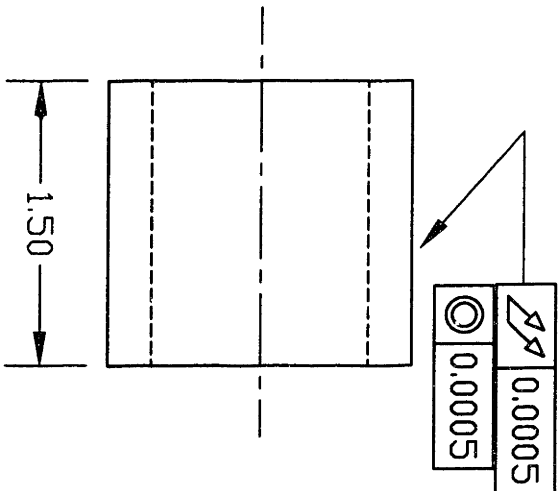
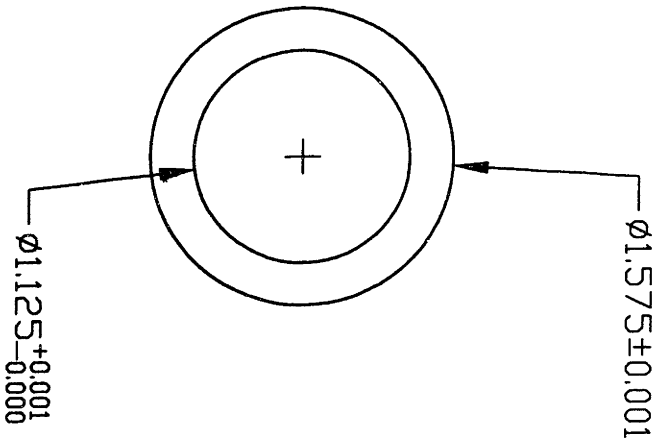
x.xxx +/- 0.020

MT'L: 303 STAINLESS STEEL

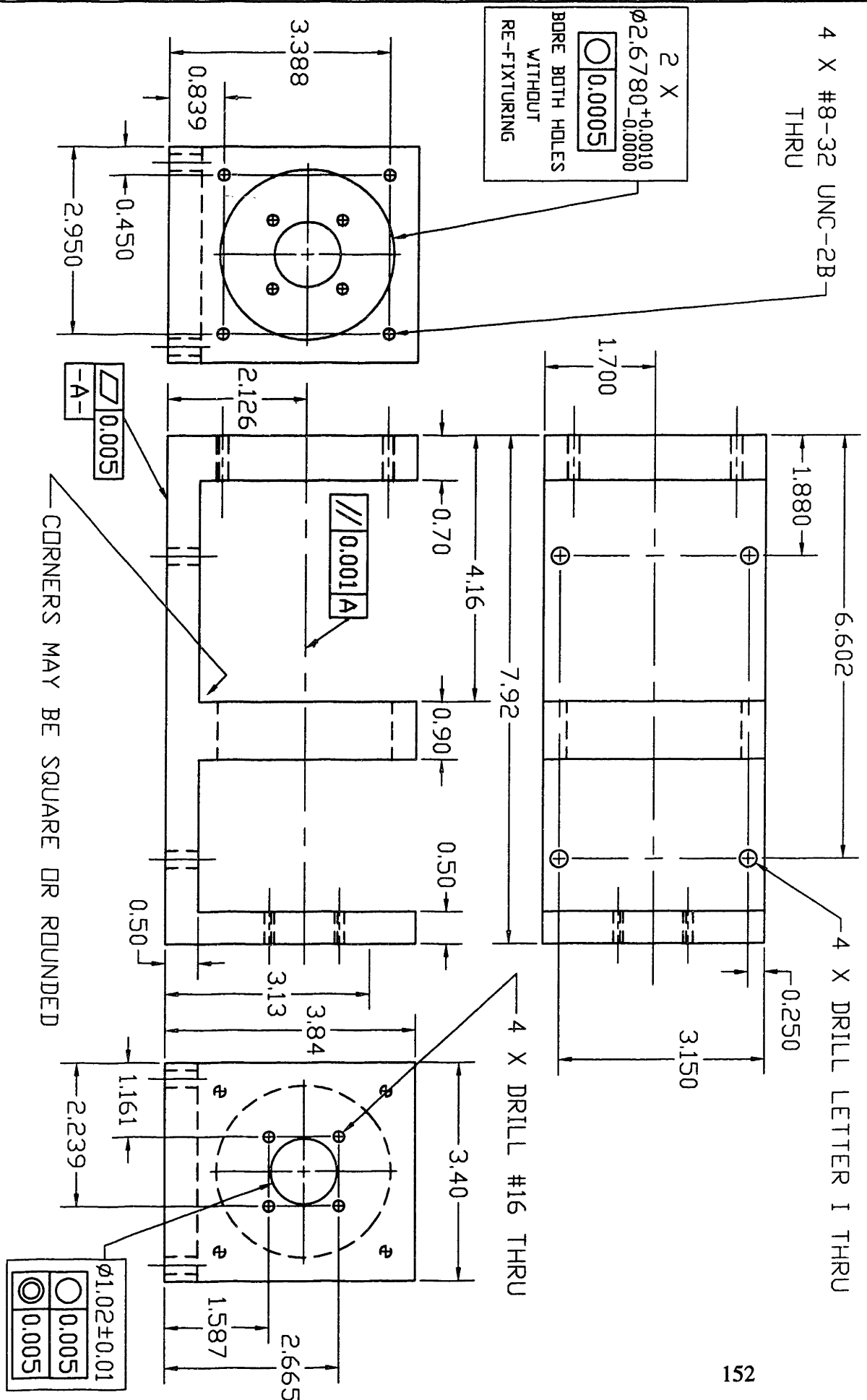
x.xxx +/- 0.002

QTY: 1

unless otherwise specified



MIT THREE-DIMENSIONAL PRINTING PROJECT	
Ako Chujioke	
SMD0TH IDLER	
PH: 617-253-7274	FAX: 617-253-0209
Rev. 1	
4-7-98	
DIMENSIONS: INCHES	TOLERANCES:
SCALE: 1:1	X.XX +/- 0.020
MT'L: ALUMINUM	X.XXX +/- 0.002
QTY: 1	unless otherwise specified

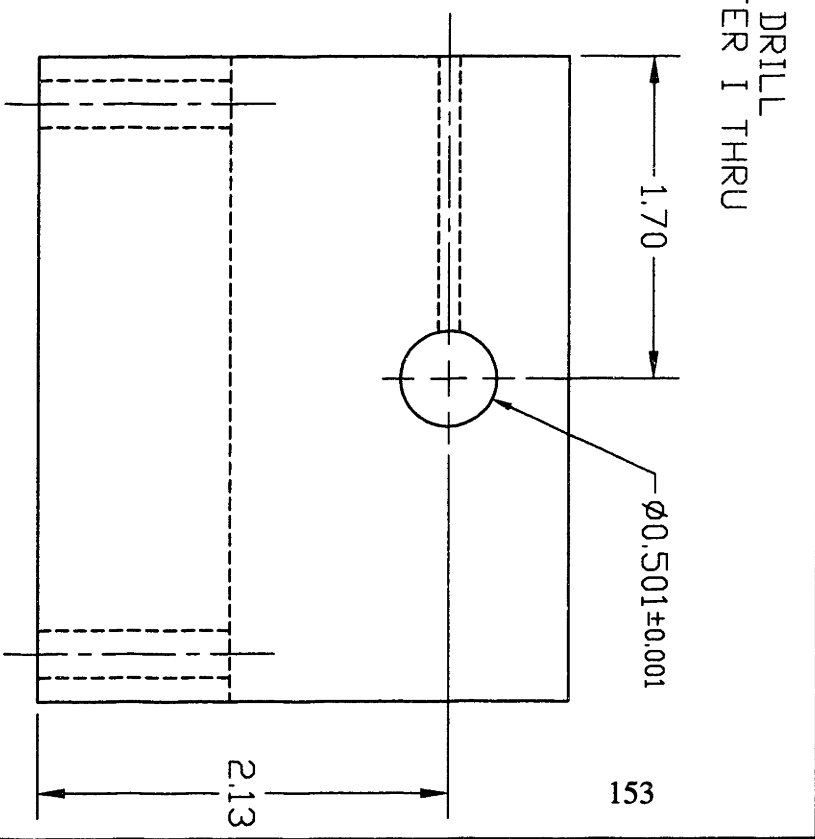
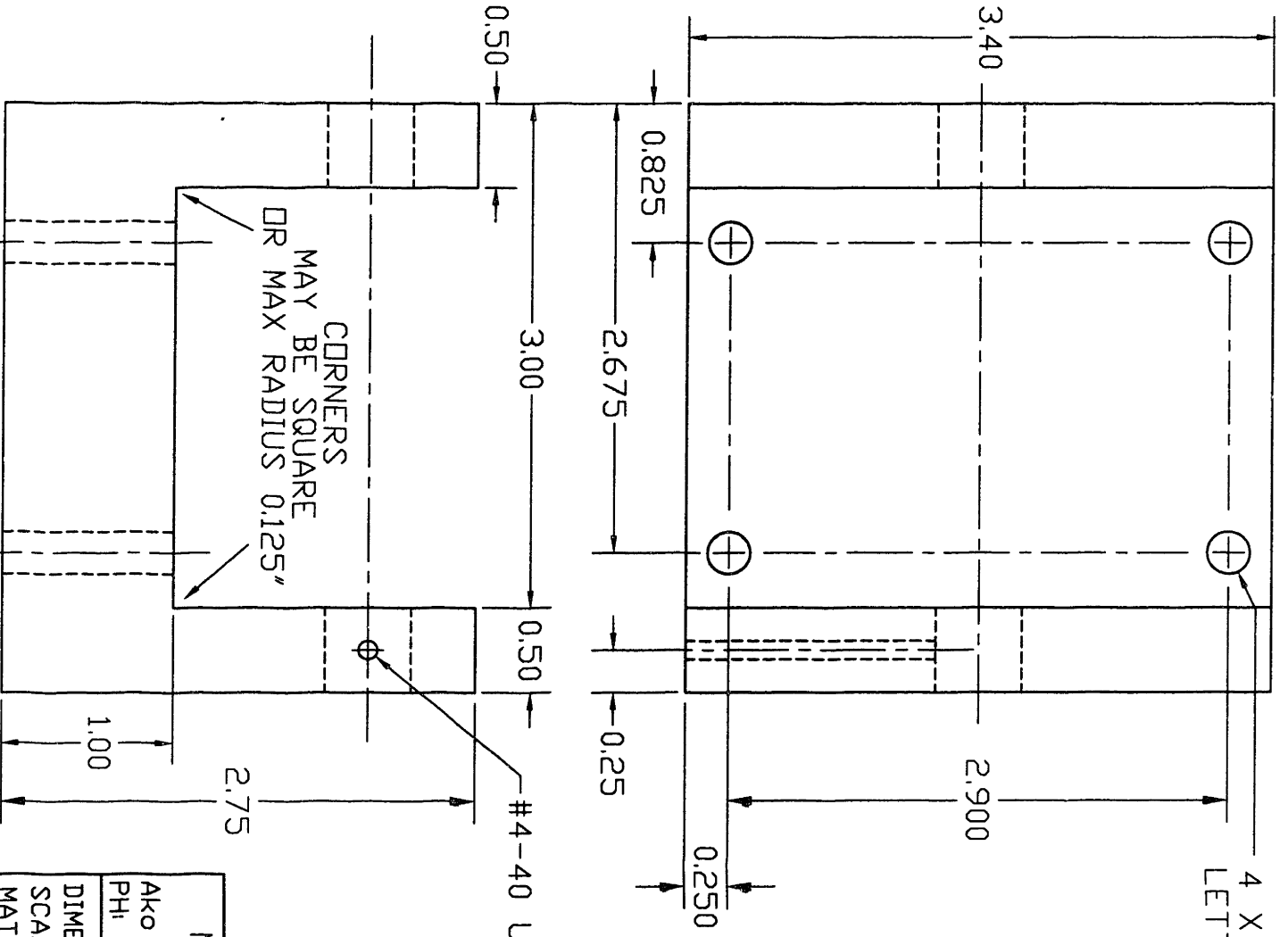


MIT THREE-DIMENSIONAL PRINTING PROJECT  
 PULLEY HOUSING

Ako Chijoke  
 PH: 617-253-5028 FAX: 617-253-0209  
 DIMENSIONS: INCHES  
 SCALE: 1:2  
 MTL: 6061 ALUMINUM  
 QTY: 1

Rev. 1  
 8-6-97

TOLERANCES:  
 x.xxx +/- 0.030  
 x.xxx +/- 0.005  
 unless otherwise specified

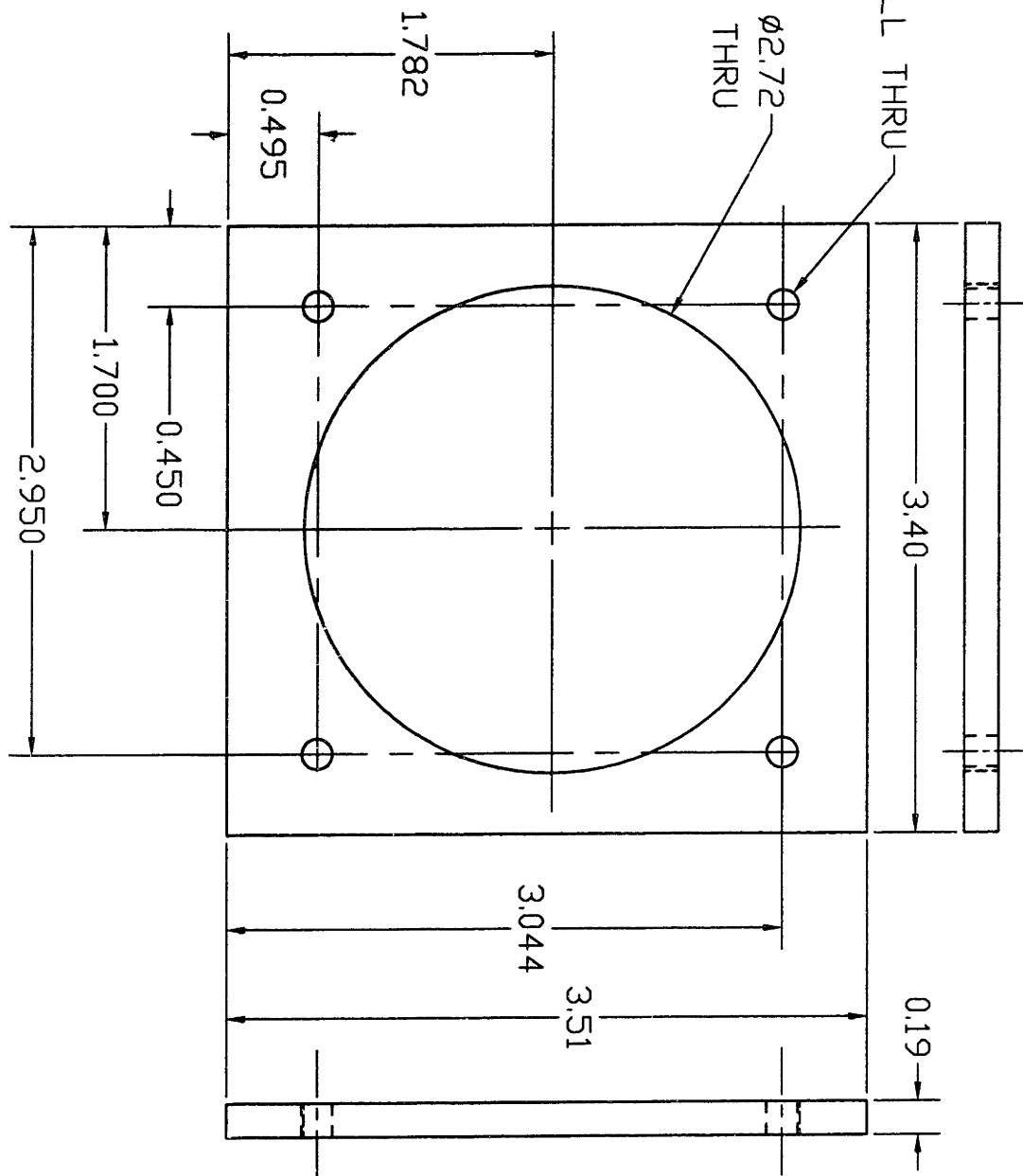


#4-40 UNC-2B THRU

CORNERS  
MAY BE SQUARE  
OR MAX RADIUS 0.125"

MIT THREE-DIMENSIONAL PRINTING PROJECT	
Ako Chijoke IDLER HOUSING	
PH: 617-253-5028	FAX: 617-253-0209
DIMENSIONS: INCHES	
SCALE: 1:1	
MAT'L: 6061 ALUMINUM	
QTY: 1	
TOLERANCES:	
x.xxx +/- 0.020	
x.xxx +/- 0.005	
unless otherwise specified	

4 X #15 DRILL THRU



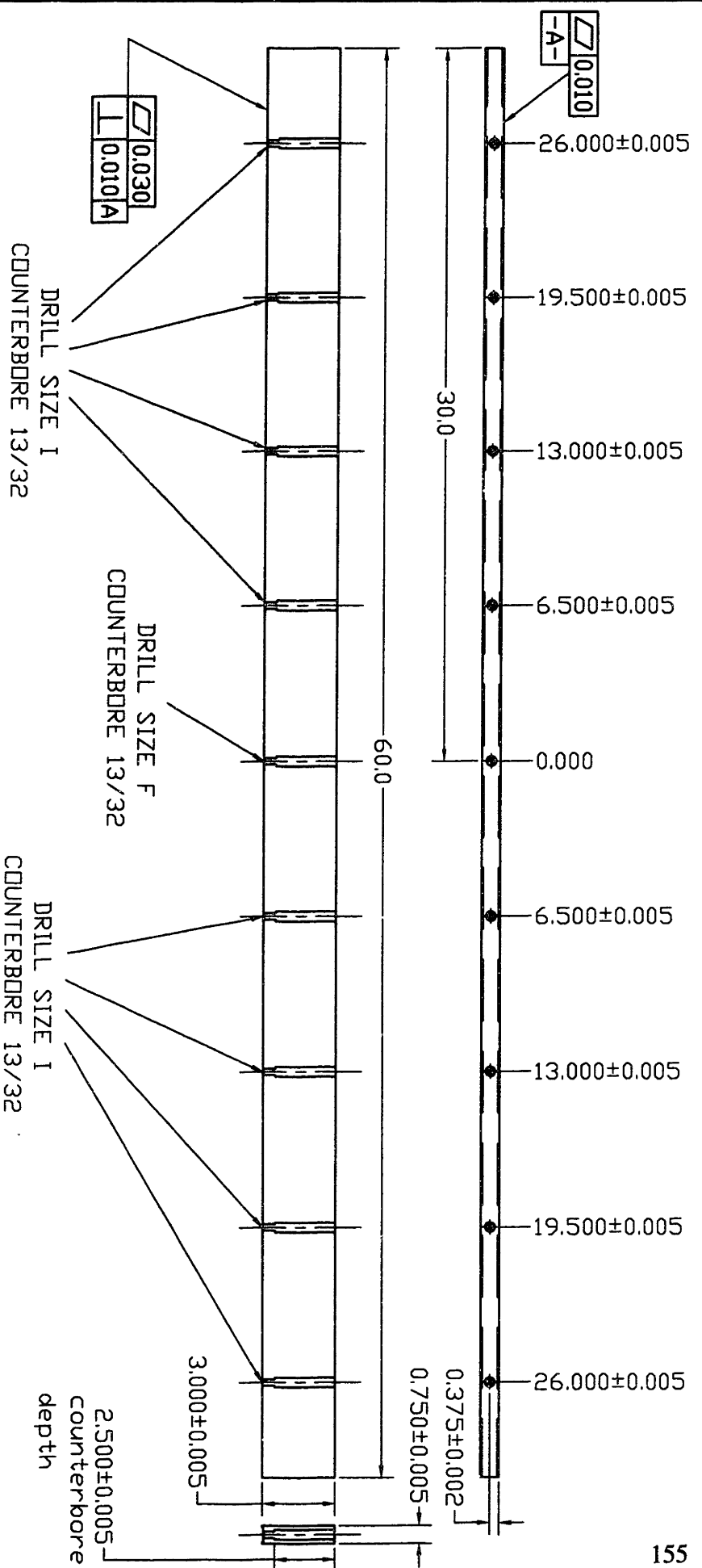
MIT THREE-DIMENSIONAL PRINTING PROJECT

ENDCAP

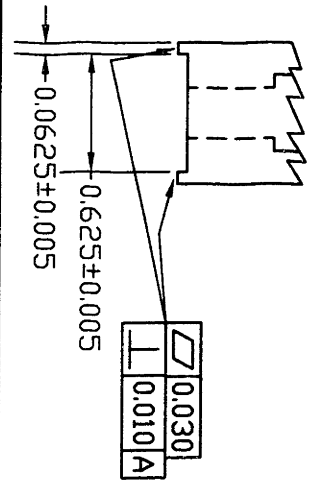
Ako Chijioke  
 PH: 617-253-5028 FAX: 617-253-0209 Rev. 2  
 9-1-97

DIMENSIONS: INCHES  
 SCALE: 1:1  
 MAT'L: 6061 ALUMINUM  
 QTY: 1

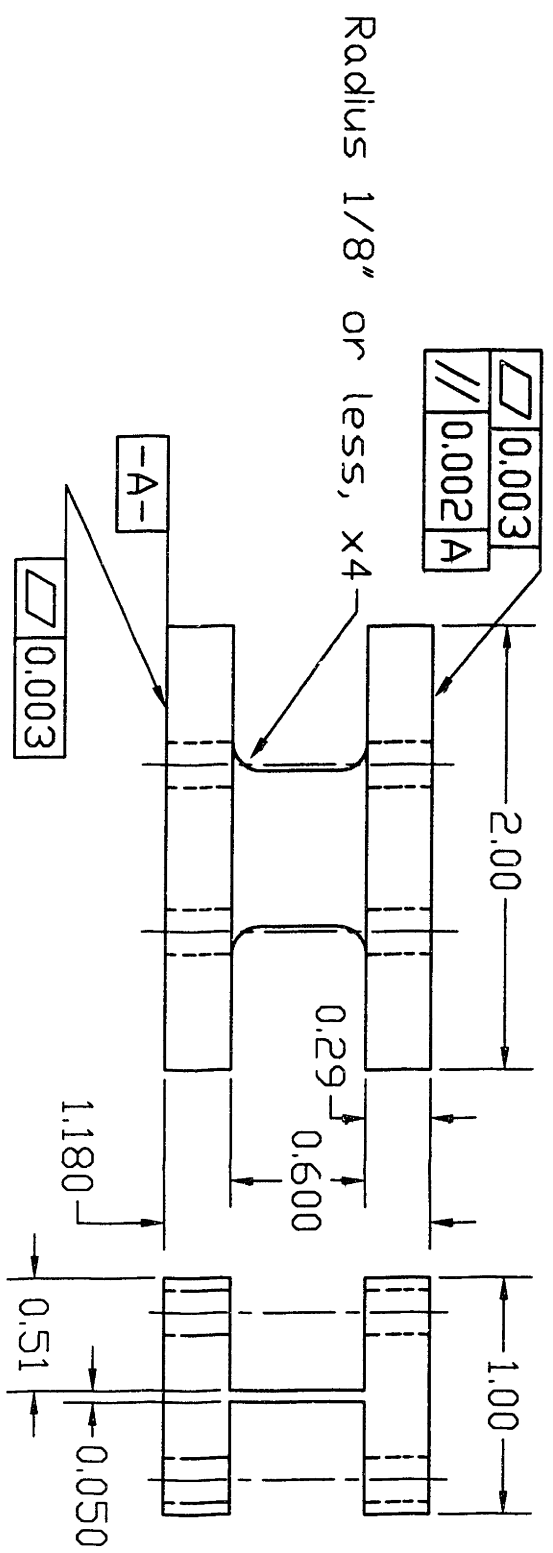
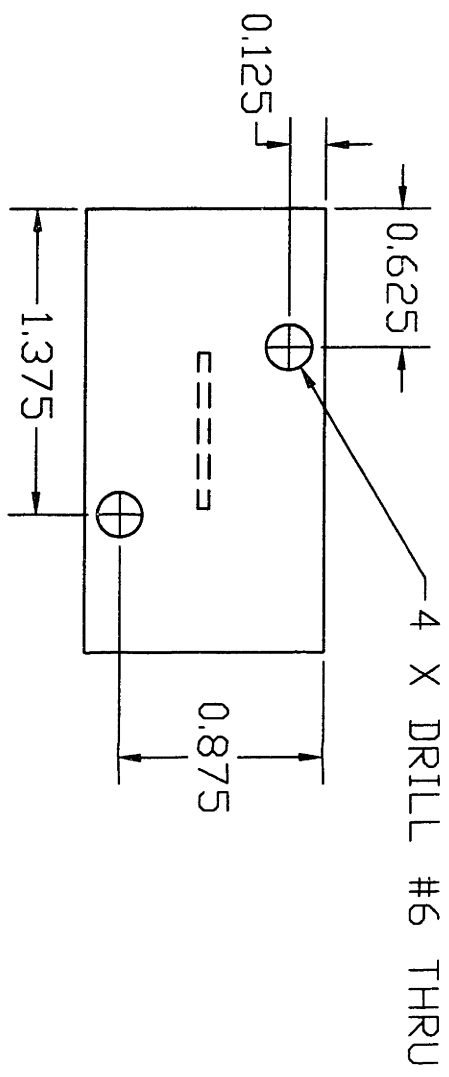
TOLERANCES:  
 X.XX +/- 0.02  
 X.XXX +/- 0.005



DETAIL OF BOTTOM SURFACE (END VIEW)



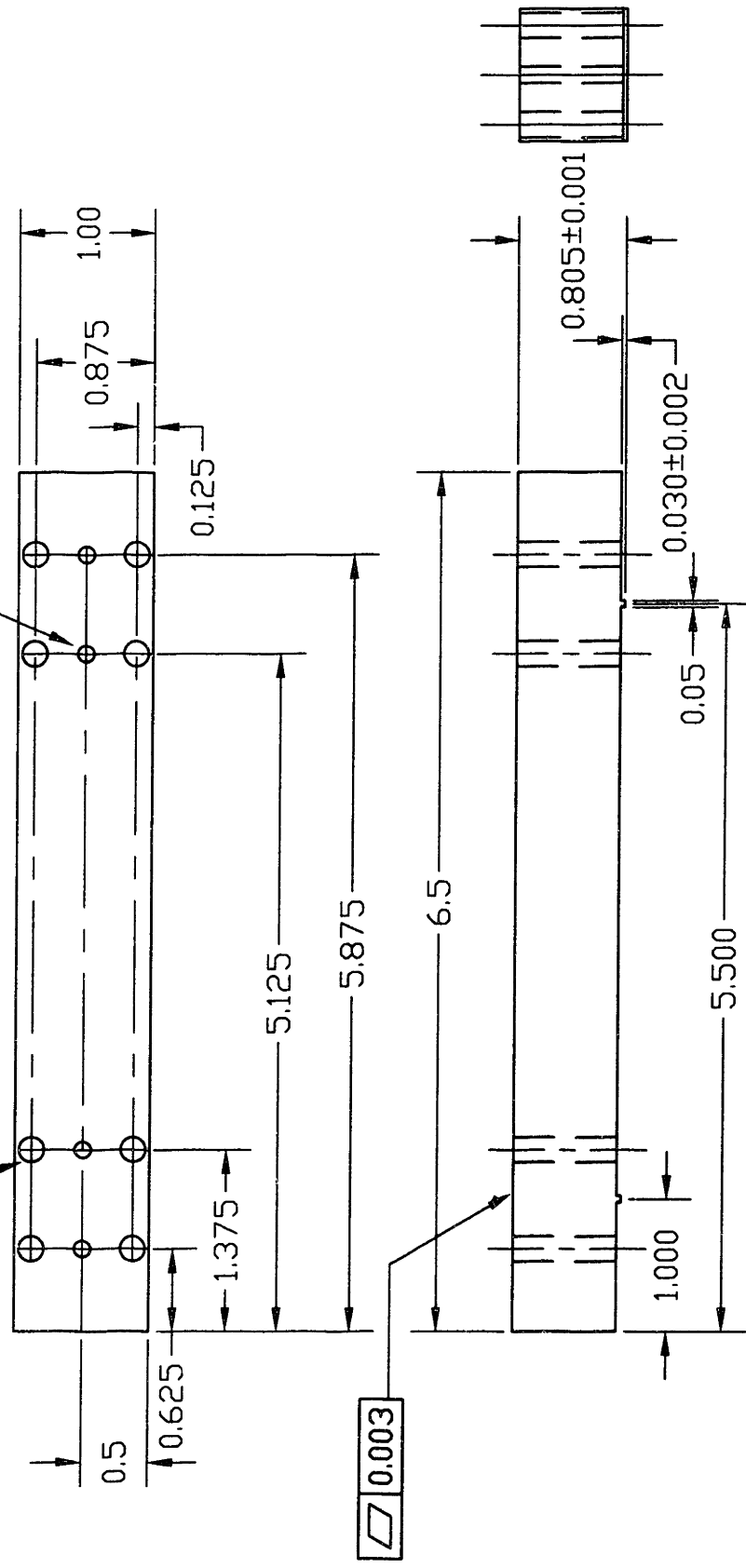
MIT THREE-DIMENSIONAL PRINTING PROJECT	
Ako Chijoke	
617-253-7274	
FAX: 617-253-0209	
ENCODER PLATE	
Rev. 3	
12/02/97	
DIMENSIONS: INCHES	
SCALE: 1:8	
MATERIAL: 3/4" ALUMINUM JIG PLATE	
QTY: 1	
TOLERANCES:	
X.X +/- 0.100	
X.XXX: as specified	



MIT THREE-DIMENSIONAL PRINTING PROJECT  
 Ako Chijioke  
 FLEXIBLE COUPLING  
 PH: 617-253-7274 FAX: 617-253-0209  
 DIMENSIONS: INCHES  
 SCALE: 1:1  
 MTL: ULTEM 1000  
 QTY: 1  
 TOLERANCES:  
 x.xx +/- 0.010  
 v.xxx +/- 0.003  
 Rev. 2  
 6-1-98

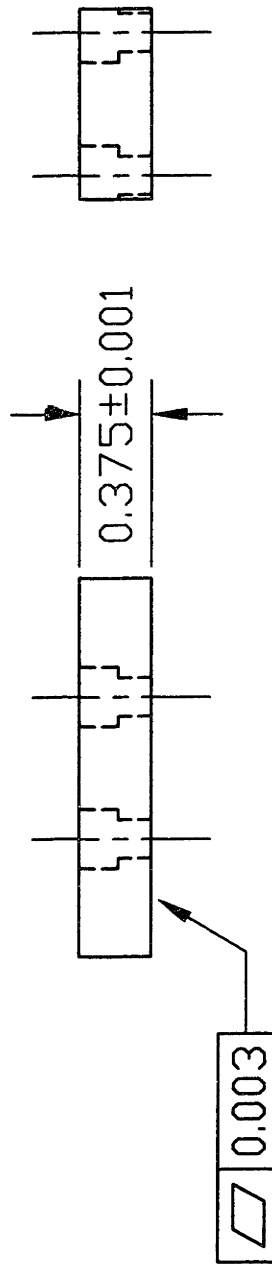
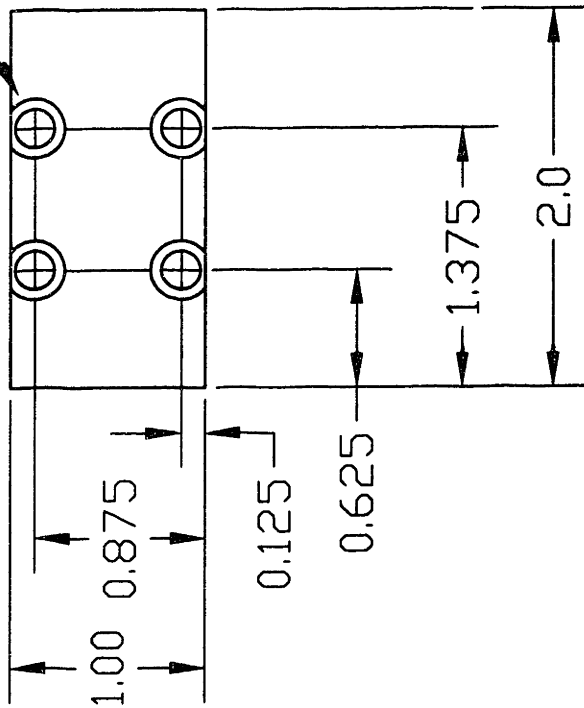


8 x #10-24 4 x DRILL 1/8 THRU



MIT THREE-DIMENSIONAL PRINTING PROJECT	
Ako Chijjoke	Rev. 2
617-253-7274	6-1-98
DIMENSIONS: INCHES	TOLERANCES:
SCALE: 0.75:1	x.x +/- 0.100
MT'L: ALUMINUM	x.xx +/- 0.010
QTY: 1	x.xxx +/- 0.005
	unless otherwise noted

4 x DRILL #6 THRU,  
COUNTERBORE 5/16  
x 0.205 +/- 0.010 DEEP

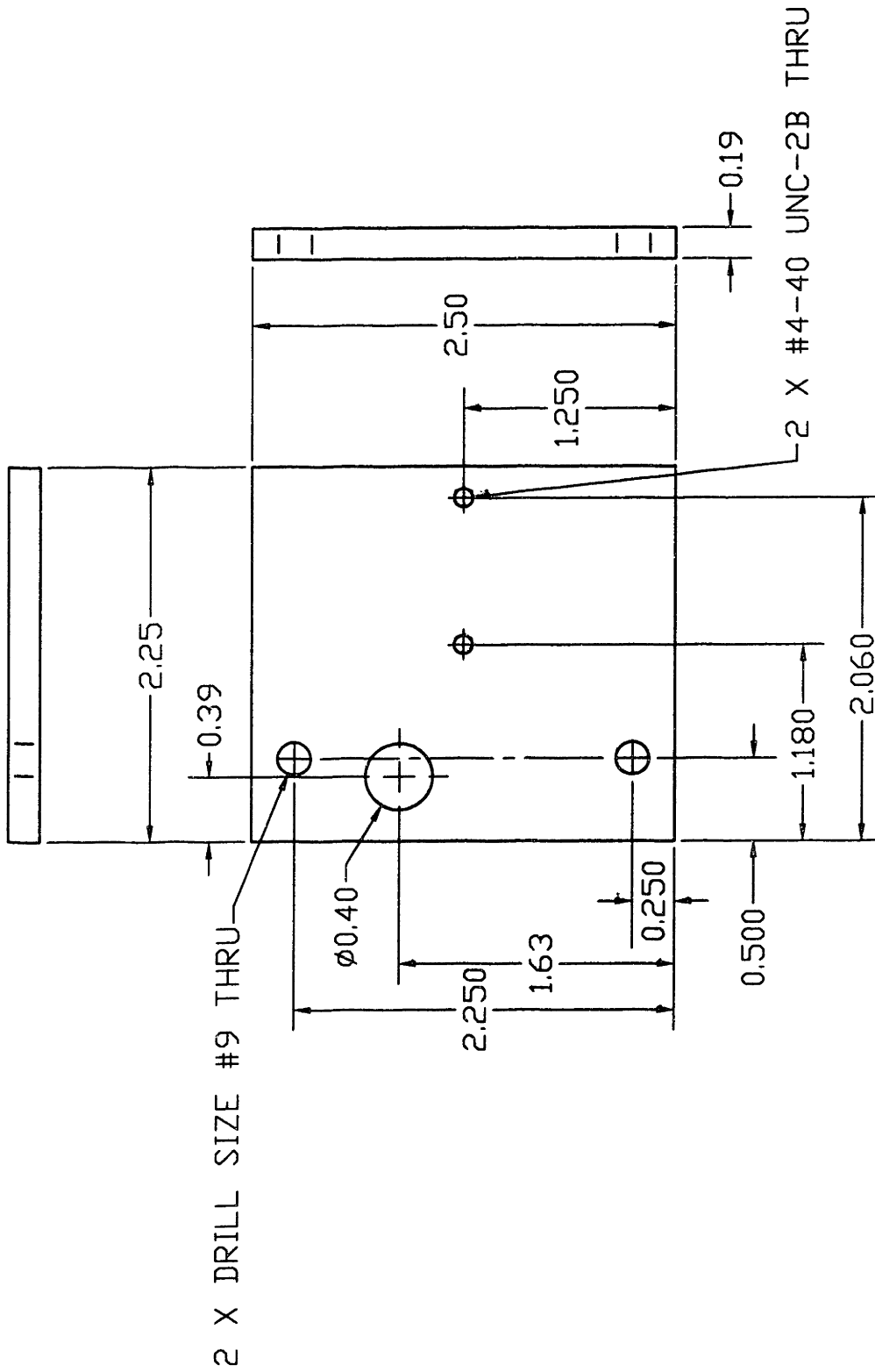


MIT THREE-DIMENSIONAL PRINTING PROJECT  
POTTED COUPLING SPACERS Rev. 2  
6-1-98

Ako Chijjoke  
617-253-7274

DIMENSIONS: INCHES  
SCALE: 1:1  
M'T'L: ALUMINUM  
QTY: 2

TOLERANCES:  
x.x +/- 0.100  
x.xxx +/- 0.010  
x.xxxx +/- 0.005  
unless otherwise noted



MIT THREE-DIMENSIONAL PRINTING PROJECT

Ako Chijjoke CARRIAGE PIECE 2 Rev. 1

PH: 617-253-5028 FAX: 617-253-0209 8-5-97

DIMENSIONS: INCHES

SCALE: 1:1

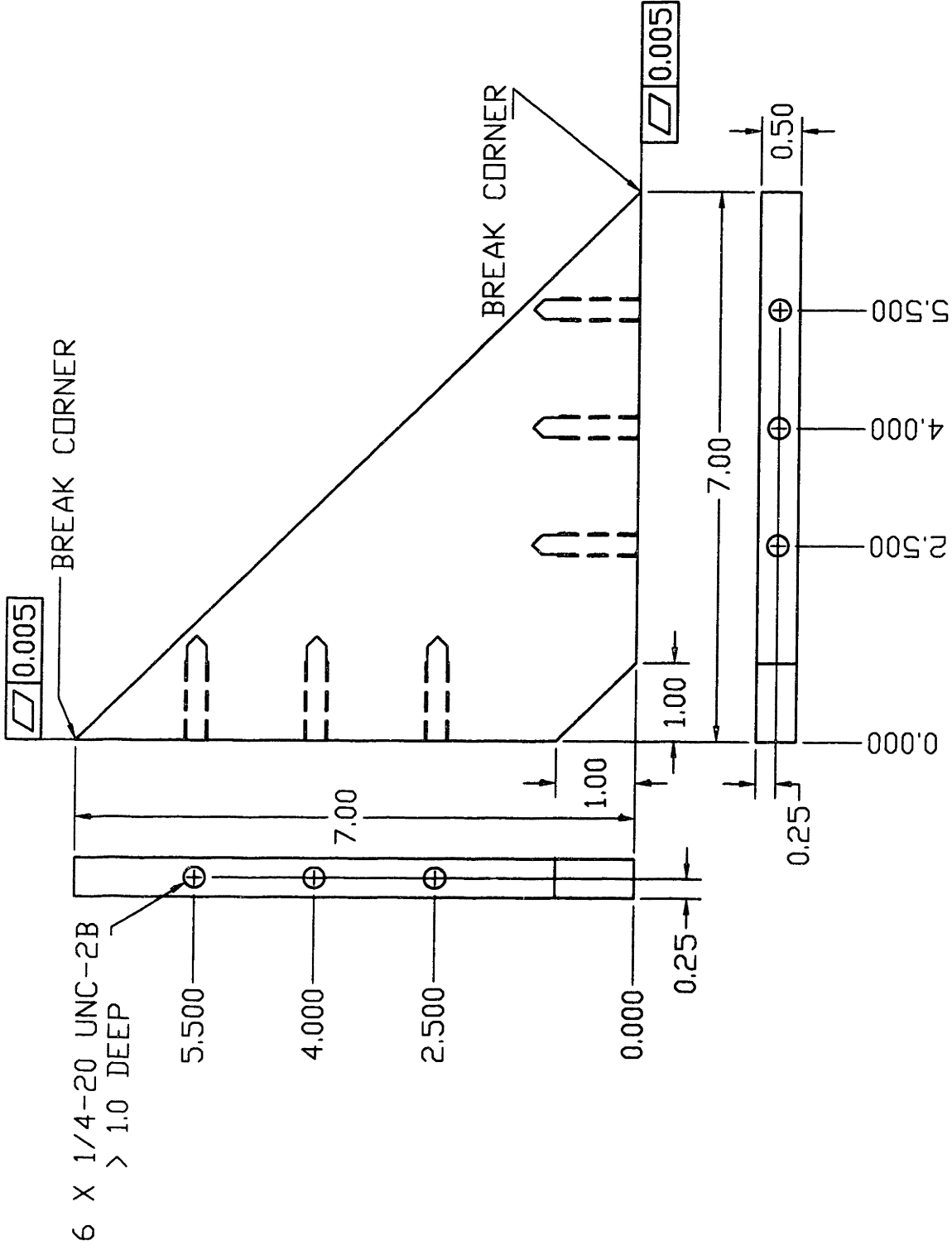
MT'L: 6061 ALUMINUM

QTY: 1

TOLERANCES:

X:XX +/- 0.020

X:XXX +/- 0.005



6 X 1/4-20 UNC-2B  
> 1.0 DEEP

5.500

4.000

2.500

0.000

0.25

7.00

1.00

1.00

7.00

0.000

2.500

4.000

5.500

0.50

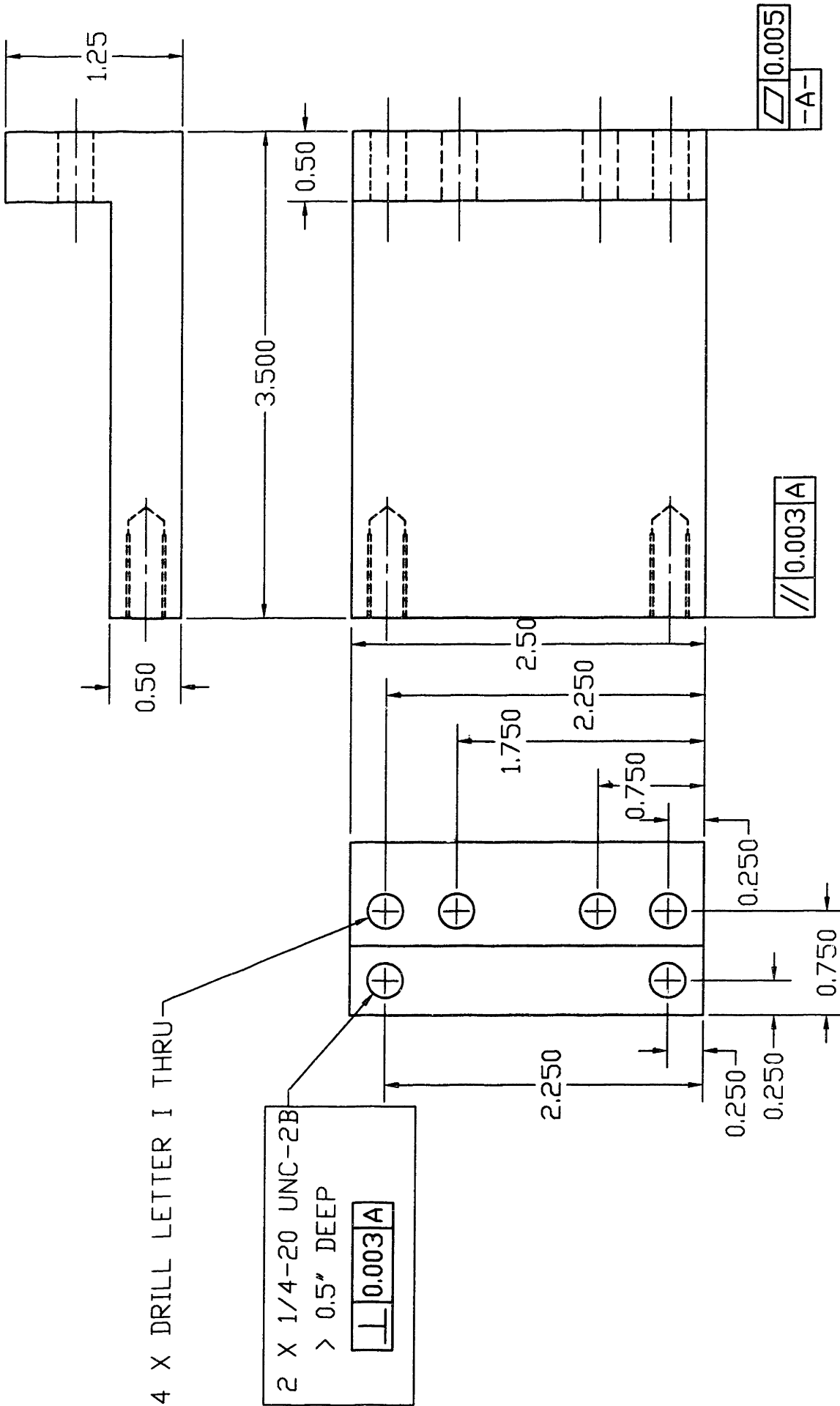
0.005

0.005

BREAK CORNER

BREAK CORNER

MIT THREE-DIMENSIONAL PRINTING PROJECT	
Ako Chjloke	MOUNT BRACE
PH: 617-253-5028	FAX: 617-253-0209
	Rev. 1
	8-7-97
DIMENSIONS: INCHES	TOLERANCES:
SCALE: 1:2	x:xx +/- 0.010
MAT'L: 6061 ALUMINUM	x:xxx +/- 0.005
QTY: 2	



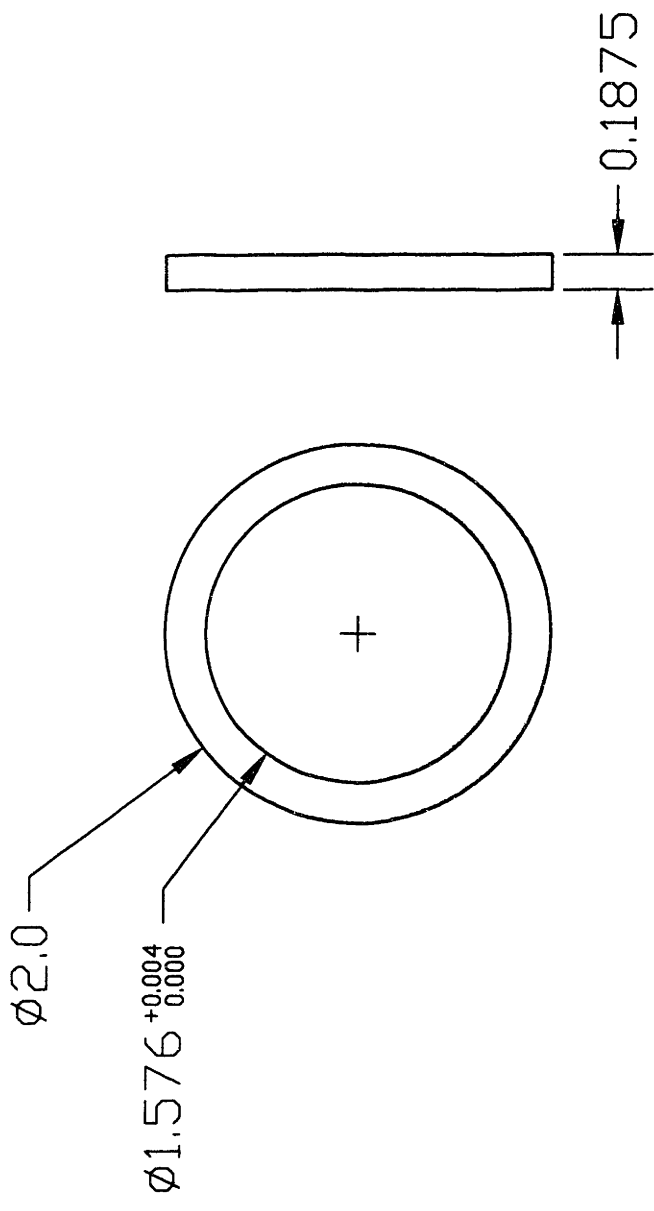
4 X DRILL LETTER I THRU

2 X 1/4-20 UNC-2B  
> 0.5" DEEP  
┘ 0.003 A

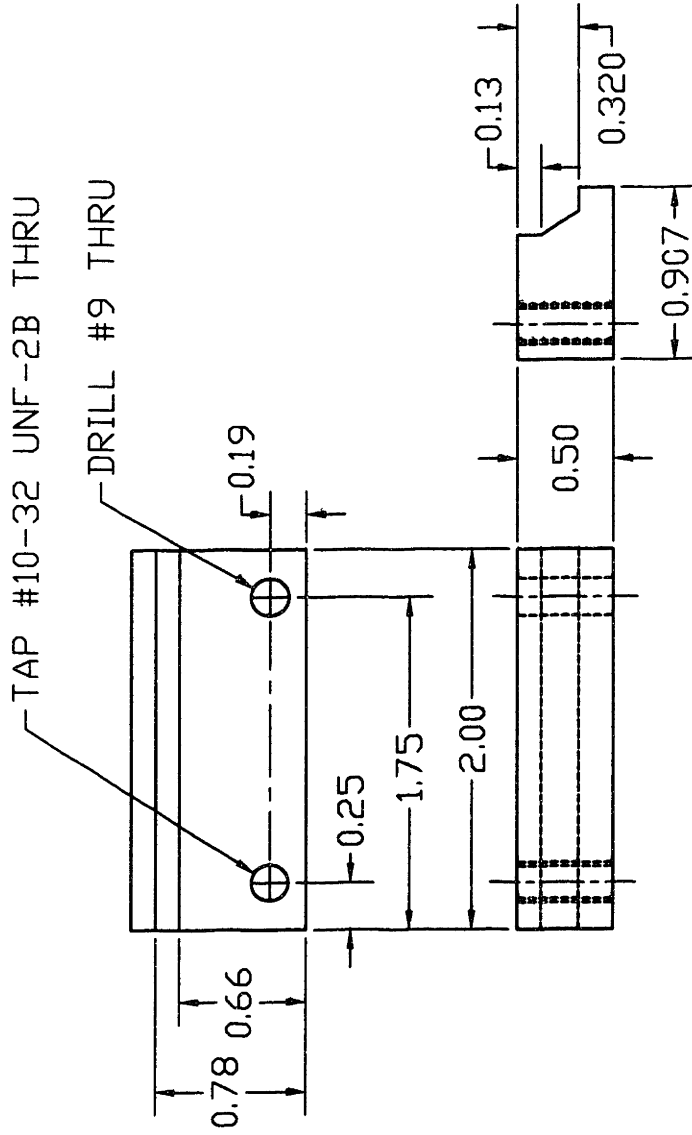
// 0.003 A

▧ 0.005  
-A-

MIT THREE-DIMENSIONAL PRINTING PROJECT	
Ako Chijjoke	POWDERBED STAND Rev. 2
PH: 617-253-5028	FAX: 617-253-0209 6-1-98
DIMENSIONS: INCHES	TOLERANCE:
SCALE: 1:1	x.xx +/- 0.020
MT'L: 6061 ALUMINUM	x.xxx +/- 0.005
QTY: 1	



MIT THREE-DIMENSIONAL PRINTING PROJECT	
Ako Chijioke	CABLE ALIGNMENT RINGS
617-253-7274	Rev. 1 1/28/98
DIMENSIONS: INCHES	TOLERANCES:
SCALE: 1:1	+/- 0.100
MT'L: ALUMINUM	unless otherwise noted
QTY: 2	

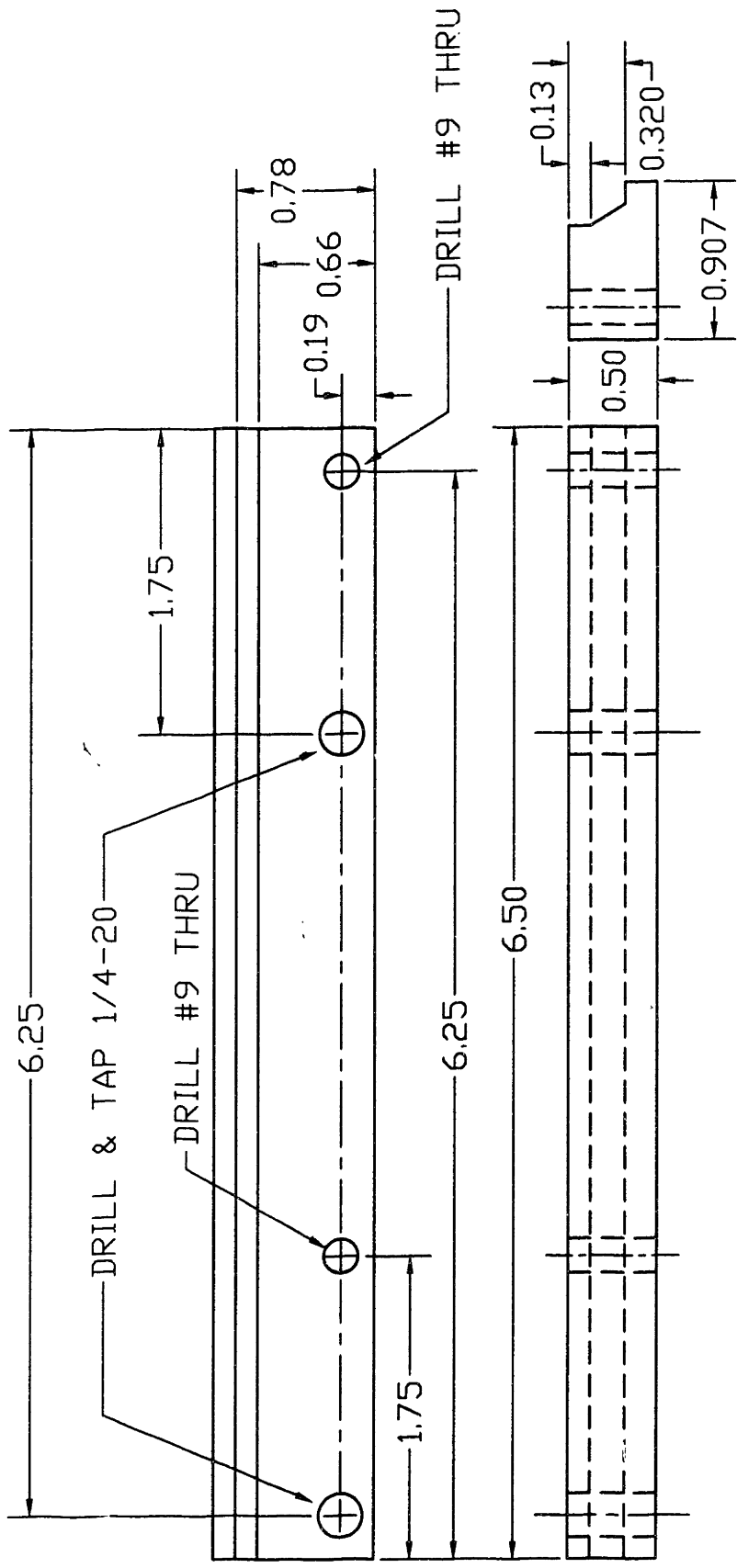


MIT THREE-DIMENSIONAL PRINTING PROJECT

Ako Chijjoke SAFETY CATCH 1 Rev. 1  
 PH: 617-253-5028 FAX: 617-253-0209 8-12-97

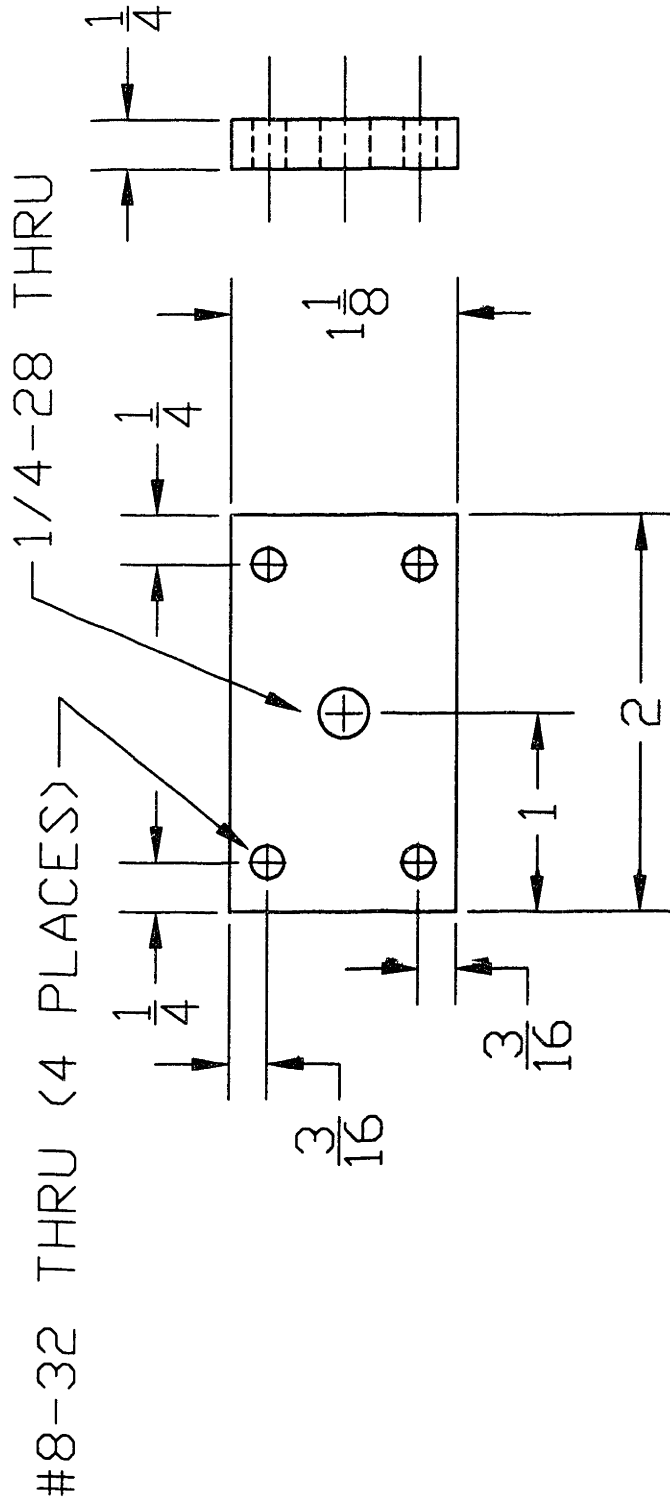
DIMENSIONS: INCHES  
 SCALE: 1:1  
 MT/L: NYLON  
 QTY: 2

TOLERANCES:  
 X:XX +/- 0.010  
 X:XXX +/- 0.005



MIT THREE-DIMENSIONAL PRINTING PROJECT		Rev. 3
SAFETY CATCH 2		6-1-98
Ako Chijjoke	617-253-2606	617-253-0209
DIMENSIONS: INCHES		
SCALE: 1:1		
MATERIAL: NYLON		
QTY: 2		
TOLERANCES:		
X.XXX +/- 0.010		
X.XXX +/- 0.002		



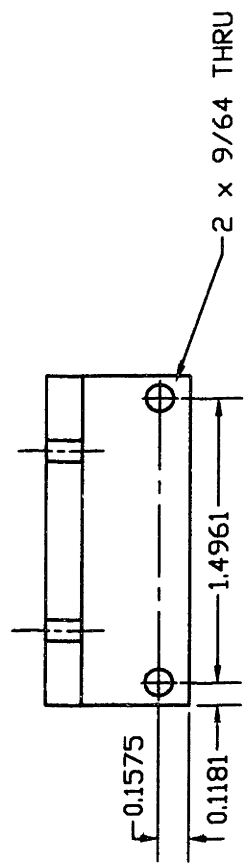
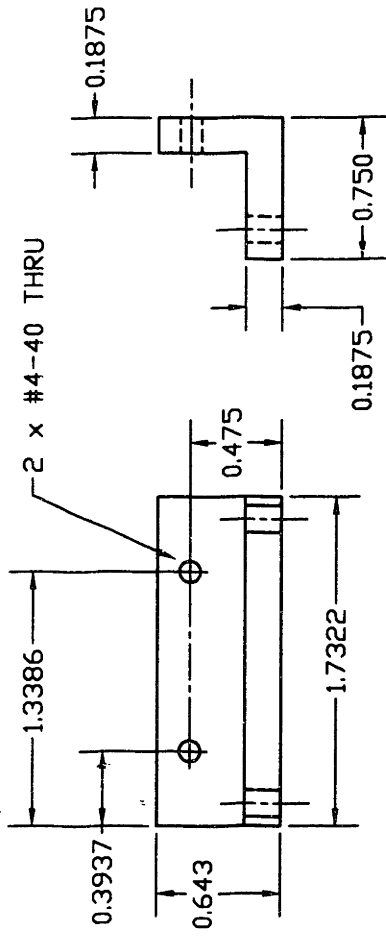


MIT THREE-DIMENSIONAL PRINTING PROJECT  
 ROD-END ANCHOR

Dave Brancazio, Ako ChiJloke  
 617-253-2606

Rev. 2  
 6-1-98

DIMENSIONS: INCHES  
 SCALE: NOT TO SCALE  
 MTL: ALUMINUM  
 QTY: 1



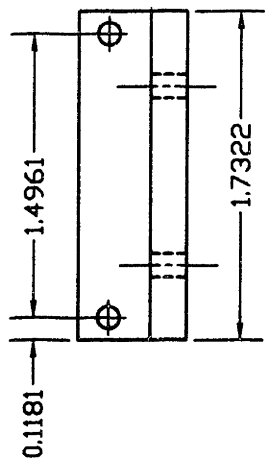
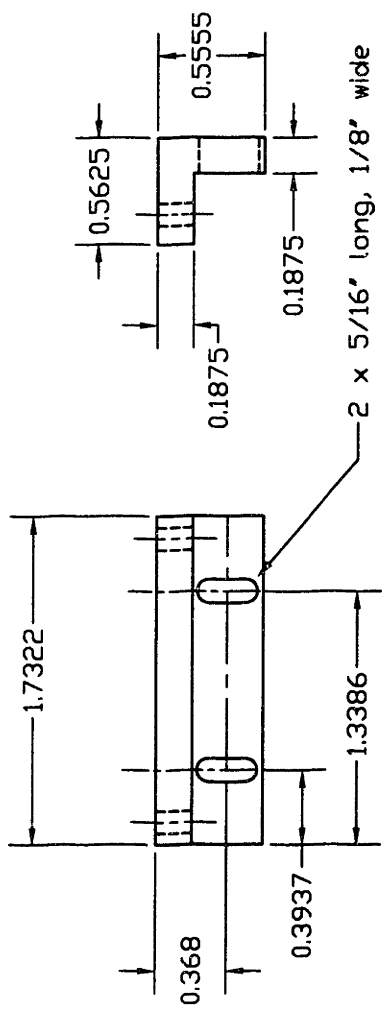
MIT THREE-DIMENSIONAL PRINTING PROJECT

Ako Chijoke  
617-253-7274

READHEAD BRACKET 1

Rev. 1  
6-1-98

DIMENSIONS: INCHES  
SCALE: 1:1  
MATERIAL: ALUMINUM  
QTY: 1

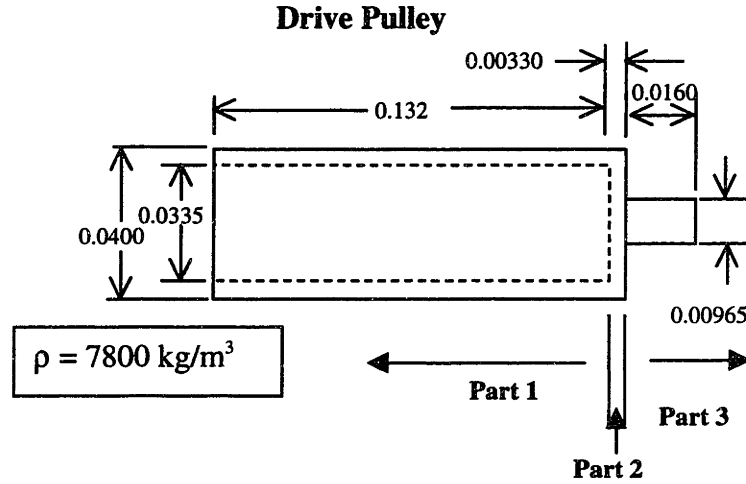


MIT THREE-DIMENSIONAL PRINTING PROJECT	
Ako Chijjoke	Rev. 1
617-253-7274	6-1-98
DIMENSIONS: INCHES	
SCALE: 1:1	
MATERIAL: ALUMINUM	
QTY: 1	

## APPENDIX B: MASS MOMENT OF INERTIA CALCULATIONS

All dimensions in meters.

### 1. DRIVE PULLEY ASSEMBLY



$$J = \int r^2 dm$$

$$J_{\text{pulley}} = J_1 + J_2 + J_3$$

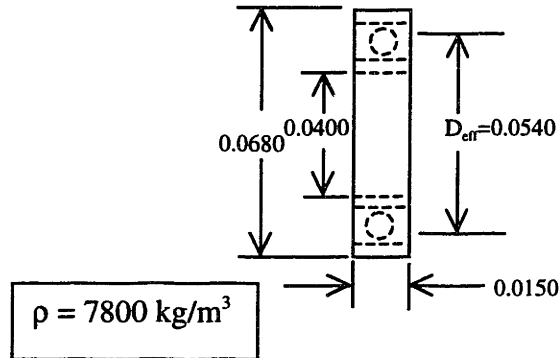
$$J_1 = \rho l \frac{\pi}{2} [r_o^4 - r_i^4] = \frac{7800 \frac{\text{kg}}{\text{m}^3} \times 0.132 \text{m} \times \pi \left[ \left( \frac{0.0400 \text{m}}{2} \right)^4 - \left( \frac{0.0335 \text{m}}{2} \right)^4 \right]}{2} = 9.82 \times 10^{-5} \text{ kg} \cdot \text{m}^2$$

$$J_2 = \frac{\rho l \pi r^4}{2} = \frac{7800 \frac{\text{kg}}{\text{m}^3} \times 0.00330 \text{m} \times \pi \times (0.0200 \text{m})^4}{2} = 6.47 \times 10^{-5} \text{ kg} \cdot \text{m}^2$$

$$J_3 = \frac{\rho l \pi r^4}{2} = \frac{7800 \frac{\text{kg}}{\text{m}^3} \times 0.0160 \text{m} \times \pi \times \left( \frac{0.00965 \text{m}}{2} \right)^4}{2} = 1.06 \times 10^{-7} \text{ kg} \cdot \text{m}^2$$

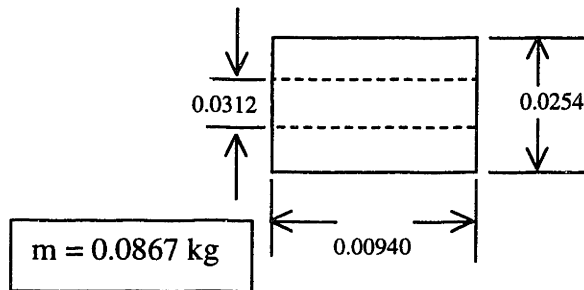
$$J_{\text{pulley}} = 1.63 \times 10^{-4} \text{ kg} \cdot \text{m}^2$$

### Drive Pulley Bearings



$$J = \frac{\rho l \pi}{2} [r_{eff}^4 - r_i^4] = \frac{7800 \frac{kg}{m^3} \times 0.0150 m \times \pi}{2} [(0.027 m)^4 - (0.020 m)^4] = 6.83 \times 10^{-5} kg \cdot m^2$$

### Flexible Coupling



$$V = \pi l (r_o^2 - r_i^2) = \pi \times 0.0312 m \times \left[ \left( \frac{0.0254 m}{2} \right)^2 - \left( \frac{0.00940 m}{2} \right)^2 \right] = 1.36 \times 10^{-5} m^3$$

$$\rho_{eff} = \frac{m}{V} = \frac{0.0867 kg}{1.36 \times 10^{-5} m^3} = 6376 \frac{kg}{m^3}$$

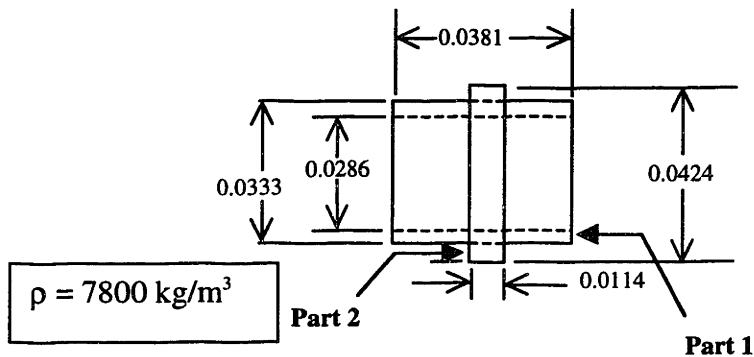
$$J = \frac{\rho_{eff} l \pi}{2} [r_o^4 - r_i^4] = \frac{6376 \frac{kg}{m^3} \times 0.0312 m \times \pi}{2} \left[ \left( \frac{0.0254 m}{2} \right)^4 - \left( \frac{0.00940 m}{2} \right)^4 \right] = 7.97 \times 10^{-6} kg \cdot m^2$$

$$J_{drive\ assembly} = 2J_{bearing} + J_{pulley} + J_{coupling}$$

$$= 2(6.83 \times 10^{-5} \text{ kg} \cdot \text{m}^2) + 1.63 \times 10^{-4} \text{ kg} \cdot \text{m}^2 + 7.97 \times 10^{-6} \text{ kg} \cdot \text{m}^2 = 3.08 \times 10^{-4} \text{ kg} \cdot \text{m}^2$$

## 2. IDLER PULLEY ASSEMBLY

### Idler Pulley



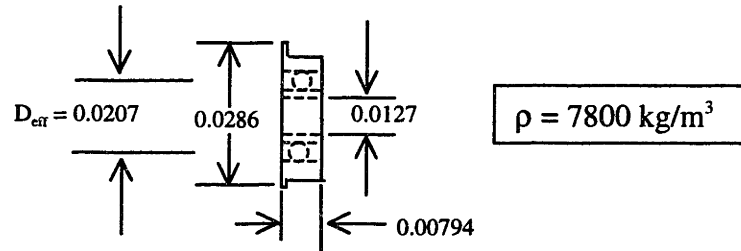
$$J = J_1 + J_2$$

$$J_1 = \frac{\rho l \pi}{2} [r_o^4 - r_i^4] = \frac{7800 \frac{\text{kg}}{\text{m}^3} \times 0.0381 \text{ m} \times \pi}{2} \left[ \left( \frac{0.0333 \text{ m}}{2} \right)^4 - \left( \frac{0.0286 \text{ m}}{2} \right)^4 \right] = 1.64 \times 10^{-5} \text{ kg} \cdot \text{m}^2$$

$$J_2 = \frac{\rho l \pi}{2} [r_o^4 - r_i^4] = \frac{7800 \frac{\text{kg}}{\text{m}^3} \times 0.0114 \text{ m} \times \pi}{2} \left[ \left( \frac{0.0424 \text{ m}}{2} \right)^4 - \left( \frac{0.0333 \text{ m}}{2} \right)^4 \right] = 1.75 \times 10^{-5} \text{ kg} \cdot \text{m}^2$$

$$J = 1.64 \times 10^{-5} \text{ kg} \cdot \text{m}^2 + 1.75 \times 10^{-5} \text{ kg} \cdot \text{m}^2 = 3.39 \times 10^{-5} \text{ kg} \cdot \text{m}^2$$

### Idler Bearings



$$J = \frac{\rho l \pi}{2} [r_o^4 - r_{eff}^4] = \frac{7800 \frac{\text{kg}}{\text{m}^3} \times 0.00794 \text{ m} \times \pi}{2} \left[ \left( \frac{0.0286 \text{ m}}{2} \right)^4 - \left( \frac{0.0207 \text{ m}}{2} \right)^4 \right] = 2.95 \times 10^{-6} \text{ kg} \cdot \text{m}^2$$

$$J_{idler \text{ assembly}} = 2J_{bearings} + J_{idler}$$

$$= 2 \times 2.95 \times 10^{-6} \text{ kg} \cdot \text{m}^2 + 3.39 \times 10^{-5} \text{ kg} \cdot \text{m}^2 = 3.98 \times 10^{-5} \text{ kg} \cdot \text{m}^2$$

### 3. CARRIAGE AND CABLE

$$J = mr^2 = 1.8 \text{ kg} \times (0.0212 \text{ m})^2 = 8.09 \times 10^{-4} \text{ kg} \cdot \text{m}^2$$

### 4. TOTAL

$$J_{total} = 8.09 \times 10^{-4} \text{ kg} \cdot \text{m}^2 + 3.98 \times 10^{-5} \text{ kg} \cdot \text{m}^2 + 3.08 \times 10^{-4} \text{ kg} \cdot \text{m}^2 = 1.16 \times 10^{-3} \text{ kg} \cdot \text{m}^2$$

## APPENDIX C: SOFTWARE DOCUMENTATION

This appendix describes the principal operating program, or Virtual Instrument (VI) that has been built for the impact observation station, *PrintingAndImaging.vi*.

### A1. Front Panel

The user interface for Labview VIs is aptly termed the front panel. The controls and indicators on the front panel of the *PrintingAndImaging.vi* program are described as follows.

#### Controls:

*Number of passes.* This is a digital (i.e. numeric) control which takes on integer values. This is how the user selects the number of consecutive passes to perform.

*PFI pin for signal to be divided.* This is a digital control which takes on integer values. This is how the user selects the number of the pin on the SCB-68 connector box to which the encoder output signal is connected. Since the wiring to this pin has been done in a semi-irreversible manner, perhaps this user control ought to be removed.

*PFI pin for counter gate.* This is a digital control that takes on integer values. It is how the user selects the pin to which the flip-flop output signal is connected.

*DIO pin for flop reset.* This is a digital control which takes on integer values. It is how the user specifies which digital output pin on the SCB-68 connector box is used to put out the flip-flop reset signal.



*Controller routines.* This is a set of two programs downloaded to the controller at the beginning of a set of passes and executed before set of commands downloaded to controller and executed before the first pass. The two programs *Init* and *Rezero* initialize the controller and rezero the carriage respectively. The user can modify these programs by changing the code in this front panel control.

*KD, KP, KI, IT, Acceleration, Servo Loop Time, Velocity.* These are all digital controls, and the means by which the user alters the commanded motion profile and motion controller parameters. Servo Loop Time is an integer control which can only take on controller-allowed values of this parameter.

*Counter output mode.* This is a digital integer control by which the user selects whether a pulse mode or toggle mode output is used.

*Drop Spacing.* This is the specified drop spacing. It is an integer digital control. If the print mode selected is pulse mode, this will equal the divisor used to generate the drop excitation signal from the encoder signal. If the print mode selected is toggle mode, this will equal twice the divisor used to generate the drop excitation signal from the encoder signal.

*Microns before strobe.* This is an integer digital control. It specifies where in the pass the strobe is to flash. It does not take into account the strobe delay, which will cause the strobe flash to actually occur a bit farther in the pass. The program will internally round the specified value to the nearest number evenly divisible by the droplet spacing.

*Microns before frame grab.* This is an integer digital control. It specifies where in the pass the frame grab trigger pulse is to occur. Note that depending on the

camera frame duration and the speed of the carriage, the value specified here must be such that the strobe flash falls within the grabbed frame.

*Print start position.* This is an integer digital control which specifies the position in microns at which a printed line is to start. The program will internally round the specified value to the nearest number evenly divisible by the droplet spacing.

*Print stop position.* This is an integer digital control which specifies the position in microns at which a printed line is to stop. The program will internally round the specified value to the nearest number evenly divisible by the droplet spacing.

*Charge cell command voltage for print.* This is the voltage put out by the multifunction signal card on the charge cell analog output line for the portion of a pass during which drops are to be printed.

*Charge cell command voltage for deflection.* This is the voltage put out by the multifunction signal card on the charge cell analog output line for the portion of a pass during which drops are not to be printed.

*Microns per pixel.* This is the resolution of the camera being used. It is used by image analysis routines that may later be incorporated into this program.

*Phase delay in microseconds.* This is the commanded phase delay. It determines the level of voltage pulse  $V_a$  applied to the strobe delay circuit.

#### Indicators:

*Analog out update rate.* This shows the actual rate at which the analog output channels are being updated, but only works if an internal clock is being used. This is not the case here, so this should be removed.

*Motion error indicators.* These indicate when the motion controller reports that the programmed error limit has been exceeded, and suspend execution of the vi.

*Imaq error out.* This indicates any error reported by the NI-IMAQ routines. Error codes can be looked up in the IMAQ Vision for G Reference Manual, Appendix C.

*Write file error out.* This indicates any error that occurs in trying to write an image file to disk.

*Counter frequency.* This indicates the frequency of the droplet excitation signal.

*Final position.* This indicates the position of the carriage after the return pass and a short wait with integral gain.

## **A2. Overall Structure**

The whole program is inside a for-next loop which executes the number of times that the user has specified as number of passes. Inside this loop is an eight-frame sequence that executes a pass. Some of the frames contain sequences of their own (nesting). These are Frame 0, which contains a sequence to do initialization and rezeroing, and Frame 3, which contains a sequence to handle the main forward pass, including generation of all necessary signals.

## **A3. Frame-by-Frame Description**

*Frame 0:* This frame does initialization and rezeroing. It checks to see if the current pass is the first, and if so, executes a seven-frame sequence that initializes the motion controller and rezeros the carriage.

*Frame 0:* Download **RESET** command to the motion controller.

*Frame 1:* Download the front panel routines to the motion controller. These routines are the initialization routine and the rezeroing routine.

*Frame 2:* Execute the initialization routine

*Frame 3:* Wait. This is done to make sure that execution of initialization routine is done before the next program execute command is sent to the motion controller. This may or may not be necessary. This could also be replaced by a TB command (see frame 6)

*Frame 4:* Execute the rezero routine

*Frame 5:* Wait. This wait is inserted to make sure that the rezero routine has a chance to get started before checking for completion. This wait is probably not necessary.

*Frame 6:* Check for program complete. A Tell Status Byte (TB) command is used (see Galil DMC 1000 manual, p250). This will return a non-zero value (bit 6 high) if it is still executing the program.

*Frame 1:* This frame takes the user input drop spacing and velocity, calculates and displays the drop frequency and converts the velocity to microns per second. Drop spacing and carriage velocity in microns/sec are wired to sequence locals for use elsewhere in the program.

*Frame 2:* This frame loads the analog output arrays. The number of points in the array is the length of the pass in microns, divided by the drop spacing, minus 2. These are two arrays, to be put out on DAC outputs 0 and 1. DAC 0 is for the charging cell output and DAC 1 for the strobe  $V_a$  voltage output. DAC 0 is loaded with the catch command voltage at all points before print line start position and after print line end position. Between print line start position and print line end position, DAC 0 is loaded with the print command voltage. DAC 1 is loaded with  $-1.0$  at all points except where the strobe flash is desired to occur, at which point it is loaded with a voltage  $V_a$  that is calculated according to the user-commanded phase delay.

*Frame 3:* This frame is the core of the program. It handles a forward pass in a 14-frame sequence. All the functions of the machine are performed – motion, printing, strobing and frame grabbing.

*Frame 0:* This routes the frame grab triggering signal, counter 0 output, to RTSI line 0 which is wired to the frame grabber RTSI trigger input 0 inside the computer.

*Frame 1:* This sets the frame grabber up. It initializes it, sets it to be triggered by a low-going pulse on RTSI line 0, and creates an image buffer to be written to.

*Frame 2:* This drives the counter gating flip flop reset line low, forcing the the flop output low.

*Frame 3:* Makes the program wait while the flop resets. Probably not necessary.

*Frame 4:* Drives the counter gating flip flop reset line high, allowing the flip flop output to go high when the flop is clocked. This occurs when the carriage passes the reference pulse actuator.

*Frame 5:* This configures counter 1 to divide the encoder signal according to the drop spacing selected by the user, and then starts the counter. The counter is set here to only count while its gate is high, so counting does not begin until the reference mark is passed. The output of counter 1 is the piezo signal, and is used to clock analog output voltages and frame grabber triggering.

*Frame 6:* This configures counter 0 to put out a pulse at the location at which a frame is to be grabbed.

*Frame 7:* This configures the multifunction board to perform analog output, writes the analog output arrays to an output buffer, and starts analog output, each value to be clocked out on {a rising edge of the counter 1 output signal}.

*Frame 8:* This performs the forward pass motion. A series of commands are sequentially downloaded to the motion controller: set Servo Loop Time, set Error Limit, set KD, set KP, set KI, set motion smoothing factor IT, set acceleration, set deceleration, set speed, set destination position, begin pass.

*Frame 9:* This snaps a picture during a pass, writes it to a file and to a window on the screen, and shuts down the frame grabber.

*Frame 10:* This shuts off analog output once all the analog output values have been clocked out.

*Frame 11:* This queries the motion controller repeatedly until it receives a response that motion is complete. A delay of 50 milliseconds is inserted between queries.

*Frame 12:* The pass now complete, this stops the counter.

*Frame 13:* Currently empty, this frame is where image analysis on the just-acquired image would be done.

*Frame 4:* This performs the reverse pass motion. This is done by a series of commands to the motion controller, just as with the forward pass.

*Frame 5:* This queries the motion controller until it receives a response that the reverse pass is complete.

*Frame 6:* This waits at the final position (0) for a few seconds with integral gain applied, so as to get the carriage exactly back to its starting position. This may not be necessary.

*Frame 7:* This queries the motion controller for the final position error.

#### **A4. Sub-VIs used**

*Download program.vi* – This downloads a program to the motion controller. It calls three Galil-supplied VIs in sequence, *open.vi*, *Downbuff.vi*, and *close.vi*.

*talkgalil.vi*- This sends a single command to the motion controller. It calls three Galil-supplied VIs in sequence, *open.vi*, *command.vi* and *close.vi*.

*Route Signal.vi* – This VI is used to assign signals on the PCI-MIO-16E-1 card to the RTSI bus. Here it is used to route counter output 0 (frame grabber trigger) to RTSI line 0. For more information on this VI see the Labview Function and VI Reference Manual, p28-14.

*Simple Error Handler.vi* – This displays an error message on the screen if an error occurs. For more information see the Labview Function and VI Reference Manual, p10-10.

*Write to Digital Line.vi* – This sets the value of a digital output. Here it is used to write to the line which is connected to the reset pin of the counter gating flip-flop. For more information on this VI see the Labview Function and VI Reference Manual, p22-3.

*New Down Counter or Divider Config.vi*: This vi configures counter 1 to divide a signal by a specified factor. The output can either be in toggle mode (change state every n counts) or in pulse mode (put out a pulse every n counts). This was modified from the original Down Counter or Config.vi to accept input from PFI pins. In this application, the input signal is the encoder signal, the user specifies the divisor and the output is the droplet excitation signal. More information on the Down Counter or Divider Config VI can be found in the Labview Data Acquisition VI Reference Manual, p18-10.

*Generate Delayed Pulse.vi*: This configures a counter to generate a pulse of a given polarity and duration after a given delay. The pulse width and delay may be defined in seconds, in which case an internal timebase is used, or in cycles of an external timebase. In this case it is used with an external timebase, and is used to

generate the frame grabber trigger pulse. For more information see the Labview Data Acquisition VI Reference Manual, page 17-3.

*Counter Start.vi* – This starts counter 1. For more information see the Labview Data Acquisition VI Reference Manual, p18-7.

*Counter Stop.vi* – This stops the counter 1. For more information see the Labview Data Acquisition VI Reference Manual, p18-7.

*AO Config.vi* – This sets up the board to perform analog output on a specified set of channels and allocates a buffer for the operation. For more information see the Labview Data Acquisition VI Reference Manual, p9-3.

*AO Write.vi* – This writes the analog output data to a buffer for buffered output. For more information see the Labview Data Acquisition VI Reference Manual, p9-8.

*AO Trigger and Gate Config.vi* – This specifies the trigger or gate mode for the analog output. In this case, ungated, no-trigger mode is specified. For more information see the Labview Data Acquisition VI Reference Manual, p11-20.

*modified AO Start.vi* – This starts the analog output, specifying the clock source. For more information see the Labview Data Acquisition VI Reference Manual, p9-5.



*AO Wait.vi* – This periodically checks for the analog output task to be done, returning when the analog output is complete. For more information see the Labview Data Acquisition VI Reference Manual, p9-7.

*AO Clear.vi* – This is used to free memory that had been allocated to analog output once the analog output task is complete. For more information on this VI see the Labview Data Acquisition VI Reference Manual, p9-2.

*IMAQ Create.vi* -This allocates a buffer for an image. For more information see the IMAQ Vision for G Reference Manual, p10-1.

*IMAQ Trigger Control.vi* –This is used here to assign RTSI line 0 on the frame grabber to the incoming trigger signal. For more information on this VI see the NI-IMAQ VIs for G Reference Manual, p2-20.

*IMAQ Attribute.vi* – This is used here to put the frame grabber in triggered-operation mode. It can be used to get or set several other parameters. For more information, see the NI-IMAQ VIs for G Reference Manual, p2-13.

*Imaq Snap Async.vi*: This function instructs the frame grabber to snap a picture as soon as a trigger signal is received. Once the trigger edge is detected, the last frame (or two fields) to have been put out by the camera will be held by the frame grabber.

For more information see the online NI-IMAQ VIs for G Reference Manual, p2-17.

*IMAQ Winddraw.vi* – This draws the image in a window on the screen. For more information see the IMAQ Vision for G Reference Manual, p12-2.

*Imaq Writefile.vi* – This writes an image to a file on disk. For more information see the IMAQ Vision for G Reference Manual, p11-5.

*Imaq Close.vi* – This closes the open imaq interface after the frame grabbing operation is complete. For more information see the NI-IMAQ VIs for G Reference Manual, p2-12.

# THESIS PROCESSING SLIP

FIXED FIELD: ill. \_\_\_\_\_ name \_\_\_\_\_

index \_\_\_\_\_ biblio \_\_\_\_\_  
▶ COPIES: Archives Aero Dewey Eng Hum  
Lindgren Music Rotch Science

TITLE VARIES: ▶  \_\_\_\_\_

NAME VARIES: ▶  Douglas

IMPRINT: (COPYRIGHT) \_\_\_\_\_

▶ COLLATION: 182 l

▶ ADD: DEGREE: \_\_\_\_\_ ▶ DEPT.: \_\_\_\_\_

SUPERVISORS: \_\_\_\_\_

NOTES:

cat'r: \_\_\_\_\_ date: \_\_\_\_\_  
page: 130  
▶ DEPT: M.E.  
▶ YEAR: 1978 ▶ DEGREE: S.M.  
▶ NAME: CHICK RE, M.L.